

Nanoparticle-based multi-dimensional optical data storage

*A thesis submitted for the degree of
Doctor of Philosophy*

by

Xiangping Li



*Centre for Micro-Photonics
Faculty of Engineering and Industrial Sciences
Swinburne University of Technology
Melbourne, Australia*

For my beloved family.

Declaration

I, Xiangping Li, declare that this thesis entitled:

“Nanoparticle-based multi-dimensional optical data storage”

is my own work and has not been submitted previously, in whole or in part, in respect of any other academic award.

Xiangping Li

Centre for Micro-Photonics
Faculty of Engineering and Industrial Sciences
Swinburne University of Technology
Australia

Dated this day, February 27, 2009

Abstract

The ever increasing demand for high data storage capacity compels the two-photon (2P) excitation based three-dimensional (3D) bit by bit optical data storage system, where the information is recorded as a localised physical or chemical change inside the volume of recording media. Due to the highly confined property 2P induced optical data storage has higher spatial resolution compared to single-photon induced recording. In addition, less scattering loss allows the information to be recorded deep into the volume of the medium, therefore greatly expanding the storage capacity. In the past decade, the 2P excitation technique has been demonstrated in a variety of materials for the feasibility of high density optical memory.

2P excitation builds up the platform for 3D optical data storage; however, several challenges have limited the development of 2P based optical data storage. First, a high 2P sensitivity and a large 2P absorption cross-section are required to produce a highly efficient recording system. Semiconductor nanoparticles such as quantum dots/rods (QDs/QRs) are attracting materials due to their broad spectra tunability over their sizes which can be controlled during the preparation process. In particular, their 2P absorption cross-sections have been found to be orders of magnitude larger than organic dyes. Second, the storage capacity is still limited by the diffraction nature of light. Lots of efforts have been spent to break the diffraction limit of light by designing a near-field probe to reduce the recording spot size. An alternative method to break the limit of the current 3D optical data storage density is to encode

the data in the physical domain of a writing beam such as polarisation or spectra.

In light of these challenges this thesis explores the application of QDs/QRs in photopolymers for highly efficient 2P recording. A new horizon of polarisation-encoded four-dimensional (4D) optical data storage is demonstrated. To exploit the new system the research conducted in this thesis concentrates on the following key areas.

First a 2P induced polarisation encoding technique is demonstrated in azo-dye-dispersed polymers in this thesis. It has been known that under 2P excitation a polarisation sensitivity can be introduced through the isomerisation process of azo dyes. However, no 2P induced polarisation-encoded multilayer data storage has been demonstrated before due to the fact that 2P induced polarisation sensitivity is much weaker than that under single-photon excitation. To this end, a birefringence interference setup is introduced to readout the polarisation sensitivity. The readout intensity of recorded bits shows an angular dependence of $\sin^2(2\theta)$ on the reading polarisation angles, which establishes the possibility of two-state polarisation multiplexing with a polarisation angle of 45 degrees. As a consequence two-state polarisation-encoded multilayer optical data storage is demonstrated using the birefringence interference method. Furthermore, the recorded information can be erased completely when the sample is exposed to UV illumination. Erasing and re-multiplexing of information in a particular layer are successfully demonstrated as well.

The isomerisation of azo dyes under 2P excitation can introduce not only polarisation sensitivity but also the refractive-index change in the volume of the medium. The 2P induced refractive-index change in the azo-dye-dispersed polymers has been investigated both theoretically and experimentally in confocal reflection

microscopy. A confocal reflection readout threshold of the axial response from a planar reflector with a refractive-index change on the order of 10^{-2} is revealed. However, the threshold is reduced when the recorded pattern is composed of an array of bits which correspond to the size of the focus. The strong forward scattering caused by the bits leads to multiple reflection between the bit and the rare surface, which enhances the image contrast and reduces the readout threshold.

To further enhance the 2P sensitivity, a novel QD-sensitised polymers doped with azo dyes are developed in this thesis. The key innovation demonstrated in this thesis is to explore the large 2P absorption cross-sections of QDs to enhance the 2P sensitivity of azo dyes via the resonance fluorescence energy transfer process. It has been discovered that the energy transfer efficiency can be tuned according to the size of QDs, determined by both spectral overlapping and fluorescence quantum yields. Characterisation evidently reveals an enhanced isomerisation efficiency of azo dyes excited by the 2P energy transfer process from QDs. As a result the QD-sensitised photoisomerisation polymer shows an enhanced refractive-index change under 2P excitation.

In addition to the high efficiency of the 2P induced refractive-index change, QR-sensitised photoisomerisation polymers can bring the localised polarisation sensitivity. To achieve this, QRs of a uniform size distribution have been synthesised for the enhanced 2P absorption as well as polarisation selective excitation property. The 2P absorption cross-sections have been characterised by both the z-scan method and 2P induced fluorescence study. The 2P absorption cross-section of QRs is found to be one order of magnitude larger than that of QDs of similar diameters. In addition to their large 2P absorption cross-sections, strong linearly polarised emission and sharp polarisation selective excitation features of QRs have been observed in orientation microscopy study.

A novel 2P induced 4D optical data storage technique in QR-sensitised photoisomerisation polymer is demonstrated for the first time in this thesis. Characterisation of photoluminescence reveals the optimised energy transfer condition. As a consequence of energy transfer an enhanced refractive-index change is observed. The sharp angular selective excitation property has built up the pronounced difference of isomerisation rates between the directions parallel and perpendicular to the laser polarisation. It has been shown that the isomerisation excited by energy transfer from QRs introduces a pronounced polarisation sensitivity. Polarisation-encoded 4D optical data storage as well as polarisation-multiplexed 3D patterning and polarisation-controlled fabrication of waveguides is successfully demonstrated.

Due to the ability of reversible modulation of the refractive-index change photorefractive polymer is another promising branch for 3D optical data storage. Developing QD/QR-sensitised photorefractive polymers for 2P localised refractive-index change is another key aspect of this thesis. The recording performance of QDs of different surface stoichiometry has been characterised. It has been discovered that the sulfur rich surfaces facilitate the local charge transfer from QDs to surrounding dyes. Enhanced recording can be readout by fluorescence, transmission and differential interference contrast (DIC) multi-modes. Using QDs as 2P sensitisers in photorefractive polymers not only enhances the recording efficiency but also enlarges the dynamic range between erasable recording and permanent recording threshold. A 2P induced 3D optical data storage in QD-doped photorefractive polymers is successfully demonstrated. The feasibility of incorporating QRs into photorefractive polymers towards 4D optical data storage is explored. The challenges are discussed as well.

The novelty of the research presented in this thesis is to propose and demonstrate

a 2P induced multi-dimensional optical data storage in photopolymers sensitised by QDs/QRs for the first time, which has opened the new horizon for high density optical data storage. In particular, the incorporation of QRs can not only enable highly efficient 2P recording but also bring out the polarisation-encoded 4D optical data storage, which can dramatically expand the storage capacity of the current 3D storage system without the efforts to break the diffraction limitation of light. The theoretical density of multi-dimensional optical memory is towards Petabytes/disk. One can anticipate the great impact in this field of high density optical data storage if a compact optical system enabling multi-dimensional data recording and reading can be integrated in the near future.

Acknowledgement

I would like to thank my supervisor, Professor Min Gu, who offered me the great opportunity to explore the Ph.D study in the fantastic field of optical data storage. From the date I started, I have been receiving tireless guidance and endless support from him, which makes the completion of my Ph.D degree possible. His energetic characters, passion for science and insightful visions are always inspiring me and in the future work. So first and foremost, I would express my sincerest gratitude to him.

Here, I would express my sincerest gratitude to my cosupervisor, Dr. James Chon as well. I would thank him for the fruitful discussions and generous experimental suggestions to make this project moving forward smoothly. Many thanks go to Dr. Daniel Day for his remarkable research foundation on this project. I would like to thank especially for Dr. Craig Bullen, Dr. Wu Shuhui and Dr. Joel Van Embden for generous support for materials preparation and helpful discussions. For external scientists involved in this project, I would thank Professor Richard Evans. His help on materials preparation and fruitful discussions and suggestions are greatly appreciated.

Many thanks go to Australian Research Council (ARC) for funding support to this project and the top-up scholarship. And many thanks own to Swinburne University of Technology and Centre for Micro-Photonics (CMP) for the funding

support throughout the whole Ph.D study. I would like to express my gratitude to CMP administrative assistants Ms. Katie Cage and Ms. Johanna Lamborn for their help with paperwork and general office tasks. And I would like to thank Mr. Mark Kevinen for making customs optical mounts for the experiment setup.

Particular thanks own to my best friend and roommate, Mr. Jiafang Li, for various helps and many discussions after work. Many thanks go to Dr. Baohua Jia for generous help since I came to Australia. And many thanks go to Mr. Brendan Chick and Mr. Peter Zijlstra for fruitful discussions during meeting and day to day business. To other CMP members, Dr. Jingliang Li, Dr. Guangyong Zhou, Dr. Hongchun Bao, Dr. Dru Morrish, Dr. Kyongsik Choi, Dr. Michael Ventura, Mr. Wei Tao, Mr. Xinyu Gao, Ms. Hong Kang, Ms. Jing Wu, Ms. Elisa Nicoletti thank them all for the help and discussion as well as the happy time with them.

Finally, I would like to acknowledge to my family to whom this thesis is dedicated. To my parents, I thank them for the endless support. Without their support this thesis cannot be completed. To my wife, Yifan Long, thank her deeply for the great patience and understanding.

Xiangping Li

Melbourne, Australia

February 27, 2009

Table of contents

Declaration	
Abstract.....	i
Acknowledgement.....	vi
Table of contents.....	viii
List of figures.....	xii
List of tables.....	xx

1 Introduction

1.1 Bit by bit optical data storage.....	1
1.1.1 Two-dimensional recording systems.....	2
1.1.2 Three-dimensional optical data storage.....	5
1.1.3 Multi-dimensional optical data storage.....	7
1.1.3.1 Concept of multi-dimensional optical data storage.....	7
1.1.3.2 Challenges of multi-dimensional optical data storage.....	8
1.2 Objectives of this thesis.....	10
1.3 Preview of this thesis.....	11

2 Review on nanoparticle-based optical data storage

2.1 Introduction.....	14
-----------------------	----

2.2	Nanoparticles.....	15
2.3	Nanoparticle-doped photoisomerisation polymers.....	17
2.3.1	Phoisomerisation of azo dyes.....	18
2.3.2	Fluorescence resonance energy transfer.....	21
2.3.3	Merits of quantum-dot-driven energy transfer.....	23
2.3.4	Quantum-dot-dispersed photoisomerisation polymers for optical data storage.....	26
2.4	Nanoparticle-doped photorefractive polymers.....	27
2.4.1	Photorefractivity in polymers.....	27
2.4.2	Quantum-dot-doped photorefractive polymers.....	31
2.4.3	Two-photon localised photorefractive effect.....	34
2.5	Chapter summary.....	36
3	Two-photon induced polarisation encoding in azo-dye-doped polymers	
3.1	Introduction.....	37
3.2	Two-photon polarisation sensitivity.....	39
3.2.1	Experimental arrangement.....	39
3.2.2	Two-photon induced polarisation sensitivity.....	40
3.3	Two-state multilayer polarisation encoding.....	42
3.4	Erasability and rewritability.....	44
3.5	Chapter conclusions.....	46
4	Confocal reflection readout thresholds in two-photon-induced optical recording	
4.1	Introduction.....	47
4.2	Confocal reflection readout threshold in a planar reflection model.....	49

4.2.1	Experiment.....	49
4.2.2	Theory.....	52
4.3	Confocal reflection readout threshold in a bit scattering model.....	57
4.4	Chapter conclusions.....	60
5	Four-dimensional optical data storage in quantum-dot/rod-dispersed photoisomerisation polymers	
5.1	Introduction.....	61
5.2	Three-dimensional optical data storage.....	63
5.2.1	Materials preparation.....	63
5.2.2	Characterisation of energy transfer performance.....	65
5.2.3	Three-dimensional optical data storage.....	68
5.2.4	Anisotropy evolution.....	70
5.3	Two-photon characterisation of quantum rods.....	72
5.3.1	Two-photon absorption cross-sections.....	72
5.3.2	Two-photon orientation microscopy.....	79
5.4	Four-dimensional optical data storage.....	82
5.4.1	Characterisation of quantum-rod-driven energy transfer.....	82
5.4.2	Characterisation of energy-transfer-driven isomerisation.....	84
5.4.3	Four-dimensional optical data storage and other photonic applications.....	89
5.5	Chapter conclusions.....	91
6	Multi-dimensional optical data storage in quantum-dot/rod-doped photorefractive polymers	
6.1	Introduction.....	93

6.2	Three-dimensional optical data storage.....	95
6.2.1	Surface modification of quantum dots.....	95
6.2.2	Two-photon localised photorefractive performance.....	98
6.2.3	Dynamic margin.....	103
6.2.4	Three-dimensional optical data storage.....	104
6.3	Feasibility of incorporating quantum rods for multi-dimensional optical data storage.....	105
6.4	Chapter conclusions.....	107
7	Conclusion	
7.1	Thesis conclusions.....	108
7.2	Future work.....	112
7.2.1	Quantum-rod-sensitised photorefractive polymers.....	112
7.2.2	Five-dimensional optical data storage.....	113
7.2.3	Compact optical system for multi-dimensional optical data storage.....	113
	Bibliography.....	115
	Publications of the author.....	134

List of Figures

1.1	Scheme of optical data storage. (a) Bits are recorded by a photoinduced localised physical change of recording media. (b) Information is retrieved back by detecting the intensity variation of a reading beam when the optical disc is scanned.....	2
1.2	Scheme of optical setups and optical discs for CDs (a), DVDs (b) and Blu-ray discs (c).....	3
1.3	Illustration of information encoded in spectra and polarisation domains in the same region of the media..	8
2.1	(a) Size-dependent luminescence and (b) schematic illustration of the size and the luminescence wavelength of CdSe-ZnS QDs. (c) Absorption spectra (solid lines) and photoluminescence (PL) spectra (broken lines) of CdSe QDs of different sizes.....	16
2.2	Schematic illustration of isomerisation of azo dye molecules under linearly polarised laser illumination.....	19
2.3	Physical view of a photorefractive process in polymers. (1) generation of space charges (2) transporting and trapping of mobile charges (3) resulting electric field (4) refractive-index modulation.....	28
2.4	(a) Experimental geometry of 2BC. The grating is written by the interference between beam 1 and beam 2. (b) 2BC experiment for PVK:ECZ:DMNPAA:TNF at 633nm with $E_0 = 30V / \mu m$. The intensity of beam 2 is monitored as beam 1 is switched on at $t = 20s$ and off at $t = 225s$. (c) Geometry of FWM is similar to 2BC except that a separate probe beam 3 is required.....	30

3.1	Schematic illustration of the experimental setup for polarisation recording and reading.....	39
3.2	Absorption spectra of the sample.....	41
3.3	The bit intensity of the recorded bits as a function of the reading polarisation angle. The sample thickness is $80\text{ }\mu\text{m}$. The image shows two vertical bits were recorded by a horizontally polarised laser beam. The recording power and the exposure time are 10 mW and 25 ms, respectively. The circles are the experimental data of bit intensity and the solid line is the fitting using $\sin^2(2\theta)$	42
3.4	Demonstration of 2P polarisation-encoded patterns in the same region in three layers of the sample. (a) and (b) show the letters P (encoded at 0 degree) and B (45 degrees) recorded in the first layer; (c) and (d) show the letters I (0 degree) and J (45 degrees) recorded in the second layer; (e) and (f) show the letters C (0 degree) and D (45 degrees) recorded in the third layer.....	43
3.5	The erasing time as a function of the recording power by the He-Ne laser of power 0.4 mW. The inset shows the readout contrast as a function of the recording power immediately after recording (circles) and after erasing by a vertically polarised He-Ne beam (triangles).....	44
3.6	Erasing and rewriting patterns in a particular layer. (a) and (b) show two letters I and J encoded in the same region in the second layer; (c) shows the area after letters I and J are completely erased by a vertically polarised He-Ne laser beam; (d) and (e) show the letters F and E are rewritten in the same region. The marked defects indicate all the patters are recorded in the same area; (f) shows the recording contrast (squares) as a function of the repeat cycle.....	45
4.1	Experimental geometry. (a) Planar reflection model readout. A planar reflection layer with refractive-index change Δn is recorded in an azo-dye-dispersed poly(methyl methacrylate (PMMA) sample. The reflection is collected by an objective with numerical aperture (NA)=1.4. (b) Bit scattering model readout of recorded bits.....	48

4.2	Experimental results of the axial image of the recording layer. (a) and (b) are the transmission and axial images of the recording layer in the sample with air at the back surface. (c) and (d) are transmission and axial images of the recording layer in the sample with Norland at the back surface. The recording power is 11 mW. The scale bar in axial images is $3\ \mu\text{m}$	51
4.3	Experimental readout of the confocal reflection intensity normalised to the reflection intensity of the front surface is plotted as a function of the recording power. The black circle and red triangle are the sample with air and Norland at the back surface, respectively.....	52
4.4	Theoretical calculation of the confocal axial response from the planar reflector with a refractive-index change of 0.005. The reflector is $5\ \mu\text{m}$ below the front surface. (a)/(b), (c)/(d), (e)/(f) and (g)/(h) are samples with air, water, Norland and PMMA sample ($n_3 = n_1$) at the back surface, respectively. The right column is the zoom-in view of the left column.....	55
4.5	Theoretical calculation of the confocal reflection intensity of the planar reflector normalised to the reflection intensity of the front surface is plotted as a function of the refractive-index variation. The black circle and red triangle are the sample with air and Norland at the back surface, respectively.....	56
4.6	Scattering-induced reflection image reconstruction. (a) and (b) are the scattering-induced reflection images of recorded bits readout at $10.3\ \mu\text{m}$ and $15\ \mu\text{m}$ below the front surface, respectively. The recording power is 10 mW and the exposure time is $200\text{ms}/\mu\text{m}^2$. (c) The readout contrast of the recorded bits is plotted as a function of the reading position.....	58
4.7	The reflection image contrast is plotted as a function of the distance between recording position and the back surface. The black circle and red triangle are the samples with air and liquid at the back surface, respectively. (b) The reflection image contrast as a function of the refractive-index mismatch at the back surface.....	59
4.8	The scattering-induced readout contrast of the recorded bits is plotted as a	

	function of the recording power in the sample with air at the back surface....	60
5.1	Principle of polarisation modulated energy transfer. (a) Random distribution of fluorescent QRs and azo dyes in the polymer matrix. (b) When a laser beam is parallelly polarised to the orientation of QRs efficient 2P excitation induced energy transfer occurs, which drives the re-orientation of azo dyes towards the perpendicular direction to the laser polarisation. (c) 2P excitation is shut off when the laser beam is perpendicularly polarised, therefore the resultant energy transfer cannot occur.....	62
5.2	(a) Absorbance of prepared CdS QDs. (b) Relative fluorescence intensity of CdS 366 (green), CdS 441 (red) and CdS 433 (blue), respectively as well the overlapping with the absorption spectrum of DR1 (black). (c) Calculated Förster distance using the standard Förster formula.....	65
5.3	Time evolution of normalised absorbance change of DR1 molecules when the polarisation direction of the probe beam is parallel (a) and perpendicular (b) to the pump irradiation polarisation direction, respectively. The black dots, green triangles, red filled triangles and blue crosses correspond to samples without QDs, with CdS 366, CdS 441 and CdS 433 respectively.....	67
5.4	DIC readout. (a) DIC images of recorded bits. (b) Readout contrast as a function of the recording power. The black dots, green empty triangles, red filled triangles, and blue cross correspond to samples without QDs, with CdS 366, CdS 441 and CdS 433, respectively. The scale bar is $10\ \mu\text{m}$	68
5.5	Time evolution of normalised absorbance change of DR1-EH molecules when the polarisation direction of the probe beam is parallel (a) and perpendicular (b) to the pump irradiation polarisation direction. Black squares and red triangles are data from sample without QDs and sample sensitised by CdS 433 respectively. The film thickness is $5\ \mu\text{m}$ and the pump intensity is $15\ \text{GW}/\text{cm}^2$	69
5.6	Demonstration of 3D optical memory. (a) DIC image of recorded bits of DR1-EH without QDs and with CdS 433 doping in PS. Scale bar is $5\ \mu\text{m}$. (b) Readout contrast as a function of the recording power. (c) to (e) demonstrate letters I, E and C recorded in the first, second and third layers,	

	respectively.....	70
5.7	Time evolution of anisotropy of film loaded with DR1 molecules (a), CdS 366 QDs (b), CdS 441 (c) and CdS 433 (d) respectively. Solid lines are guides for eyes.....	72
5.8	(a) Open aperture z-scan response of CdS QDs of three different sizes. Blue circles, red triangles and green squares are data of CdS 430, CdS 437 and CdS 451 respectively. The solid lines are fitting with Eq. (5.2). (b) Log-log plot of two-photon absorption (TPA) cross-sections of CdS QDs versus their diameters ($1GM = 10^{-50} cm^4 \cdot s \cdot photon^{-1}$). Red line is the linear fitting yields a power-law proportionality of 3.6.....	74
5.9	(a) Absorption (blue) and fluorescence (red) spectra of as-prepared CdS QRs. (b) TEM images of well washed QRs. (c) Counts of statistics of width (blue) and length (red) of CdS QRs.....	75
5.10	Open aperture z-scan response of CdS QRs in chloroform solution. Blue circles are measured normalised transmittance and red line is fitting with Eq. (5.2).....	77
5.11	Plot of TPA cross-sections of CdS QRs (blue circles) and CdS QDs 430 (red squares) as a function of the excitation wavelength.....	78
5.12	Fluorescence intensity dependence of the CdS QRs emission under 2P excitation on a log-log scale. The slope of linear fitting is 2.007.....	79
5.13	(a) Fluorescence images of a circled emitting spot acquired at emission polariser angles of 0 and 90 degrees, respectively. The image scale is $5 \mu m$. (b) The emission intensity of the circled emitting spot is plotted as a function of the emission polarisation angle. The solid line is fitting with $\cos^2(\theta)$	80
5.14	(a) Fluorescence images of a circled emitting spot acquired at excitation polarisation angles of 0, 30, 75 and 90 degrees, respectively, where the emission polariser was fixed at the vertical direction. The image length scale is $5 \mu m$. (b) The emission intensity of the circled emitting spot is plotted as a function of the excitation polarisation angle. The solid line is fitting with a	

	dependence of $\cos^4(\theta)$	81
5.15	Absorption and emission spectra of CdS QRs as well as sufficient spectral overlapping with the absorption spectra of DR1-EH.....	82
5.16	(a) Schematic illustration when donors are far away from acceptors, no energy transfer (ET) occurs and FL is emitted from QRs. If donors and acceptors are within the Förster distance, azo dyes are excited by ET. (b) The FL intensity of the QR-dispersed PS sample is plotted as a function of the inter-molecule separation of DR1-EH. The inset is the FL images for different concentrations of azo dyes.....	83
5.17	(a) DIC images of written bits recorded at the power range from 15 to 30 mW. (b) The readout bit intensity of pure energy-transfer-driven isomerisation induced recording is plotted as a function of the recording power. (c) The readout bit intensity of pure energy-transfer-driven isomerisation induced recording at 30 mW in samples blended with azo dyes of different concentrations.....	85
5.18	(a) Normalised absorption change of the controlled sample dispersed DR1-EH only. (b) Pure energy-transfer-driven isomerisation induced absorbance evolution. Blue squares and red circles are data acquired when the excitation polarisation is parallel and perpendicular to the probe polarisation direction, respectively. The solid lines are the early isomerisation rate fitting with a linear dependence.....	87
5.19	(a) Anisotropy evolution of the QR-sensitised sample under linearly polarised illumination. The solid line is the guide for eyes. (b) Anisotropy enhancement of a QR-sensitised sample compared to the QD-sensitised sample is plotted as a function of time. The solid line is the guide for eyes. (c) Plot of the energy-transfer-preserved polarisation ratio of recorded bits as a function of the reading polarisation angle after baseline correction. Red circles and blue squares are data from QD- and QR-sensitised samples, respectively. Solid curves are fitting with $\cos(4\theta)$	88
5.20	Demonstration of polarisation-encoded 4D optical data storage. (a) to (f) are letters I/J, E/F and C/D recorded in the first, second and third layers,	

	respectively, in the polarisation direction of 45 and 0 degrees and retrieved back using corresponding polarised reading beams.....	89
5.21	Photonic applications of localised polarisation control. (a) DIC images of polarisation multiplexed patternings. Top-view images of distinct patterns are retrieved by rotating the polarisation direction of the reading beam at 45 (b) and 0 (c) degrees, respectively. (d) DIC images of polarisation controlled waveguide fabrication. Top-view images of upper and lower arms are readout at a polarisation angle of 45 (e) and 0 (f) degrees, respectively.....	90
6.1	Charge transfer enhancement by surface modification. (a) Gradual deposition of unpassivated S atoms on the surface of QDs serves as hole traps leading to suppression of radiative recombination of photoexcited QDs. (b) The experimental configuration for 2P induced recording. Surface modified QDs were incorporated into photorefractive polymers, blending with nonlinear dye and PVK matrix.....	95
6.2	Surface stoichiometry engineering using SILAR method. (a) Dynamic evolution of absorption spectra after injection of additional S precursors. I corresponds to QDs of Cd rich surface achieved when the mol concentration ratio of Cd to S is 1.2:1 in the reaction pot. II and III correspond to mixed surface and S rich surface at mol concentration ratio of 1:1.25 and 1:1.5 respectively. (b) Relative PL intensity of QDs I, II and III divided by the absorbance of illuminating beam at the wavelength of 400 nm. The inset shows the TEM image of S rich surface QDs. The scale bar is 20 nm.....	97
6.3	Scheme of localised photorefractivity. (a) Energy levels and local charge transfer at the interface between QDs and DABM molecules. (b) Nonlinear response and enhancement by molecule re-orientation as a consequence of local electric field introduced by charge transfer at the interface.....	99
6.4	(a) PL readout images of recorded bits at the recording power from 7.5 to 35 mW. The scale bar is 10 μm . The inset shows the recording configuration. (b) The readout contrast of recorded bits is plotted as a function of the recording power. Black squares, red dots, green triangles and blue triangles are data from the controlled sample dispersed DABM only and samples	

	dispersed CdS QDs with Cd rich surface, mixed surface and S rich surface, respectively.....	101
6.5	Transmission (a) and DIC (c) readout images of recorded bits at the recording power from 12.5 to 35 mW. All scale bars are 10 μm . Transmission (b) and DIC (d) readout contrasts of recorded bits are plotted as a function of the recording power. The black squares, red dots, green triangles, and blue triangles correspond to the controlled sample dispersed DABM only and samples dispersed with CdS QDs of Cd rich surfaces, mixed surfaces and S rich surfaces, respectively.....	102
6.6	(a) DIC readout contrast of recorded bits in samples dispersed with CdS QDs of S rich surfaces before (black squares) and after (red circles) exposed to UV illumination is plotted as a function of the recording power. (b) The recording threshold power (red circle) and permanent recording threshold power (green asterisk) as a function of surface stoichiometry. Solid lines are guide for eyes.....	103
6.7	Demonstration of multilayer information storage in photorefractive polymers sensitised by CdS QDs of S rich surfaces. Letter A (a), Letter B (b) and Letter C (c) are recorded in the first, second and third layer, respectively. The scale bar is 20 μm	104
6.8	DIC (a) and FL (b) readout images of recorded bits in QR-sensitised photorefractive polymers. The recording power is 40 mW and exposure time is 25 ms for each bit. The insets are the zoom-in views of one bit. The scale bar is 10 μm	106

List of Tables

1.1	Major groups work on 3D optical data storage and their reported storage capacity.....	6
2.1	Merits of reported QD-dispersed photorefractive polymers to date.....	32
2.2	Several usages of QDs in photorefractive polymers and corresponding advantages.....	34

Chapter 1

Introduction

1.1 Bit by bit optical data storage

Since we came into the age of information technology, there has been ever increasing demand for high data storage capacity. Several types of data storage systems have been introduced in the past several decades such as audio cassettes (0.1Mbit/cm^2), floppy disks (1.86Mbit/cm^2), hard disks (158Gbit/cm^2) and flash memory cards (100Gbit/cm^2) (from Wikipedia). Each technology comes with new expansion of the storage capacity but also with its own limitation. The increasing requirement for recording media to be low cost, a high memory density, high resistance to intense electromagnetic radiation, compact and portable compels the emergency of optical data storage system such as compact discs (CDs), digital video discs (DVDs) and Blu-ray discs (Blu-rays) [1].

The principle of bit by bit optical data storage is to utilise photons to introduce a localised physical or chemical property change as information storing processes such as photoinduced fluorescence or reflectance variation. When an optical disc is

scanned, pre-stored information can be retrieved back as the intensity of the reading beam to be “on” or “off”, as illustrated in the Fig.1.1.

Due to their low cost, ease to write/erase and portability, optical disc based information memory has become a popular and fastly expanding business. Considering an optical disc of diameter of 12 cm and thickness of 1.2 mm, the storage capacity is mainly limited by the size of the recorded bits. To reduce the bit size and increase the memory density optical data storage has been evolving constantly in the past twenty years. The storage capacity has been expanded from 700 Mbytes/disc (CDs) [1] to tens Gbytes/disc (DVDs, Blu-ray) [1] to 300 Gigabytes/disc (Multilayer optical storage) [2].

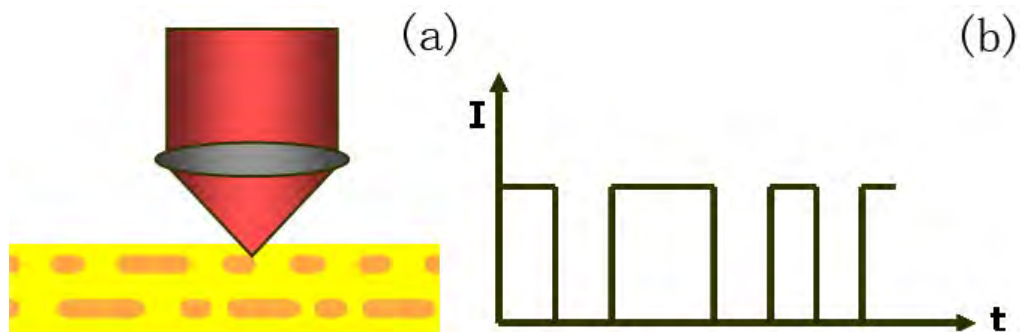


Fig. 1.1: Scheme of optical data storage. (a) Bits are recorded by a photoinduced localised physical change of recording media. (b) Information is retrieved back by detecting the intensity variation of a reading beam when the optical disc is scanned.

1.1.1 Two-dimensional recording systems

The optical data storage started with two-dimensional recording systems, where only one layer of data (in an x-y plane) is recorded beneath the surface of a recording medium. In 1983 CDs were first announced to the market as high quality and portable storage media [1]. Over 200 billion CDs were sold in the last 25 years [1]. The technique involved in CDs is to differentiate the reflected intensity between pits

(recorded areas) and lands (areas without recording). The CDs are fabricated such that the light reflected from pits is destructively interfered producing a low signal intensity compared with that from lands as shown in Fig. 1.2 (a).

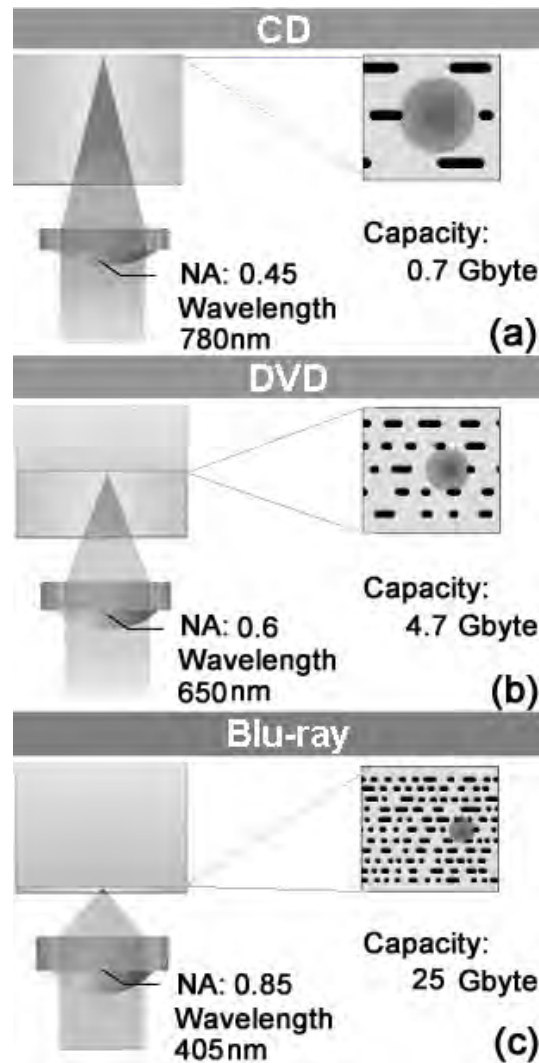


Fig. 1.2: Scheme of optical setups and optical discs for CDs (a), DVDs (b) and Blu-ray discs (c).

The standard design for an optical system of rewritable CDs, shown in Fig. 1.2 (a), utilises a laser diode operating at the wavelength of 780 nm for recording and reading. The laser beam is focused by a low numerical aperture (NA) objective

(NA=0.45) into the optical disc. The information is written in one layer of 1.2 mm beneath the cover layer. Considering the diffraction-limited case after the beam pass through the objective, the resolution of such a system can be written as [3]

$$r = 0.61 * \lambda / NA, \quad (1.1)$$

where λ is the wavelength, NA is the numerical aperture of the objective. The wavelength inside the cover layer is around 520 nm assuming that the refractive-index of the cover layer is 1.5. The calculated focal spot size is approximately $1.4 \mu m$. To minimise the error rate the standard optical discs for CDs adopt a track pitch of $1.6 \mu m$, which limits the storage the capacity up to 700 Megabytes/disc, provided that the diameter of a disc is 12 cm.

CDs quickly fell behind of the requirement of high density storage devices. In the following 10 years DVDs and recently Blu-rays have emerged as replacement of CDs for the fastly increasing requirement for more storage capacity. As seen from Eq. 1.1 the system resolution is dependent on two parameters: wavelength and NA. Improving the system resolution by either reducing the recording wavelength or increasing the NA of the writing objective will lead to a dramatic expansion of the storage capacity without increasing the size of the recording medium.

The technique involved in DVDs is using a shorter wavelength laser diode (650 nm) and a higher NA objective (NA=0.6) to produce a smaller focused spot, therefore improving the system resolution and reducing the track pitch to $0.74 \mu m$, as shown in Fig. 1.2 (b). Although the information is still recorded in one layer at 0.6 mm below the cover layer, the single layer storage density has been expanded to 4.7 Gigabytes/disc.

Blu-ray discs operate at a much shorter wavelength of 405 nm and increase the

NA to 0.85 which allows more information to be stored in the same area with a focal spot size reduced to 580 nm, as shown in Fig.1.2 (c). The track pitch can be decreased further to $0.32\ \mu\text{m}$, therefore the storage capacity has been pronouncedly expanded to 23 Gigabytes/disc. To avoid the scattering loss and unwanted optical effect when propagating through the cover layer, the information is recorded 0.1 mm beneath the surface.

As the data layer is closer to the surface, Blu-ray discs are more vulnerable to scratches and require scratch protection coatings, thus significantly increasing the manufacturing costs. The estimated cost for a Blu-ray disc is twenty times of a DVD, however the capacity of a Blu-ray disc is only 5 times that of a DVD. The technique involved in DVDs and Blu-ray discs makes such that further increasing the area memory density beyond 25 Gigabytes is very unlikely due to the pronounced increase in the cost for larger NA objectives or a laser diode shorter than 400 nm.

1.1.2 Three-dimensional optical data storage

As the information is only recorded one layer beneath the surface approximate 99.99% of the volume of the recording medium is left unused. The further development has been conducted into three-dimensional (3D) optical data storage, such as double layer DVDs and double layer Blu-ray discs. An additional axial dimension has been introduced, where information is recorded in the x-y-z space. However, when a recording beam is focused deep into the volume of an optical medium, scattering loss occurs. The shorter the wavelength the stronger the scattering loss [4]. The energy cannot be delivered efficiently for multilayer recording. It is very difficult to manufacture a three-layer DVD or Blu-Ray disc. This challenge compels the two-photon (2P) excitation based multilayer optical data storage systems [5, 6].

In contrast to single-photon process, 2P absorption occurs when two photons are absorbed simultaneously. As the 2P absorption is dependent on the square of the intensity of an incident light beam [7, 8], the excitation can be confined to a small region within the focus of the objective. In other words, 2P excitation has a higher spatial resolution compared to single-photon excitation, which allows the information to be written and retrieved back distinctly without unwanted crosstalk from neighboring layers. The second advantage of 2P excitation is that the beam can propagate deep into the volume by using an infrared wavelength which suffers less scattering by the medium. The 2P energy can be delivered efficiently to multilayers inside the volume without significant degradation.

Author	Year	Material	Density	Ref
Strickler, et al.	1991	Photopolymerisable gel	0.3 Tbits / cm ³	[6]
Cumpston, et al.	1999	Photopolymersiable polymer	--	[9]
Parthenopoulos, et al.	1989	Photochromic polymer	--	[5]
Toriumi, et al.	1997	Photochromic material	1 Gbits / cm ³	[10]
Kawata, et al.	1998	Photorefractive crystal	33 Gbits / cm ³	[11]
Day, et al.	1999	Photorefractive polymer	5 Gbits / cm ³	[12]
Bhawalkar, et al.	1998	Photobleachable polymer	1 Tbits / cm ³	[13]
Gu, et al.	1999	Photobleaching polymer	3 Gbits / cm ³	[14]
Glezer, et al.	1996	Photofabricating voids in silica	17 Gbits / cm ³	[15]
Day, et al.	2002	Photofabricating voids in polymer	2 Gbits / cm ³	[16]
McPhail, et al.	2002	Liquid crystal dispersed polymer	0.2 Tbits / cm ³	[2]
Walker, et al.	2008	Photochromic polymer	0.3 Tbits / cm ³	[8]

Table 1.1 Major groups work on 3D optical data storage and their reported storage capacity.

Since the first demonstration of 2P excitation based 3D optical data storage [5], the 2P technique has been widely applied into a variety of materials for high density memories, including photopolymerisable materials [6, 9], photochromic materials [2, 5, 8, 10] photorefractive materials [11, 12], photobleaching materials [13, 14] and void-fabricatable materials [15, 16]. Table 1.1 lists the major groups working on 2P absorption based 3D optical data storage and their reported memory density. In particular, a prototype of 2P optical disc has been characterised with a reported capacity of $0.3 \text{ Tbits} / \text{cm}^3$ and a recording and reading speed comparable with the current DVD technique [8].

1.1.3 Multi-dimensional optical data storage

The storage capacity of 2P excitation based 3D optical memory is still limited by the resolution of recorded bits which is confined by the diffraction nature of light. The theoretical limit of capacity is approximately $3.5 \text{ Tbits} / \text{cm}^3$ by using an objective of NA=1.4 after aberration correction [17]. In addition, the nonlinear absorption establishes the fact that the probability of 2P excitation is significantly weaker than that of the single-photon excitation process [7]. A large 2P absorption cross-section is necessary for this system to be practical. The need for new techniques to break the diffraction limitation compels the emergence of multi-dimensional optical data storage.

1.1.3.1 Concept of multi-dimensional optical data storage

The concept of multi-dimensional optical data storage, so called “the third generation optical data storage”, (we call CDs, DVDs and Blu-rays the first generation optical data storage and 3D data storage the second generation), is to record multi-states of

information in the same 3D spatial position of a recording medium. The information can be multiplexed into additional physical dimensions of a writing beam such as spectra or polarisation, as illustrated in Fig. 1.3. The multi-dimensional encoding technique is potentially promising to increase the current storage capacity by orders of magnitude with introducing the polarisation or spectral dimensions, which is not limited by the spatial resolution of recorded bits. This thesis is committed to polarisation encoding technique only. The concept of recording the polarisation state of a writing beam has been reported in a few experiments using organic dyes [18, 19] and liquid crystals [20] as polarisation sensitisers. However, there is no demonstration of polarisation-encoded four-dimensional (4D) optical data storage yet.

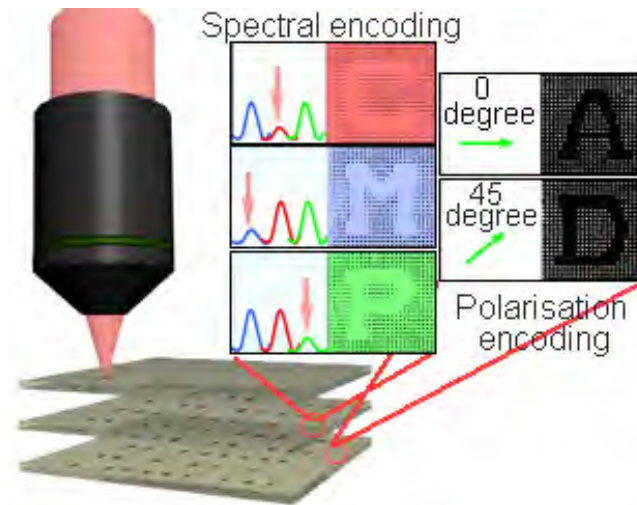


Fig. 1.3: Illustration of information encoded in spectra and polarisation domains in the same region of the media.

1.1.3.2 Challenges of multi-dimensional optical data storage

As discussed in the previous section, reports on polarisation encoding techniques are few and its technological development in optical memory is still in its early stage. Applying a polarisation encoding technique in multi-dimensional optical data storage

which allows the increase in memory capacity not limited by the spatial resolution of recorded bits still remains challenges. The primary challenges for implementation of the multi-dimensional encoding are summarised in the following.

Two-photon sensitivity. 2P absorption is dependent on the square of the intensity of the incident light. The nonlinearity establishes the fact that the probability of 2P excitation is significantly weaker than that of a single-photon excitation process [7]. As a result an ultra-short pulsed laser such as a femtosecond laser is usually used for efficient nonlinear excitation. Organic dye molecules are generally 2P excitable; however the low 2P sensitivity impedes their wide application in terms of devices. Semiconductor nanoparticles such as quantum dots (QDs) and quantum rods (QRs) are promising candidates due to their broad spectral tunability over sizes [21] and larger 2P absorption cross-sections [22]. However, dispersing nanoparticles homogeneously into a recording medium itself is quite challenging.

Sharp selective excitation. Besides a high 2P sensitivity a recording medium needs to be polarisation selectively excitable, as multi-states information is recorded in the same spatial region. Further there should be no interference with the chemical or physical features recorded by the second polarisation state during both recording and reading. A sharp polarisation selective absorption property is necessary for efficient polarisation encoding. This tolerance determines the number of states that can be encoded simultaneously in the polarisation domain. Nanoparticles can be promising candidates for this solution due to their optical properties can be tuned dependent on their sizes as well as shapes [21, 23]. The concept of incorporating semiconductor nanoparticles in multi-dimensional optical data storage has never been explored yet.

Compatible optics design. As discussed above a sharp polarisation selective excitation property of a recording medium is required, an optical system which can

pick up and deliver the differently polarised writing and reading beams is necessary. Polarisation control elements are needed for encoding and decoding the polarisation information.

1.2 Objectives of this thesis

The objective of this research is to explore the performance of nanoparticles (specifically QDs/QRs in this thesis) in 2P induced bit by bit optical storage and develop polarisation-encoded multi-dimensional optical data storage systems in nanoparticle-dispersed polymers. This objective is achieved in two ways.

First, a 2P induced polarisation encoding technique in photopolymers doped with azo dyes is constructed and characterised. This is the first demonstration of 2P induced rewritable polarisation-encoded 4D optical data storage. A birefringence interference system is developed to decode the polarisation information multiplexed in the same spatial area. This system serves as a key reading system for polarisation-encoded multi-dimensional optical data storage.

To gain an understanding of 2P induced refractive-index change of azo dyes dispersed in polymers, axial images of 2P induced refractive-index change are investigated both theoretically and experimentally in a confocal reflection microscope. The threshold effect on the refractive-index change is investigated on both a planar reflector model and a bit scattering model.

To improve the 2P sensitivity of azo-dye-dispersed polymers, the concept of using cadmium sulfide (CdS) QDs as 2P energy transfer donors is proposed and demonstrated for the first time. Extensive investigations particularly with regard to energy transfer induced refractive-index change are undertaken. To open the

possibility of application in polarisation-encoded multi-dimensional optical memory, CdS QRs with functionality of polarisation selective absorption property are synthesised and incorporated as 2P sensitisers. 2P absorption cross-sections, polarisation selective excitation and emission properties of QRs, which are crucial for 2P polarisation-encoded data storage, are studied. Polarisation-encoded 4D optical data storage as well as various polarisation-controlled photonic applications is demonstrated.

Second, the concept of the 2P absorption induced localised charge separation and the subsequent photorefractive effect in QD-dispersed photorefractive polymers is proposed and demonstrated. To gain an insight of the dependence of the surface charge transfer on their surface states CdS QDs with different surface stoichiometry are investigated. Extensive investigations, particularly fluorescence quenching, refractive-index variation enhancement and rewritable dynamic margin, are carried out to characterise the surface charge transfer and the localised photorefractive effect. To open the possibility towards multi-dimensional optical data storage, the feasibility of incorporating QRs into photorefractive polymers is also explored.

1.3 Preview of this thesis

The research undertaken in this thesis includes materials preparation and system development of QD/QR-dispersed polymers for multi-dimensional optical data storage. The core concept presented is to utilise QDs/QRs as 2P sensitisers due to their large 2P absorption cross-sections [22], and the polarisation absorption functionality [24, 25] for polarisation-encoded multi-dimensional optical data storage.

Chapter 2 introduces the foundation of the research undertaken in this thesis. An

introduction of semiconductor nanoparticles and their primary optical properties are given in Section 2.2. The recent development of optical data storage in nanoparticle-dispersed photoisomerisation materials via energy transfer process is reviewed in Section 2.3. The principle of Förster energy transfer and the concept of photoisomerisation of azo dye molecules are introduced. Special attention is given to the development of QD/QR-sensitised photoisomerisation polymers via energy transfer process for optical data storage. Section 2.4 describes the general photorefractivity in polymers as well as the photorefractive effect in nanoparticle-doped photorefractive polymers. To date, the reported work on nanoparticle-incorporated photorefractive polymers for optical data storage is reviewed. A summary of this chapter is given in Section 2.5.

Chapter 3 demonstrates the first 2P induced rewritable polarisation-encoded multilayer optical data storage in azo-dye-dispersed polymers. The birefringence interference setup for polarisation sensitivity readout is introduced and the 2P excitation induced polarisation sensitivity is characterised in Section 3.2. The ability of two-state polarisation encoded multilayer storage is demonstrated in Section 3.3. The conditions of erasable and rewritable recording is discussed and demonstrated in Section 3.4. A chapter conclusion is drawn in Section 3.5.

Using confocal reflection microscope to readout the 2P induced refractive-index change in azo-dye-dispersed polymers is presented in Chapter 4. In Section 4.2, the readout threshold on the 2P induced refractive-index change is studied both theoretically and experimentally based on the planar reflector model. A reduction of the threshold is identified when strong forward scattering caused by recorded bits leads to multiple reflection between the bit and the back surface in Section 4.3. Factors which affect the quality of reconstructed refractive-index images in such a bit scattering model are carefully investigated. Conclusions are drawn in Section 4.4.

Chapter 5 investigates the energy transfer performance and demonstrates polarisation-encoded 4D optical data storage in QD/QR-sensitised photoisomerisation polymers. In Section 5.2 the feasibility of incorporating QDs in photoisomerisation polymers as 2P energy transfer donors is demonstrated. As a consequence energy-transfer-driven 3D optical data storage is demonstrated. To gain understanding of QRs under 2P excitation, 2P absorption cross-sections are measured and the polarisation selective excitation property is characterised in Section 5.3. In Section 5.4 the refractive-index change enhancement and the polarisation sensitivity of QR-driven isomerisation are characterised. Finally, the application of QRs and azo dyes dispersed polymers in polarisation-encoded 4D optical data storage as well as in various polarisation-controlled photonic applications are demonstrated. A chapter conclusion is drawn in Section 5.5.

Incorporating QDs/QRs into photorefractive polymers towards 4D optical data storage is explored in Chapter 6. Section 6.2 demonstrates 2P induced localised photorefractive effect in CdS QD-sensitised photorefractive polymers. In particular, the recording performance of QDs with different surface stoichiometry is characterised for multi-modes readout. As a result 3D optical storage in QD-dispersed photorefractive polymers is demonstrated. In Section 6.3 the feasibility of incorporation QRs into photorefractive polymers towards multi-dimensional optical data storage is explored. A few key challenges are discussed. A chapter conclusion is drawn in Section 6.4.

Chapter 7 summarises the work undertaken in this thesis. Conclusions are drawn in Section 7.1. Future works including the development of instruments and five-dimensional storage systems are discussed in Section 7.2.

Chapter 2

Review on nanoparticle-based optical data storage

2.1 Introduction

Ever since the introduction of semiconductor nanoparticles in 1990's, great efforts of researchers have been spent to explore their application in optical data storage systems due to their attractive optical properties. The performance of nanoparticles in a variety of recording media and recording mechanisms has been investigated. Developing nanoparticle- and photoisomerisation-material-doped polymers via fluorescence energy transfer process is of significance. This is largely attributed to many advantages of nanoparticles including a broad spectral tuning range, a large excitation efficiency and a high photostability, which are inaccessible to traditional organic materials. Dispersing nanoparticles in photorefractive polymers is another promising approach due to their high photocharge generation efficiency and tunable spectral response range.

This chapter reviews the recent development of nanoparticle-based optical data

storage. An overview of general principles and features of semiconductor nanoparticles is given in Section 2.2. The concept of Förster energy transfer as well as application of nanoparticles in photoisomerisation materials via an energy transfer process is reviewed in Section 2.3. Special attention is given to photoisomerisation effect of azo dye molecules. The advantages of incorporating nanoparticles in energy transfer investigation are discussed. The concept of applying nanoparticle-driven energy transfer in optical data storage is described. Section 2.4 reviews major principles of the photorefractive effect in polymers and the technique highlight of nanoparticle-dispersed photorefractive polymers. The concept of the two-photon (2P) localised photorefractive effect is summarised. Chapter is summarised in Section 2.5.

2.2 Nanoparticles

Nanoparticles, specifically focused on quantum dots (QDs) and quantum rods (QRs) in this thesis, are fragments of semiconductors consisting of thousands of atoms with the bulk bonding geometry and surface states eliminated by enclosure in a material of a larger band gap [21]. These nanoparticles are often composed of atoms from groups II-VI or III-V elements in the periodic table such as CdS (cadmium sulfide), CdSe (cadmium selenide) and CdTe (cadmium telluride). The dimension of these particles which is important to their optical and electronic properties, is typically on a scale from 0.2 to 100 nm. With a size reduced to a nano-scale, the electronic energy states become discrete and the surface-to-volume ratios of materials are large, which significantly changes the fundamental optical and electronic properties from the bulk material. Therefore, these features lead to a size-tunable optical property which sparks QDs/QRs with potential applications in every discipline of sciences.

The most striking feature of QDs is their broad spectral tunability over their

sizes which can be controlled by the temperature, the duration and ligand molecules used in the preparation process [21]. As the size decreases, the electronic excitation blue shifts to higher energy bands. The discrete energy states also lead to a dependence of the fluorescence wavelength on the size. This leads to a broad spectral tunability and the capability of multi-wavelength excitation. In other words, it offers a plenty of room to control the desired wavelength response by a judicious choice of the composition over the size. Typical size-dependent emission spectra spanning the visible region as well as the corresponding absorption spectra are shown in Fig. 2.1 [26].

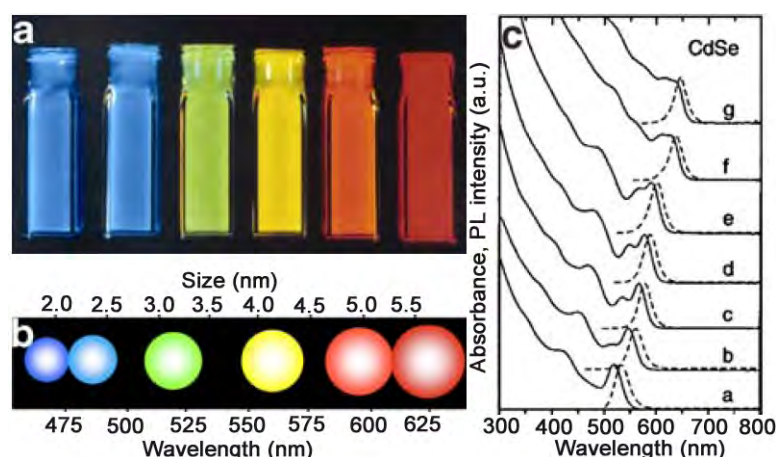


Fig. 2.1: (a) Size-dependent luminescence and (b) schematic illustration of the size and the luminescence wavelength of CdSe-ZnS QDs. (c) Absorption spectra (solid lines) and photoluminescence (PL) spectra (broken lines) of CdSe QDs of different sizes [26].

The second important characteristic of QDs is the influence of their surface states on the optical and electronic properties. The absorption of a photon with energy above the band gap creates an electron-hole pair. As the surface is not perfect, surface defects in nanoparticles create temporary “traps” for electrons or holes and prevent the radiative recombination of electron-hole pairs. Passivation of nanoparticles with organic molecules is necessary to avoid the aggregation of nanoparticles and increase the fluorescence quantum yield [21]. Another way to

protect the surface atoms from oxidation and improve the photostability is to grow a monolayer of shell materials of larger band gap on the surface of core particles. The quantum yield of QDs with judicious design of shell structures can be close to 90% [27].

The ability to tailor the shapes of QDs results in the production of rod-shape nanoparticles, also known as QRs. Apart from size-dependent optical properties attributed to the strong confinement of electrons and holes in low dimensional materials [21], the wavefunction can be further manipulated by elongating spherical QDs into one-dimensional rod shapes. It allows linearly polarised emission as well as angular selective excitation features [24, 25] whereas spherical QDs do not have. Furthermore, the fluorescence of QRs can be reversibly switched on and off by an external electric field [28]. These unique properties can further expand nanoparticles in various photonic applications.

2.3 Nanoparticle-doped photoisomerisation polymers

Photoisomerisation is the ability to alternate between two different chemical structures with different absorption spectra as a response to the irradiation of light of an appropriate wavelength [29]. The fuse of photoisomerisation materials with polymer sciences provides promising candidates for optical memory due to their easy procedure of preparation and rewritability. Owing to their tunable spectral response, high sensitivity and high fluorescence quantum yield, investigation of incorporating QDs/QRs into photoisomerisation materials via energy transfer processes has been carried out. In particular, developing nanoparticle-dispersed photoisomerisation polymers is of significance. This section reviews the recent development of

nanoparticle-dispersed photoisomerisation polymers.

2.3.1 Photoisomerisation of azo dyes

The widely studied isomerisable dyes are spirobenzopyran derivatives and diarylethene derivatives, which are also characterised as photochromic materials due to the isomerisation-caused dichroic property. Photoisomerisable dye spirobenzopyran-dispersed polymers were first demonstrated for 2P induced high density three-dimensional (3D) optical data storage using the photochromic property [5]. Isomer A having shorter absorption bands can be 2P excited to isomer B with longer absorption bands and red emission [5]. 2P excitation has also been adopted for fluorescence readout from isomer B in the written bits. However, this fluorescence readout is destructive, where information is partly erased during the reading process. This is attributed to the reverse isomerisation reaction from isomer B to isomer A. Nondestructive readout has been developed by detecting the small difference of refractive-index between the two isomer states in the longer wavelength which cannot stimulate the photoisomerisation process [10, 30].

Another widely investigated photoisomerisable dyes are azobenzene (azo) derivatives. The exciting feature of azo groups is such that photoisomerisation of the two isomer states introduces not only dichroism but also birefringence [31, 32]. It has been well known that the polarisation state of a writing beam can be recorded as a polarisation sensitive refractive-index change [18, 33-35].

It is known that azo dyes containing the aromatic group can exist in two configurations, a *trans* state and a *cis* state, as illustrated in Fig. 2.2 [36, 37]. The photoisomerisation process starts by photoexciting *trans* molecules into *cis* isomers. The *trans* states with their optical axis parallel to the polarisation direction of the

laser beam are preferentially excited to *cis* states. As azobenzene *trans* isomers are generally more stable than *cis* isomers. The molecules in *cis* states can relax back to *trans* states through either spontaneous thermal relaxation or reverse *cis-trans* isomerisation cycles [32]. During the reverse isomerisation process some isomers relax back to the initial *trans* states as before illumination, while the others rotate their optical axis by 90 degrees from the initial states (Fig. 2.2) [38]. The *trans* molecules that return to the initial states are re-excited to *cis* isomers. As a consequence of multiple *trans-cis-trans* cycles, the number of *trans* isomers with optical axis perpendicular to the polarisation direction of the laser beam increases, therefore leading to an anisotropic refractive-index modulation [18, 39].

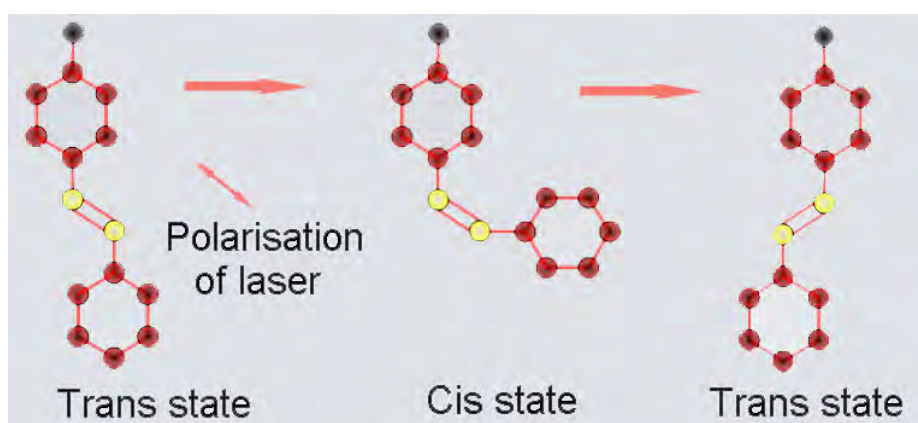


Fig. 2.2: Schematic illustration of isomerisation of azo dye molecules under linearly polarised laser illumination.

As described above the photoisomerisation of azo dyes under linearly polarised laser illumination leads to re-alignment of their optical axis towards the direction perpendicular to the polarisation state of the laser beam. To characterise the photoisomerisation real-time dichroism kinetics is investigated by a pump probe experiment [40]. The probe beam in the absorption band of *trans* states with much weaker intensity is polarised either parallel or perpendicular to the polarisation direction of the pump beam. Two competing processes involved are orientational

hole burning and pure photoorientation [40]. If *trans* isomers are photoisomerised to *cis* isomers but not rotated, the population of *cis* states increased and a hole is burning in the *trans* states. Absorbance in both parallel and perpendicular direction decreases with $\Delta A_{//} = 3\Delta A_{\perp}$, where $\Delta A_{//}$ and ΔA_{\perp} are the absorbance change in the parallel and perpendicular direction, respectively [40]. Pure orientation occurs when *trans* molecules are efficiently rotated and *cis* isomers are negligible. The absorbance in parallel direction decreases whereas absorbance in perpendicular direction increases with $\Delta A_{//} = -2\Delta A_{\perp}$ [40]. Under 2P excitation the photoisomerisation is more complicated. High power irradiation induced photobleaching occurs which leads to the isotropic absorbance decrease. Then non-bleached molecules are photoaligned perpendicular to the polarisation direction of the pump beam [41].

The anisotropic distribution of *trans* isomers builds up the birefringence which allows the polarisation state of a writing beam to be recorded. Azo-dye-dispersed polymer materials have been investigated for both holographic memory and bit-oriented storage [18, 42-44]. Single-photon induced polarisation encoding has also been demonstrated in azo dye bonded copolymers [18]. Three letters were multiplexed in three polarisation states of a writing beam at polarisation angles of 0, 60, and 120 degrees, respectively. The ability of erasing and rewriting in the same spatial position was successfully demonstrated as well. However, this multiplexion is only achieved in one layer beneath the surface of the recording medium since single-photon excitation cannot be delivered efficiently inside the volume.

It has been known that 2P excitation can also introduce photoisomerisation of azo dyes embedded in a polymer matrix [41, 45], and a polarisation sensitivity can also be introduced by 2P orientational hole burning and photoorientation effect. As a consequence a proof-of-concept experiment of polarisation sensitive refractive-index change has been demonstrated by 2P excitation [35]. A 2.5 times difference in the

readout intensity of recorded bits using parallelly and perpendicularly polarised reading beam was observed by polarisation reflection confocal microscope [35]. However, the multi-photon orientation is less efficient to rotate *trans* isomers in the perpendicular direction than single-photon orientation [41, 45]. Significant cross talk impedes the demonstration of 2P induced polarisation-encoded multilayer data storage until this thesis. A detecting system with an improved polarisation sensitivity is necessary. To demonstrate 2P induced polarisation-encoded multilayer data storage in such a system is the first aim of this thesis. The corresponding detail is discussed in Chapter 3.

2.3.2 Fluorescence resonance energy transfer

Fluorescence resonance energy transfer, also known as Förster resonance energy transfer (FRET), is a distance dependent interaction between excited electronic states of fluorophores [46]. A donor molecule can non-radiatively transfer its absorbed energy to another nearby acceptor molecule. For the occurrence of efficient FRET several conditions are required [46, 47]. First, the emission band of the donor has to overlap significantly with the absorption band of the acceptor. Second, the separation of donor-to-acceptor has to be usually within several nanometres. Third, as FRET is a process of dipole-dipole coupling the emission dipoles and the absorption dipoles must have a favorable mutual orientation. Last, the donor must have a high fluorescence quantum yield. The efficiency of energy transfer η is dependent on the donor-to-acceptor separation distance r with an inverse 6th power law due to the dipole-dipole coupling mechanism and given as [46]

$$\eta = \frac{1}{1 + (r/R_0)^6}, \quad (2.1)$$

where R_0 is defined as the Förster distance at which the energy transfer efficiency is 50%. The Förster distance depends on both the spectral overlapping of the

emission from the donor with the absorption from the acceptor and the mutual dipole-dipole orientation, expressed as followings [46]

$$R_0^6 = \frac{9 \cdot (\ln 10) \cdot \kappa^2 \cdot J(\lambda) \cdot Q}{128 \cdot \pi^5 \cdot n^4 \cdot N_A}, \quad (2.2)$$

where κ^2 is the mutual dipole orientation factor, Q is the fluorescence quantum yield of the donor in the absence of the acceptor, n is the refractive-index of the medium, N_A is Avogadro's number, and $J(\lambda)$ is the spectral overlapping and given as [46]

$$J(\lambda) = \int f_D(\lambda) \cdot \varepsilon_A(\lambda) \cdot \lambda^4 d\lambda, \quad (2.3)$$

where $f_D(\lambda)$ is the normalised emission spectrum from the donor and $\varepsilon_A(\lambda)$ is the molecular extinction coefficient from the acceptor. $\kappa^2 = 2/3$ is often assumed in a system where dyes are freely rotating and can be considered as isotropic orientation. When the dipoles are parallel to each other κ^2 has the maximum value of 4 [46].

FRET has been widely adopted as an important tool for biomedical applications including optical sensing [48] and fluorescence labeling [49]. Most important, the reversible modulation of the fluorescence intensity of the donors via switching on and off the energy transfer process builds up the key concept of all-optical switching as well data storage. This reversible switching has been achieved by alternating between the two isomer states of photoisomerisation dyes upon single-photon irradiation which show dichroic features [50, 51]. 2P 3D storage has been convincingly demonstrated in a photoisomerisable dye diarylethene and fluorescent fluorophore fluorene dispersed samples [52, 53]. During the recording process the closed form of diarylethene is photoisomerised to an open form which has an absorption band not overlapped with the emission band from fluorene. As a consequence strong 2P fluorescence from fluorene has been successfully readout in the written regions [52, 53].

The fluorescence energy transfer process can also be utilised to enhance the absorption efficiency of materials with a small 2P absorption cross-section, especially photoisomerisation and photochromic dyes. Energy transfer based 3D optical data storage has been proposed to improve the 2P writing efficiency [54]. The 2P absorption cross-section of majority photochromic and photoisomerisation dyes generally is small in the range of $0.1 \sim 10 GM$ ($1 GM = 10^{-50} cm^4 \cdot s \cdot photon^{-1}$). The effective absorption cross-section of photoisomerisation dye indolyl flugide from isomer A to isomer B is only $0.05 GM$. Rh6G with a large 2P cross-section of $200 GM$ and a high fluorescence quantum yield has been used as 2P energy transfer donors. The effective 2P cross-section of indolyl flugide has been increased to $2.7 GM$ excited by 2P fluorescence energy transfer from Rh6G, which is over 50 times magnification [54]. Similarly, the FRET method has been applied to improve the 2P induced emission of DNA intercalators in conjugated polymers. An enhancement factor of over 35 has been achieved owing to the contribution from fluorescence energy transfer [55]. These results build up the bench mark to utilise QDs in 2P based optical data storage via fluorescence energy transfer processes.

2.3.3 Merits of quantum-dot-driven energy transfer

The incorporation of QDs into energy transfer related photonic applications can greatly enhance the impact in this field due to their unique optical properties such as their broad absorption tunability [21], high molar extinction coefficients (2 orders of magnitude higher than organic dyes) [56] and resistance to photodegradation and photobleaching. Compared to their counterparts of conventional fluorophores the tunable emission spectra property enables better control of spectral overlapping with specific acceptors [57, 58]. Growing a monolayer of shell materials of larger band gaps on the surface of core particles can further increase the fluorescence quantum

yield and improve the photostability, therefore enabling a larger Förster distance. The quantum yield of QDs with judicious design of shell structures can be close to 90% [27]. Investigation of using QDs as both energy transfer donors and acceptors has been carried out. Herein, this section reviews the recent investigation of using QDs in fluorescence energy transfer processes in terms of the superiority they offer.

Tunable spectral overlapping: Because organic dyes usually have broad absorption spectra and emission bands with long tailing, significant cross-talk is often observed in fluorescence energy transfer involved investigations. However, QDs have narrow emission bands which can also be favorably tuned to a desired emission wavelength according to their sizes. Therefore, the degree of spectral overlapping between QDs and the given acceptors can be tuned to facilitate the occurrence of fluorescence energy transfer.

This has been demonstrated in the configuration of CdSe-ZnS core-shell QDs as donors and Cyanine3 (Cy3) molecules as acceptors [57]. Three QDs of different sizes were prepared with their emission peak at wavelengths 510, 530 and 555 nm, respectively, to vary the degree of spectral overlapping with the absorption band of Cy3 molecules which has an absorption peak around wavelength 550 nm. The calculation reveals that the configuration of 555 nm emitting QDs have the largest spectral overlap integral as well as the Förster distance and 510 nm emitting QDs are expected to have the lowest energy transfer efficiency due to the smallest overlap integral and Förster distance. This difference in spectral overlap was confirmed by the experimental results of fluorescence intensity quenching of QDs as well as the emission enhancement of dyes, which were used as a means to characterise the fluorescence energy transfer efficiency [57]. A similar result was reported between CdSe-ZnS core-shell QDs and photoisomerisation dye spiropyran as well [59]. This tunable fluorescence energy transfer efficiency over the sizes of QDs can be applied

to 2P induced optical data storage, which opens the possibility of efficient 2P recording while avoiding the destructive reading process.

Large extinction coefficients: Due to large extinction coefficients of QDs, one order of magnitude higher than organic dyes [60], QDs can be either excellent energy transfer donors to efficiently absorb and transfer the excitation or desirable acceptors to efficiently absorb the transferred energy. Fluorescence of small size QDs was quenched while the emission from large QDs was enhanced in a closely packed CdSe QDs solid [61]. This observation establishes the possibility of using QDs as donors or acceptors in fluorescence energy transfer investigations.

Their large 2P absorption cross-sections [22] open the horizon of using QDs in 2P photonic applications via fluorescence energy transfer processes. 2P-driven fluorescence energy transfer is limited by the difficulty to choose donor-acceptor pairs with substantial spectral overlap for high energy transfer efficiency while non-overlap between 2P absorption spectra to avoid direct excitation of acceptors. Pronounced difference in absorption coefficients can be produced between QD donors and organic dye acceptors due to orders of magnitude difference in the 2P absorption cross-sections [22], which provides a solution for 2P fluorescence energy transfer investigations. CdSe-ZnS QDs with 2P absorption cross-sections on the order of $10^4 GM$ were used as light-harvesting fluorophores to excite Cy3 molecules via the 2P fluorescence energy transfer process [62]. Due to 10^4 smaller in 2P absorption cross-sections, background from direct excitation of Cy3 was eliminated almost completely, which is common in the case of single-photon excitation.

Highly luminescent and photostable: For efficient energy transfer donors are required to have a high fluorescence quantum yield, as expressed in Eqs. (2.1) and (2.2). As discussed before, shell structures with larger band gaps on the surface of core

particles can significantly enhance the PL quantum yields above 50% [63], and even close to 90% [27]. The shell structures cannot only enhance the photoluminescence efficiency, but also improve the photostability. Stable photoluminescence of CdSe-ZnS QDs was reported over a long term in imaging [64]. The fluorescence intensity of QDs was stable and there was no deterioration during continuous illumination. In comparison organic dye fluorescein isothiocyanate labeled fluorescence signal degraded quickly to 20% of its initial brightness within 5 mins [65]. The superior photobleaching threshold and photostability of QDs are desirable in optical data storage for long term usage.

2.3.4 Quantum-dot-dispersed photoisomerisation polymers for optical data storage

Reversible modulation of QD photoluminescence using photoisomerisation dye spiropyran as fluorescence energy transfer acceptors have been investigated in solutions [59, 66]. Under UV illumination the spiro-isomers can convert into mero-isomers which have significant spectral overlap with the emission of QDs. Switching on and off the fluorescence of QDs by alternating isomer states of spiro- and mero- forms establishes the key concept of data writing and reading. Later using photoisomerisation dye spirooxazine to modulate fluorescence of organic nanoparticles was implemented in a more practical Polyvinyl alcohol film [67]. PL of organic nanoparticles can be reversibly modulated by the photoisomerisation of spirooxazine with a high on/off contrast. Experiment of fluorescence imaging readout was demonstrated under single-photon excitation [67].

However, there has been no real demonstration of optical data storage in QD-dispersed photoisomerisation polymers. In addition, the novel concept of

incorporating QDs into photoisomerisation polymers via the 2P fluorescence energy transfer process has never been explored till this thesis. Using QDs as fluorescence energy transfer donors in photopolymers doped with azo dyes for 2P induced 3D optical data storage is one of the originalities of this research. In particular, the incorporation of QRs in azo-dye-doped polymers for 2P induced polarisation-encoded multilayer data storage is proposed and demonstrated for the first time in this thesis. The details will be described in Chapter 5.

2.4 Nanoparticle-doped photorefractive polymers

Photorefractivity is an alternative promising candidate for 3D optical data storage owing to its ability to spatially modulate the refractive-index in the volume of a recording medium. In particular, photorefractive polymers are appealing materials as they enable the high nonlinear performance which underpins the many areas of photonics. The incorporation of QDs into photorefractive polymers shows an enormous potential owing to the broad spectral tuning range and the high charge photogeneration efficiency, which are inaccessible to traditional photorefractive materials. This section reviews the recent development in the field of QD-doped photorefractive polymers [68]. The merit and functionality of these hybrid materials are summarised and future challenges are discussed. The application of QD-doped photorefractive polymers for 2P localised photorefractive effect is introduced, which facilitates a promising new area of high density optical data storage.

2.4.1 Photorefractivity in polymers

The photorefractive effect in polymer was first experimentally demonstrated by Moerner in 1990 [69]. A photorefractive polymer is a multifunctional optoelectronic medium which fuses both the photoconductivity and the electro-optic effect into the

same material [70]. Typically it consists of a polymer matrix, a plasticiser, a high concentration of nonlinear dye molecules and a small amount of sensitizers with each component performing a particular role. Fig. 2.3 illustrates the physical view of the photorefractive process. In the first step, sensitizers photogenerate space charges in the “bright area”, which results from the spatially inhomogeneous illumination from the two-beam interference. The second physical process of the photorefractivity is to transport the generated charges along the polymer. Generally the mobile charges can drift or diffuse into the “dark area” under an external electric field bias. To drive the transport a component of the external electric field E_0 should exist along the direction of the grating vector K_G . Thirdly, the impurities and defects in the polymer are able to trap the mobile charges for a period of time. As a consequence, the separation of the space charges introduces a sinusoidal internal electric field. Finally, the electro-optic effect of the nonlinear optical dye molecules introduces a refractive-index change through both the linear Pockels effect and the nonlinear Kerr orientation effect [71-73].

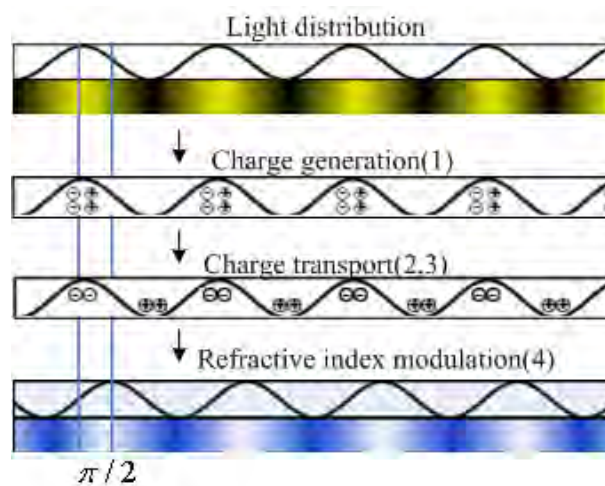


Fig. 2.3: Physical view of a photorefractive process in polymers. (1) generation of space charges (2) transporting and trapping of mobile charges (3) resulting electric field (4) refractive-index modulation.

The important feature of the photorefractive effect is its complete reversibility. The trapped charges can be released back by exposing the material to homogeneous UV irradiation or heat. The trapped space charges recombine and the space charge field becomes neutralised. Subsequently the refractive-index modulation disappears.

Two methods widely used to characterise photorefractive effect are two-beam coupling (2BC) and four wave mixing (FWM) [72-74]. A typical experimental configuration for a 2BC measurement is illustrated in Fig. 2.4 (a). A sample consisting of poly (N-vinyl carbazole) (PVK): 9-ethylcarbazole (ECZ): 2,5-dimethyl-4-p-nitrophenylazo anisole (DMNPAA): 2,4,7-trinitro-9-fluorenone (TNF) at weight concentration ratio of 53:16:30:1 is prepared. An inspection of the transmission intensity of the two incident beams as a function of time under an external electric bias in Fig.2.4 (b) reveals that one beam gains the energy while the other beam loses its energy. Chopping either of the two incident beams causes the other beam to recover to its original intensity level. As the 2BC gain is given by $\Gamma \propto \Delta n \times \sin \Phi$, where Δn is the refractive-index modulation and Φ is the phase shift of the index grating [73], which has been used as an important property to characterise the refractive-index modulation of the material. The gain coefficient can be experimentally determined using

$$\Gamma = \frac{1}{L} \ln[(I_{2(in)} \times I_{1(out)}) / (I_{2(out)} \times I_{1(in)})], \quad (2.4)$$

where L is the optical length of the amplified beam, $I_{(in)}$ and $I_{(out)}$ are the incident and transmitted beam intensity, respectively [73, 74].

FWM has been widely used as an indispensable tool for investigation on the kinetics of refractive-index gratings. The experimental configuration is quite similar to 2BC except that a separate probe beam propagating in the opposite direction to

either of the two writing beams is also required, shown in Fig.2.4 (c). Since the diffraction efficiency η is square sinusoidally dependent on Δn , it can be used as a way to characterise the refractive-index change, which is experimentally given as

$$\eta = I_4 / I_3, \quad (2.5)$$

where I_4 is the transmitted intensity of the probe beam I_3 [73]. $1/\tau_w$ is another important parameter to characterise the response rate of the photorefractive effect in the material, where τ_w is the characteristic growth time for the diffraction efficiency to reach the steady state [73].

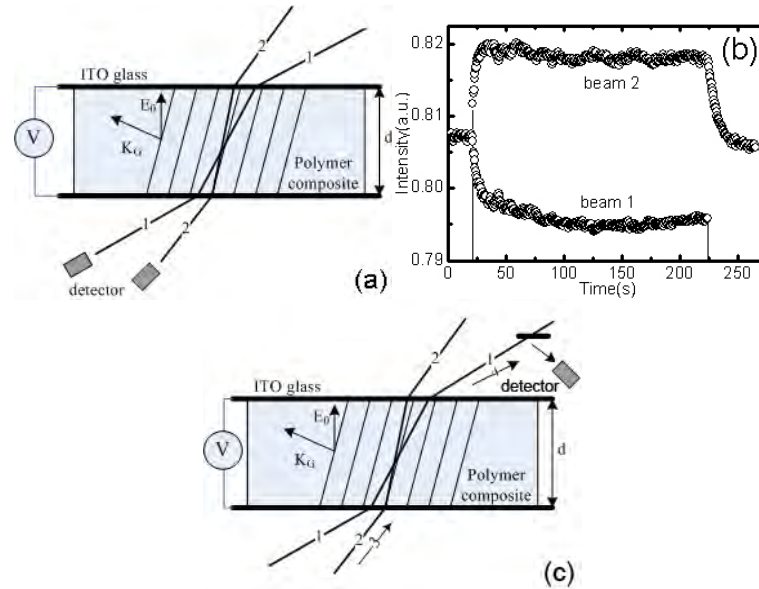


Fig. 2.4: (a) Experimental geometry of 2BC. The grating is written by the interference between beam 1 and beam 2. (b) 2BC experiment for PVK:ECZ:DMNPAA:TNF at 633nm with $E_0 = 30V / \mu m$. The intensity of beam 2 is monitored as beam 1 is switched on at $t = 20$ s and off at $t = 225$ s. (c) Geometry of FWM is similar to 2BC except that a separate probe beam 3 is required.

The information can be recorded as refractive-index gratings in the volume of a photorefractive polymer. The recording and reading setup for holographic storage [75] is beyond the topic of this thesis. An alternative method for recording information as refractive-index change inside the volume of photorefractive materials

is bit-orientated optical memory [11, 12], which is the subject of this thesis committed to. A single writing beam rather than two-beam interference is focused by an objective to introduce a localised photorefractive effect. The details are discussed in the following.

2.4.2 Quantum-dot-doped photorefractive polymers

Among all available organic sensitisers, C60 [76] and TNF [77] are the most frequently utilised photocharge generators in high performance photorefractive polymers. However, these sensitisers as with most organic sensitisers suffer from a narrow spectral tuning range. Organic photosensitising in the infrared (IR) range is generally unstable [78]. Particularly, not many organic sensitisers are available at the telecommunication wavelengths of 1.3 and 1.55 μm . Secondly, they are less efficient in photocharge generation [79]. Furthermore, photobleaching under intense light irradiation limits their applications in device wise.

QD-dispersed photorefractive polymers offer enormous advantages over their counterparts sensitised by organic molecules. Since the first demonstration of the photorefractive effect in a QD-dispersed photorefractive polymer in 1999 [80], a variety of hybrid photorefractive polymers containing various nanoparticles with different compositions and structures have been intensely investigated. A summary of these studies in terms of the nanoparticles concentration, the photorefractive response rate, the 2BC gain and the diffraction efficiency is presented in Table 2.1, while the advantages of QD-dispersed polymers are shown in Table 2.2 and summarised in the following.

Nanoparticles	C (wt%)	$\frac{1}{\tau_w} (s^{-1})$	$\Delta n \times 10^{-3}$	$\eta(\%)$	$\lambda(nm)$	$\Gamma(cm^{-1})$	Ref
CdS	0.191	0.137	--	8	514	59.5	[80]
PbS (HgS)	0.99	0.05	--	--	1310	30.9(4.3)	[81]
CdS	2	>0.02	--	72	514	30	[82]
PbS	2	0.5	--	--	1340	185	[83]
PbSe	10	--	3.1	40	1550	86.4	[84]
CdSe	0.44	0.04	0.18	0.15	633	--	[85]
CdSe/CdS	0.1	0.06	0.35	1.3	633	--	[86]
CdSe-HPA	0.4	0.077	0.912	9.3	633	13.2	[87]
CdSe/ZnS	0.4	0.04	0.3	4.21	633	30.6	[88]
CdSe/ZnS	1	0.02-0.1	0.09	0.23	633	7.2	[89]
CdTe	1.15	5	0.45	20	633	25	[90]
CdSe	1	0.5	--	--	633	48.3	[91]
CdSe	0.2	--	--	--	633	35	[92]
CdS	1	>0.1	--	4.4	633	78.4	[93]
CdSe	1	10	--	20	633	--	[94]
Alq ₃	2	0.035	--	--	633	424	[95]

Table 2.1. Merits of reported QD-dispersed photorefractive polymers to date.

Broad spectral tunability and high photogeneration efficiency: QDs are appealing photosensitisers primarily because of their broad spectral tunability and high photogeneration efficiency [80, 83, 86, 94]. By judiciously designing the size and composition of QDs one can tune the optical response of photorefractive polymers ideally to a desirable wavelength range. CdS, CdSe and CdTe QDs [80, 82, 85-94] have been widely studied to achieve the photorefractive sensitivity in the visible wavelength range, while PbS and PbSe QDs [81, 83, 84] have been incorporated in the photorefractive polymers in the telecommunication wavelength range between 1.3 and 1.5 μm .

At a given weight percentage QDs are more efficient in photocharge generation than organic sensitisers. Under an electric field the photocharge generation efficiency of the CdS-dispersed PVK-based PR material was found to be one order of magnitude higher than that in the material sensitised by C60 [79]. Tunable

photorefractive performance has been observed by surface processing of QDs [86-89, 94]. Facilitating a high efficiency of the charge generation as well as a fast grating build-up response was reported when small molecules were attached to the surface of QDs [87, 94]. A high photorefractive performance was observed in the material containing core/shell QDs where a shell of wide-band-gap materials was grown on the surface of the core particles to form an effective potential barrier to the recombination for holes immobilised on the particle surface [86, 88, 89].

Improved charge mobility: In addition to the high charge generation efficiency an increasing hole mobility has been observed in a QD-doped PVK-based material, an enhancement not shown in organic-dye-doped polymers [96, 97]. The carrier mobility is dependent on the sample thickness as well as the QD concentration. As the carrier mobility in semiconductor is much higher than that of the polymer matrix, increasing the QD doping concentration leads to active participation of QDs in the carrier transport process by absorbing and re-ejecting the mobile carriers. Therefore an enhanced hole mobility has been observed [96, 97].

Improved trap efficiency: Beyond the merits discussed above QDs can also be used as trap mechanisms to improve the photorefractive performance, since it has been well known that introducing a trapping layer to photorefractive materials can enhance the photorefractive effect [98]. An improved photorefractive performance was achieved by incorporating nanoparticles in photorefractive polymers as electron trappers rather than sensitisers [95]. By a judicious choice of the nanoparticle type such that the valence band lies below the lowest unoccupied molecular orbitals of the sensitising molecules, a small amount of nanoparticle doping can efficiently trap the photogenerated electrons due to the electron affinity gradient while mobile holes remain mobile. This electron affinity gradient induced charge separation can even occur without an external electric field [99].

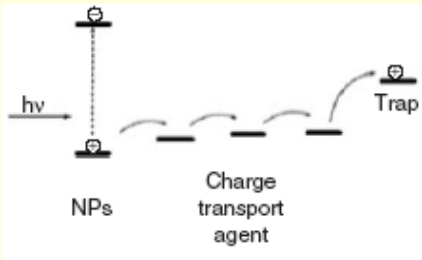
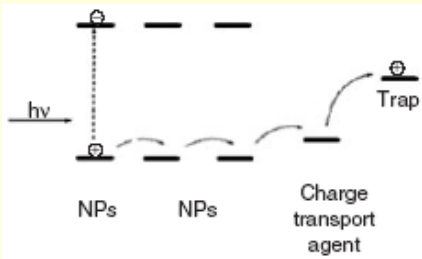
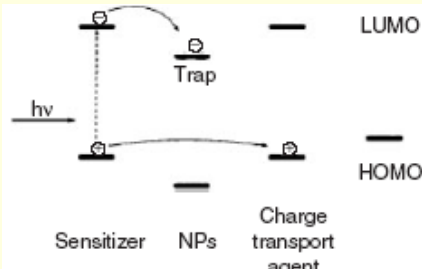
Property and use	Scheme of NPs function	Advantages
As charge generators (Photogeneration efficiency)		Broad spectra tunability over size. High photogeneration efficiency compared with organic sensitizers
To improve charge mobility (Photoconductivity)		Controllable in charge mobility by tuning doping concentration
To improve trap efficiency (Electron affinity)		Tunable trap density by careful choosing energy level and concentration of nanoparticles

Table 2.2 Several usages of QDs in photorefractive polymers and corresponding advantages.

2.4.3 Two-photon localised photorefractive effect

Photorefractive polymers have been widely used in photonic devices [100]. Some of the photonic applications of a photorefractive polymer are not based on the formation of a long-range refractive-index grating but rather on localised refractive-index changes in the absence of an external field. Although in defining and characterising the photorefractive effect an external electric field is generally required to facilitate space charge hopping through the matrix, it may not be necessary for the presence of

an external electric field to introduce the charge separation and the resultant refractive-index modulation in a short range [101]. Due to its highly confined property, 2P absorption has been widely used to generate many localised effects. In such a system a high numerical aperture (NA) objective is utilised to focus a single writing beam to generate a large electric field gradient within the focus rather than to produce long range gratings by two-beam interference. As a result, a localised refractive-index change can be introduced for 3D optical data storage in both photorefractive crystals [11] and polymers [12] without the use of an external electric field. The feasibility of 2P excitation in a photorefractive polymer has also been demonstrated through a 2BC experiment [102].

As discussed in Section 2.4.2, tuning the electron affinity gradient between QDs and surrounding polymer matrix can facilitate the occurrence of the charge separation, which provides the bench mark for the investigation on surface modification of QDs for optical data storage. In addition, 2P excitation can introduce a large electric field gradient within the focus of a high NA objective to favor the charge transporation, which opens the possibility of localised photorefractive effect in QD-dispersed photorefractive polymers under 2P excitation. With the large 2P absorption cross-sections of QDs, two orders of magnitude higher than organic sensitisers [22], 2P excitation can greatly expand the impact of QD-dispersed photorefractive polymers for 3D optical data storage. However, the concept of incorporating QDs into photorefractive polymers for 2P induced localised photorefractivity as well as its application in optical data storage has never been explored till this thesis. The 2P induced localised photorefractive performance in QD-doped photorefractive polymers and the dependence of the photorefractive performance on the surface processing of QDs are studied in this thesis. The details are discussed in Chapter 6.

2.5 Chapter summary

This chapter introduces the unique optical properties of QDs and reviews the recent development of QD-dispersed polymer materials towards optical data storage.

Photoisomerisation polymers doped with azo dyes have been known for the capability of recording the polarisation state of a writing beam under both single-photon and 2P excitation. However, a detecting system with an improved polarisation sensitivity is required for 2P induced polarisation-encoded multilayer optical data storage. A birefringence interference setup will be introduced and the 2P induced polarisation-encoding technique will be investigated in such a system in Chapter 3 and 4. Incorporating QDs into photoisomerisation materials via fluorescence energy transfer processes shows its superiority over organic sensitisers under single-photon excitation. In particular, QDs have a large 2P absorption cross-section. However, the application of QD/QR-dispersed photoisomerisation polymers into 2P induced multi-dimensional optical data storage, which is of significance, has never been explored. This novel concept will be studied for the first time in Chapter 5. The use of QDs in photorefractive polymers has significantly enhanced the photorefractive performance owing to lots of merits they offer. Applying 2P excitation in QD-dispersed photorefractive polymer for localised photorefractive performance has never been explored. Incorporating QDs/QRs into photorefractive polymers for 3D optical data storage will be explored in Chapter 6.

Chapter 3

Two-photon induced polarisation encoding in azo-dye-doped polymers

3.1 Introduction

Due to its highly localised excitation nature, two-photon (2P) excitation by a laser beam focused through a high numerical aperture (NA) objective enables a higher storage density compared with single-photon excitation [5]. Furthermore, infrared illumination permits recording into the inner volume of a thick recording medium. In the last decade, 2P excitation has been widely used in three-dimensional (3D) bit by bit optical data storage. 2P induced multilayer optical recording has been successfully demonstrated in various erasable and non-erasable materials [2, 11, 12, 30, 103-105]. In the diffraction limited case, it can be estimated that the highest 3D data density under 2P excitation by a laser beam of wavelength 800 nm is approximately a few Tbits/cm³ [17].

Applying 2P absorption in photoisomerisation polymers loaded with azo dyes

opens the possibility of polarisation-encoded optical data storage. However, two factors impede the demonstration of 2P induced polarisation-encoded multilayer storage in azo-dye-dispersed polymers. First, the 2P sensitivity of azo dyes is low. To achieve a practical recording either the concentration of dyes has to be increased to enhance the nonlinear absorption coefficients or 2P absorption cross-section of dye molecules has to be enhanced. Second, the polarisation sensitivity introduced by 2P excitation is significantly weaker than single-photon excitation [41]. A detecting system with an improved 3D polarisation sensitivity is required.

The aim of this chapter is to investigate the feasibility of rewritable 2P induced polarisation-encoded multilayer optical data storage in azo-dye-blended polymers [106], which is the bench mark for quantum dot/rod (QD/QR)-based studies. To read out 3D polarisation sensitivity, a birefringence interference setup is introduced. The 2P induced polarisation sensitivity is characterised in such a system. The condition for erasable and rewritable recording is also investigated.

The structure of this chapter is organised as following. Section 3.1 presents the introduction. In Section 3.2 a birefringence interference setup for reading out 3D polarisation sensitivity is introduced. Experimental characterisation of the 2P induced polarisation sensitivity in such a system is performed. Section 3.3 demonstrates the two-state polarisation multiplexing in multilayer data storage. The erasability and re-multiplexing are demonstrated in Section 3.4. The chapter conclusion is drawn in Section 3.5.

3.2 Two-photon polarisation sensitivity

3.2.1 Experimental arrangement

The experimental setup for 2P recording was a typical microscopy system as schematically illustrated in Fig. 3.1 [107]. A linearly polarised Ti:sapphire ultrashort pulsed laser beam of pulse width 100 fs and repetition rate 82 MHz (Spectra-Physics Tsunami) at wavelength 780 nm was employed as a light source for 2P excitation. A quarter wave plate and a Glan-Thompson prism were used to control the polarisation state of the recording beam. After passing through the system the expanding of the pulse duration is estimated to be less than 200 fs. An objective (NA=0.7; 20X) was used to focus the excitation beam onto the recording sample. A commercial transmission microscope (Olympus BX50) and a high NA objective (NA=1.4; 60X) were used for readout of multilayer information. To avoid any erasure of recorded bits in the reading process, we used the Ti:sapphire laser at a continuous wave (CW) mode with one fifth of the power of the recording beam. The sample was placed in between two orthogonal polarisers as illustrated in Fig. 3.1, which were simultaneously rotated to choose a reading polarisation state during readout. Such a reading system is equivalent to a polarisation interference system for a birefringent medium [100], but also gives the 3D imaging ability.

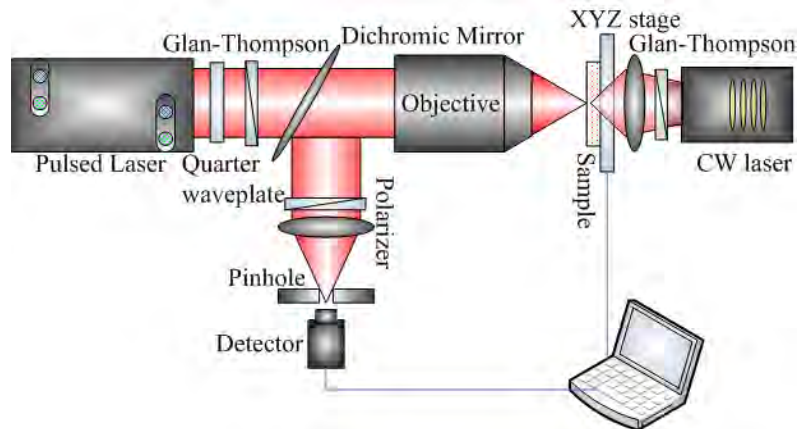


Fig. 3.1: Schematic illustration of the experimental setup for polarisation recording and reading.

3.2.2 Two-photon induced polarisation sensitivity

Azo dye 2,5-dimethyl-4-(p-nitrophenylazo)anisole (DMNPAA) has been used as dye chromophores in photorefractive polymer [12, 70]. In fact, just like the other azo dye molecules, its optical axis can be orientated to the perpendicular direction of a linearly polarised excitation beam via multiple *trans-cis-trans* photoisomerisation process as discussed in Section 2.3.1. It has been demonstrated that the DMNPAA doped photorefractive polymer can be excited under 2P absorption [12]. It is therefore possible to achieve a 2P induced polarisation sensitivity via the *trans-cis-trans* isomerisation process if DMNPAA is doped in an appropriate polymer matrix. To this end, we doped DMNPAA in un-plasticised polystyrene (PS) rather than the conventional system of poly (N-vinyl carbazole) (PVK) plasticised with 9-ethylcarbazole (ECZ) as neither charge transport nor plasticisation are needed in this process. The sample was prepared in the following way. A mixture consisting of 30 wt. % of DMNPAA and 70 wt. % of PS was dissolved in chloroform. Then the solution was evaporated at 60 °C for 20 mins to get rid of solvents. The sample was placed on a glass slide between spacers and heated at 200 °C for 3 mins. The polymer sample was sandwiched and cooled down to room temperature quickly.

The absorption spectra of the prepared sample is shown in Fig. 3.2. There is no linear absorption above 650 nm, therefore a femtosecond pulsed laser beam at wavelength 780 nm can be used for 2P excitation, which corresponds to resonant single-photon excitation around 390 nm located in the maximum absorption band of DMNPAA molecules. The 2P absorption cross-section we measured according to [108]

$$I_d = I_0 / [1 + (N\sigma_2/h\nu)I_0d], \quad (3.1)$$

where I_0 is the incident intensity in the focus, N is the number of molecules inside

the focus, d is the thickness of the sample, $h\nu$ is the photon energy and σ_2 is the 2P absorption cross-section. The measured 2P absorption cross-section of DMNPAA is $1 \times 10^{-48} \text{ cm}^4 \cdot \text{s} \cdot \text{photon}^{-1}$ while the single-photon-induced recording cannot be observed up to the intensity of $0.5 \text{ GW} / \text{cm}^2$.

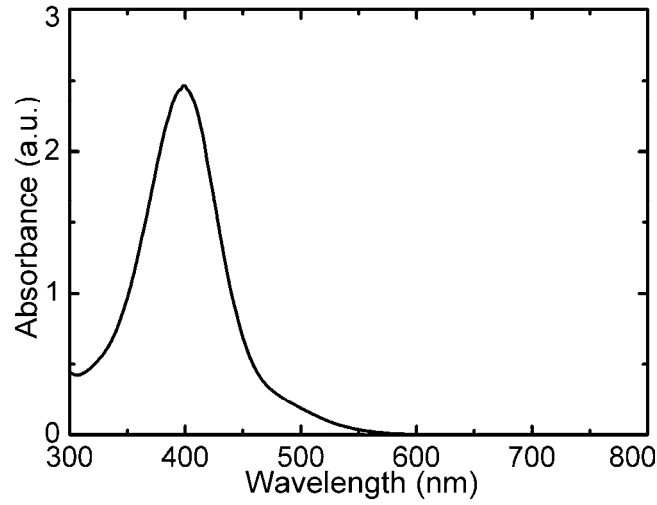


Fig. 3.2: Absorption spectra of the sample

To characterise the 2P induced polarisation sensitivity several bits were recorded by a linearly polarised femtosecond laser beam. The images in the inset of Fig. 3.3 show the readout intensity of two bits as a function of the reading polarisation angle. It can be found that the highest and lowest intensity positions occur when the angles between the recording and reading beam polarisation directions are 45 and 90 degrees, respectively. In other words, the readout intensity has an angular dependency of $\sin^2(2\theta)$ where θ is the angle between the polarisation directions of the recording and reading beams. Such an angular dependence is consistent with the theoretical prediction (solid curve) of the polarisation interference measurement through a birefringent medium [100]. This result confirms that the observed angular dependency is caused by the 2P induced birefringence property via multiple *trans-cis-trans* photoisomerisation process, where the optical axis of the excited

molecules is intended to be orientated to the direction perpendicular to the polarisation of the recording beam [18, 35]. This 2P induced polarisation sensitivity is the physical basis of the polarisation-encoded multilayer data storage method.

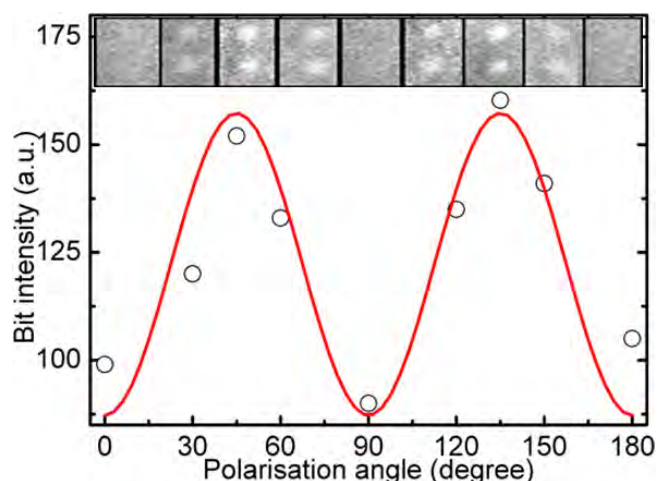


Fig. 3.3: The bit intensity of the recorded bits as a function of the reading polarisation angle. The sample thickness is $80\ \mu\text{m}$. The image shows two vertical bits were recorded by a horizontally polarised laser beam. The recording power and the exposure time are 10 mW and 25 ms, respectively. The circles are the experimental data of bit intensity and the solid line is the fitting using $\sin^2(2\theta)$.

3.3 Two-state multilayer polarisation encoding

In fact, not all molecules in the focus volume can be aligned to the perpendicular direction of the recording polarisation because of their initial random orientation. In addition angular dependence of readout intensity establishes the probability of polarisation multiplexing with little cross-talk between encoded information when the polarisation angle is 45 degrees shown in Fig. 3.3. Therefore, one can encode two polarisation states in the same layer by separating the two polarisation directions of recording beams at an angle of 45 degrees.

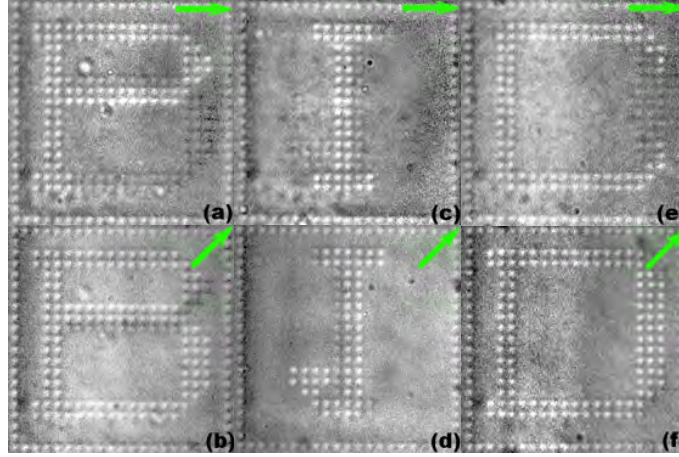


Fig. 3.4: Demonstration of 2P polarisation-encoded patterns in the same region in three layers of the sample. (a) and (b) show the letters P (encoded at 0 degree) and B (45 degrees) recorded in the first layer; (c) and (d) show the letters I (0 degree) and J (45 degrees) recorded in the second layer; (e) and (f) show the letters C (0 degree) and D (45 degrees) recorded in the third layer.

Fig. 3.4 demonstrates 2P induced polarisation-encoded six patterns recorded in three layers. In each layer, two letters are recorded when the polarisation direction of the recording beam is orientated at 0 and 45 degrees, respectively. Each pattern consists of 21×21 bits with a bit spacing of $4 \mu\text{m}$. Each bit was recorded with the given exposure condition (recording power of 16 mW and exposure time of 25 ms). The separation between the adjacent layers is $30 \mu\text{m}$. Patterns P/B, I/J and C/D were multiplexed in the first, second and third layers, respectively. Thus the estimated memory density of our system is approximately 50 Gbits per disc. However, due to the depolarisation effect of high NA objectives up to 30% [109], the bit intensity does not drop to zero (as shown in the inset of Fig. 3.3) therefore leading to a small amount of cross-talks. The depolarisation effect introduced by a writing objective of NA=0.7 is less than 10% [109]. Under this recording condition all recorded bits can be erased completely as the readout contrast drops to zero after erasing, which eliminates the possibility of any irreversible changes in the storage medium.

3.4 Erasability and rewritability

Since the aligned molecules can relax back to their original states, the recorded bits can be erased completely when exposed to an environment temperature higher than T_g ($T_g \sim 45^\circ\text{C}$) or a He-Ne beam of perpendicular polarisation to the recording beam. Fig. 3.5 shows the erasing time as a function of the recording power by the He-Ne laser of power 0.4 mW. Under our recording condition, the recorded bits can be completely erased in 3 mins. The quadratic dependence of erasing time on the recording power also confirms 2P absorption induced recording as the erasing process is a single-photon process. The inset illustrates the bit readout contrast as a function of the recording power. The contrast is given following $R = (I - I_b)/(I + I_b)$, where I is the bit intensity and I_b is the background. The circles present the results read out immediately after recording while the triangles are the results read out after erasing. For a recording power level between 5 and 20 mW, the recorded bits are erasable and rewritable with high contrast. Using the 2P absorption coefficient we calculated the heat decay into the matrix during the irradiation

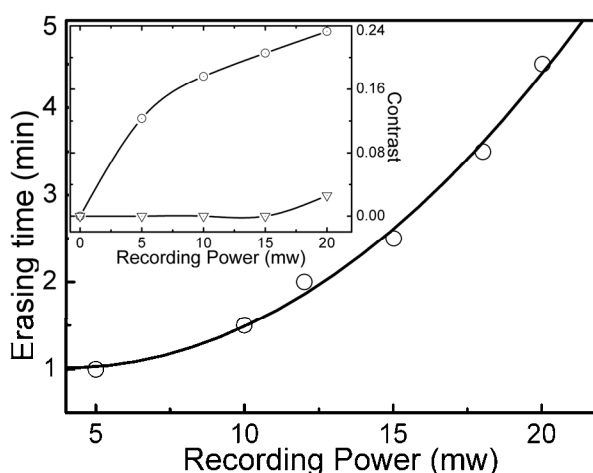


Fig. 3.5: The erasing time as a function of the recording power by the He-Ne laser of power 0.4 mW. The inset shows the readout contrast as a function of the recording power immediately after recording (circles) and after erasing by a vertically polarised He-Ne beam (triangles).

and estimated the temperature rise to $\sim 60^\circ\text{C}$ at recording power of 5 mW and exposure time of 25 ms [110] provided that thermal conductivity and specific heat capacity of PS is $0.08\text{ W/m}\cdot\text{K}$ and $1.3\text{ kJ/kg}\cdot\text{K}$ respectively. Beyond 20mW, permanent recording was observed mainly caused by thermal damage to the matrix. It should be pointed out that the erasable and rewritable condition is dependent on the chosen polymer matrix. It has been noted (not shown here) that if DMNPAA is doped in a loose matrix PVK: ECZ (concentration of 30:54:16), it is more difficult to achieve a stable erasable and rewritable region.

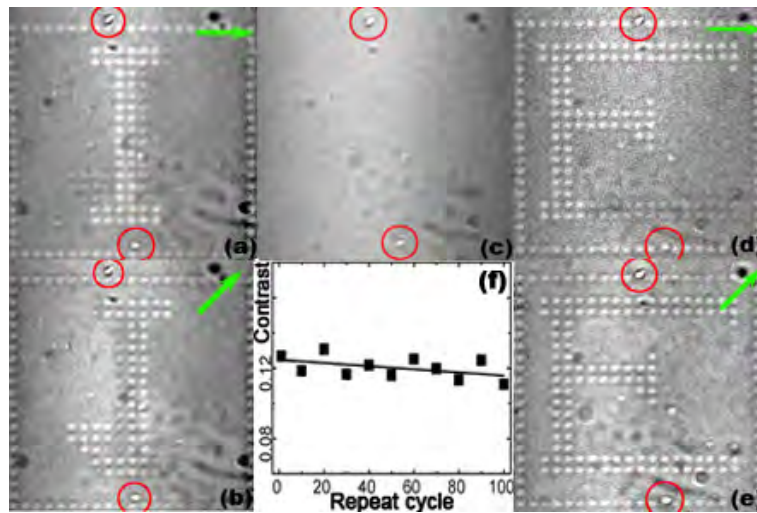


Fig. 3.6: Erasing and rewriting patterns in a particular layer. (a) and (b) show two letters I and J encoded in the same region in the second layer; (c) shows the area after letters I and J are completely erased by a vertically polarised He-Ne laser beam; (d) and (e) show the letters F and E are rewritten in the same region. The marked defects indicate all the patterns are recorded in the same area; (f) shows the recording contrast (squares) as a function of the repeat cycle.

Fig. 3.6 demonstrates the erasing and re-multiplexing of information in a particular layer. Figs. 3.6 (a) and (b) show the two letters I and J recorded in the second layer with polarisation encoding at 0 and 45 degrees. For erasing a vertically polarised He-Ne laser was focused by an objective (NA, 1.4; 60X) to scan the given layer for 3 mins. Both patterns were completely erased as shown in Fig. 3.6(c). In Fig.

3.6(d) and (e) two new patterns F and E were rewritten in the same area at 0 and 45 degrees of the recording polarisation, respectively. The repeat cycle of our sample we estimated should be at least 1000 times because there was no significant degradation after erasing and rewriting test up to 100 times at a recording power of 10 mW and an exposure time of 25 ms (see Fig. 3.6(f)).

3.5 Chapter conclusions

This chapter has demonstrated the 2P induced polarisation encoding technique for multilayer bit by bit data storage in a DMNPAA chromophore doped polymer. The polarisation sensitivity introduced by 2P excitation in azo-dye-dispersed polymers has been observed and characterised using the polarisation interference setup. The angular dependence of the readout intensity via a relation of $\sin^2(2\theta)$ establishes the possibility of two-state polarisation multiplexing with a polarisation angle of 45 degrees. Two letters have been successfully encoded in the same region in each of the three layers and read out distinctly layer by layer using the polarisation interference method. A storage capacity of 50 Gbits/disc has been achieved so far. Erasing and re-multiplexing of information in a particular layer have also been successfully demonstrated. The understanding of the azo-dye-dispersed polymer materials and the polarisation interference optical system gives rise to a scientific foundation to develop the multi-dimensional optical data storage technique based on QDs/QRs.

Chapter 4

Confocal reflection readout thresholds in two-photon-induced optical recording

4.1 Introduction

It has been demonstrated that two-photon (2P) excitation can induce the refractive-index change in a variety of materials including photochromic, photorefractive and photoisomerisation materials [11, 12, 35, 103, 106, 111, 112], although the strength of the refractive-index change varies in those materials. Confocal reflection scanning microscopy is a powerful tool for the image reconstruction of the three-dimensional (3D) refractive-index variation in a thick sample due to its nature of preventing the out-of-focus signal [3, 113]. The 2P induced refractive-index change in photochromic materials is on the order of 10^{-2} and has been successfully readout using confocal reflection microscopy [29, 114-116]. 2P induced refractive-index change in photorefractive polymers is typically less than 1% and it has been demonstrated that confocal reflection readout exhibits a threshold of

the recording power [16]. In Chapter 3, it has been demonstrated that 2P induced refractive-index change in the azo-dye-dispersed polymers can facilitate the four-dimensional (4D) optical data storage.

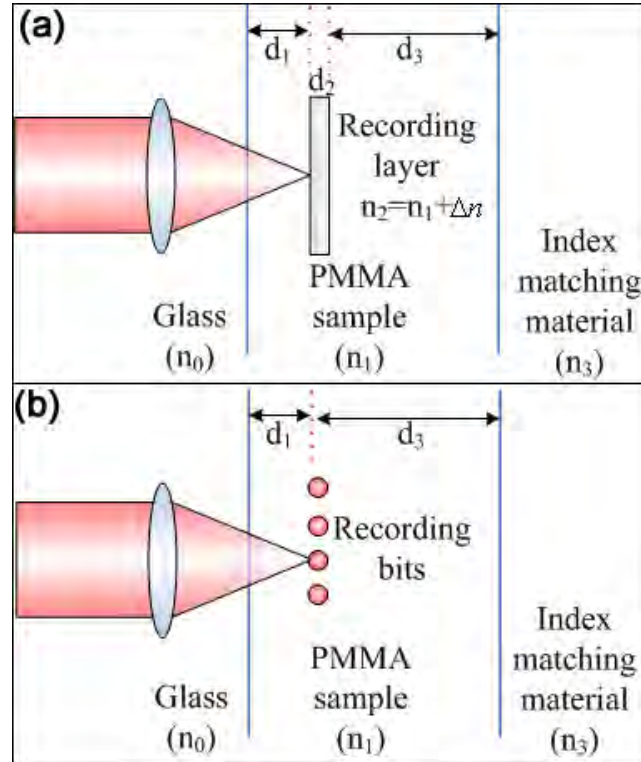


Fig. 4.1: Experimental geometry. (a) Planar reflection model readout. A planar reflection layer with refractive-index change Δn is recorded in an azo-dye-dispersed poly(methyl methacrylate) (PMMA) sample. The reflection is collected by an objective with numerical aperture (NA)=1.4. (b) Bit scattering model readout of recorded bits.

The 2P induced refractive-index change ranges from 0.003-0.01 in the azo-dye-dispersed photoisomerisation polymer [35, 106, 112, 117-119]. It can be expected the confocal reflection readout threshold in this case should highly depend on the recording power as well as the recorded structure shape. In this chapter, the confocal reflection readout thresholds in two cases in the azo-dye-dispersed polymers are studied [120]. One is the planar structures that are much larger than the wavelength of the reading beam (Fig. 4.1 (a)) and the other is the array of bits that

correspond to the focus size of a recording beam (Fig. 4.1 (b)). The axial response of the planar reflection model (Fig. 4.1 (a)) is used to determine the confocal reflection readout threshold both theoretically and experimentally. A scattering model (Fig. 4.1 (b)) is used to characterise confocal reflection readout of the 2P induced refractive-index change.

This chapter is organised as following. Section 4.1 presents the introduction. In Section 4.2 the confocal reflection readout thresholds in the planar reflection model are investigated experimentally and theoretically. The axial response is characterised at different refractive-index mismatch at the back surface of the sample. The threshold in the bit scattering model is studied in Section 4.3. The chapter conclusion is drawn in Section 4.4.

4.2 Confocal reflection readout threshold in a planar reflection model

4.2.1 Experiment

To record planar structures in a thick azo-dye-dispersed photoisomerization polymer, we prepared a poly(methyl methacrylate (PMMA) medium dispersed with 10 wt.% of Disperse Red 1 (DR1), and a thickness of $19 \pm 1 \mu\text{m}$. The refractive-index of the PMMA sample was measured to be 1.498 ± 0.002 using the traditional Becke line method with a serial of refractive-index liquids (Cargille Laboratories). A linearly polarised Ti:sapphire ultrashort pulsed laser beam of pulse width 100 fs and repetition rate 82 MHz (Spectra-Physics Tsunami) at a wavelength of 720 nm was employed as a light source for 2P excitation. A high numerical aperture (NA) objective (NA=1.4) was used to focus the excitation on the sample to induce a layer

of the refractive-index change (Fig. 4.1 (a)).

For confocal reflection readout the 2P induced refractive-index change, the overlap of the passband of the reading objective with the spacial frequency of the recorded bit is required [109]. The experiment was conducted such that the same laser beam and objective were used for imaging. The reflected signal was focused by a lens with a focal length of 200 mm onto a pinhole with a diameter of $30\text{ }\mu\text{m}$ in front of the photomultiplier tube. The axial response from the planar reflector scanned axially is a measure of the capability for axial imaging [121] and gives rise the threshold of the recoding power in confocal reflection readout. To readout the axial image of the recording layers, two immersion media were used. One sample was with air at the back surface ($n_3=1.0$) and the other was with Norland 63 ($n_3=1.52$, Norland Products Inc.) at the back surface.

A planar reflector is recorded $5\text{ }\mu\text{m}$ below the first surface by scanning a square of $10\text{ }\mu\text{m}$ by $10\text{ }\mu\text{m}$ in the sample with a power of 11 mW and an exposure time of $300\text{ms}/\mu\text{m}^2$. The transmission image of the reflecting layer which is recorded $5\text{ }\mu\text{m}$ below the first surface is shown in Fig. 4.2 (a). The axial images of the reflecting layer in the sample with the air back surface are shown in Fig. 4.2 (b). A similar experiment is performed in the sample with the Norland back surface, as shown in Figs. 4.2 (c) and (d). The first reflection peak corresponds to the cover-glass ($n=1.523$, Deckglaser)/PMMA sample interface and the third peak corresponds to the PMMA sample/back surface. We call hereafter the former the first peak, and the latter the main peak. The middle reflection peak comes from the planar reflection of the recorded layer, which locates at $5\text{ }\mu\text{m}$ below the first peak. In a controlled experiment the reflection peak disappeared when no reflecting layer was recorded, which confirmed that the middle reflection intensity peak came from the reflecting

layer. It is seen that the axial image can be detectable in our system as long as the refractive-index change is above the response threshold.

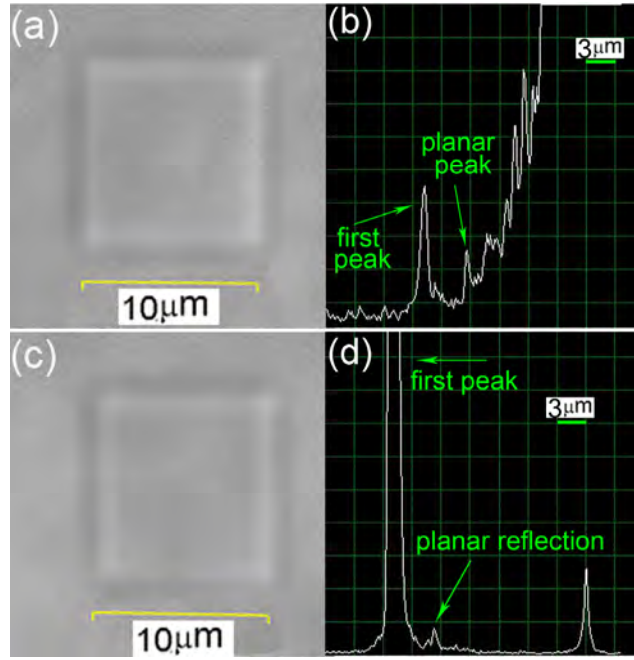


Fig. 4.2: Experimental results of the axial image of the recording layer. (a) and (b) are the transmission and axial images of the recording layer in the sample with air at the back surface. (c) and (d) are transmission and axial images of the recording layer in the sample with Norland at the back surface. The recording power is 11 mW. The scale bar in axial images is $3 \mu\text{m}$.

To demonstrate the threshold effect of the axial response, the recording power is varied to produce planar reflectors with different index changes. The readout intensity of the planar reflection normalised to that from the front surface, which has a refractive-index mismatch of 0.025 and is detectable in the system, is plotted as a function of the recording power in Fig. 4.3. There is a clear threshold effect on the axial response from the planar reflector of a small refractive-index change introduced by the DR1 molecules under 2P irradiance. Below a recording power of 11 mW (intensity of $140 \text{ GW}/\text{cm}^2$), the refractive-index change is too small to introduce any resolvable axial image response. Above that, the reflection from the refractive-index change layer can be resolved, which corresponds to a calculated refractive-index

change of 10^{-2} . In particular, the intensity of the axial response increases dramatically when the deformation of PMMA is observed. This threshold effect is consistent with previous results [16, 111].

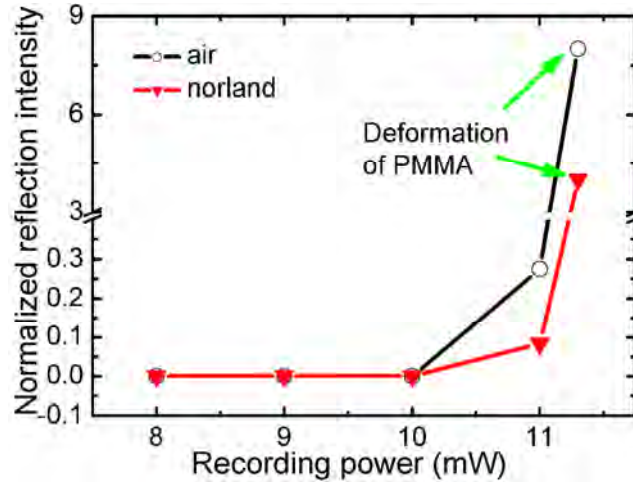


Fig. 4.3: Experimental readout of the confocal reflection intensity normalised to the reflection intensity of the front surface is plotted as a function of the recording power. The black circle and red triangle are the sample with air and Norland at the back surface, respectively.

4.2.2 Theory

To confirm the observation in Figs. 4.2 and 4.3, we consider an aberration-free confocal reflection system, when a planar object is scanned along the axis [3, 121]. The detected reflection intensity as a function of the defocused distance z can be written as [121, 122]

$$I(z) = \left| \int_0^a r(\theta) \exp(2ikn_0 z \cos \theta) \sin \theta \cos \theta d\theta \right|^2, \quad (4.1)$$

where $r(\theta)$ is the reflection coefficient for the planar structure. For linear polarised illumination, the effective reflection coefficient for parallel and perpendicular polarisation is given by [118]

$$r(\theta) = (r_\sigma - r_\pi) / 2. \quad (4.2)$$

According to Born and Wolf [123], the reflection coefficient for the beam through a

three-layer structure is

$$r_{\sigma/\pi} = \frac{r_{01\sigma/\pi} + r_{12\sigma/\pi} \exp(2ikn_x d_x \cos \theta_x)}{1 + r_{01\sigma/\pi} r_{12\sigma/\pi} \exp(2ikn_x d_x \cos \theta_x)} \quad (4.3)$$

where r_{01} and r_{12} are reflection coefficients of the first interface and the second interface, respectively. n_x and d_x are the refractive-index and the thickness of the middle medium. θ_x is the refracted angle of the beam inside the middle medium from the normal to the front surface.

For the experiment configuration as shown in Fig. 4.1 (a), the sample can be treated as a five-layer structure. The reflection coefficients for each interface can be given

$$r_{01\sigma} = \frac{n_0 \cos \theta_0 - n_1 \cos \theta_1}{n_0 \cos \theta_0 + n_1 \cos \theta_1} \quad (4.4)$$

$$r_{01\pi} = \frac{n_1 \cos \theta_0 - n_0 \cos \theta_1}{n_1 \cos \theta_0 + n_0 \cos \theta_1} \quad (4.5)$$

$$r_{12\sigma} = \frac{n_1 \cos \theta_1 - n_2 \cos \theta_2}{n_1 \cos \theta_1 + n_2 \cos \theta_2} \quad (4.6)$$

$$r_{12\pi} = \frac{n_2 \cos \theta_1 - n_1 \cos \theta_2}{n_2 \cos \theta_1 + n_1 \cos \theta_2} \quad (4.7)$$

$$r_{23\sigma} = \frac{n_2 \cos \theta_2 - n_1 \cos \theta_3}{n_2 \cos \theta_2 + n_1 \cos \theta_3} \quad (4.8)$$

$$r_{23\pi} = \frac{n_1 \cos \theta_2 - n_2 \cos \theta_3}{n_1 \cos \theta_2 + n_2 \cos \theta_3} \quad (4.9)$$

$$r_{34\sigma} = \frac{n_1 \cos \theta_3 - n_3 \cos \theta_4}{n_1 \cos \theta_3 + n_3 \cos \theta_4} \quad (4.10)$$

$$r_{34\pi} = \frac{n_3 \cos \theta_3 - n_1 \cos \theta_4}{n_3 \cos \theta_3 + n_1 \cos \theta_4} \quad (4.11)$$

Substituting Eqs. (4.4) - (4.11) into Eq. (4.3), we can derive the total reflection coefficient of the five-layer structure. This rigorous theory incorporates the depletion

of the incident beam as it travels through the structure, aberration caused by focusing through the refractive media as well as multiple reflections [121, 122].

To study the reflection intensity from a planar reflector with a small refractive-index change in front of a large refractive-index mismatched interface, we show in Fig. 4.4 the numerical analysis of the axial response from the five-layer structure by variation of the refractive-index n_3 of the matching materials at the back surface. Figs. 4.4 (a)/(b), (c)/(d), (e)/(f) and (g)/(h) are the reflection from the sample when air, water ($n_3=1.33$), Norland and PMMA samples ($n_3=n_1$) are at the back surface, respectively. The right column is the zoom in view of the left column. For calculation the refractive-index change of the planar reflector is presumed to be 0.005, and recorded $5\ \mu\text{m}$ below the front surface of the sample of a thickness of $0.3\ \mu\text{m}$ and $d_3=13\ \mu\text{m}$.

Three peaks are expected, corresponding to the reflection from the front surface, the planar reflector and the back surface, respectively. There is no reflection from the back surface when the refractive-index is completely matched as shown in Figs. 4.4 (g) and (h). It is clear that the main peak loses its symmetry due to the aberration when there is refractive-index mismatching at the front surface. The sidelobes on the right side of the main peak are dominated by phase aberration which is determined by the refractive-index mismatch at the front surface. As we increase the refractive-index n_3 of the matching materials at the back surface to match the PMMA sample, the strength of sidelobes in the backwards direction, dominated by multiple reflection, are reduced. In the meantime the absolute reflection intensity from the planar reflector is also reduced due to the exclusion of the multiple reflection contribution (see Figs. 4.4 (c)/(d) and (e)/(f)).

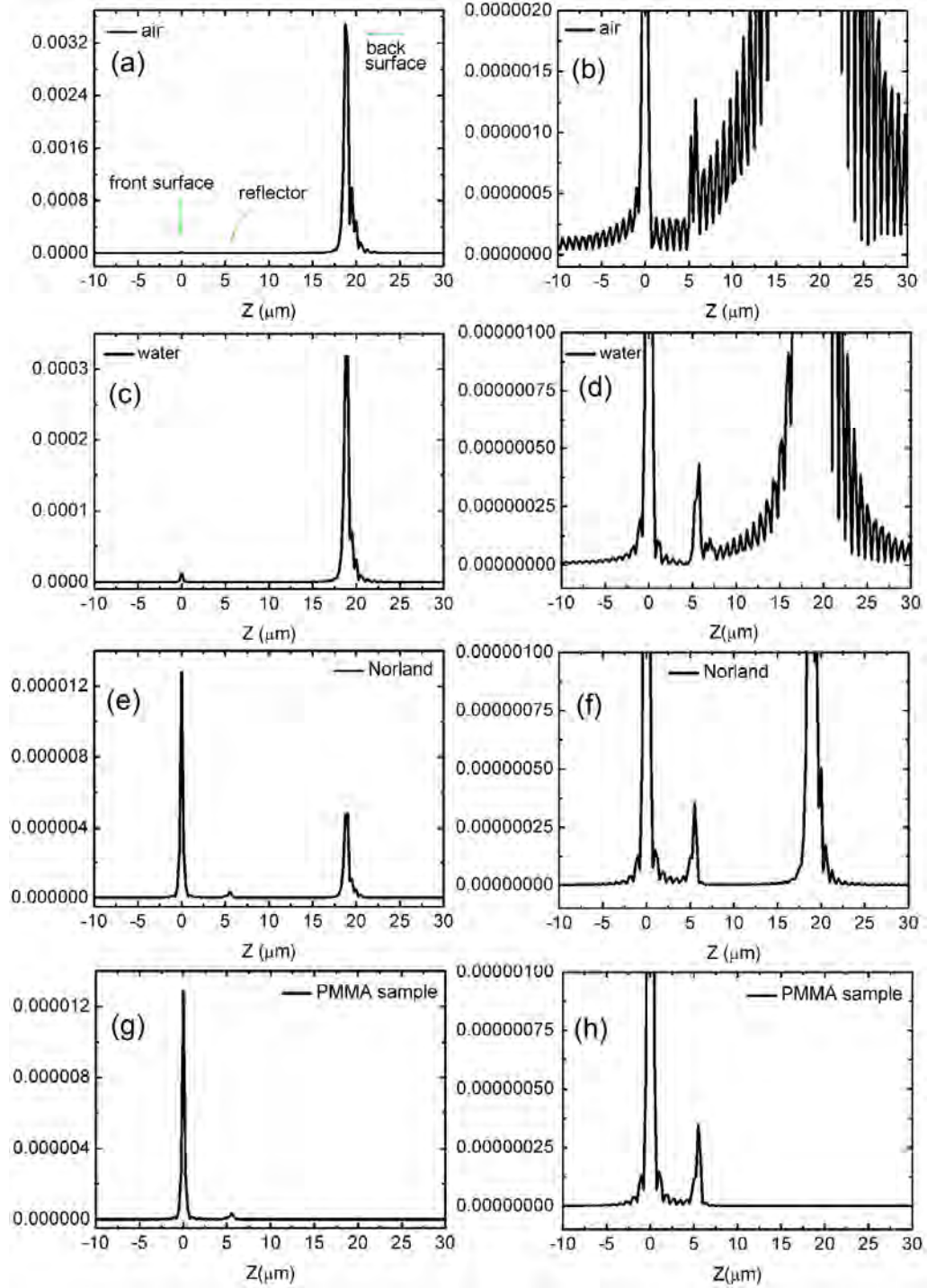


Fig. 4.4: Theoretical calculation of the confocal axial response from the planar reflector with a refractive-index change of 0.005. The reflector is 5 μm below the front surface. (a)/(b), (c)/(d), (e)/(f) and (g)/(h) are samples with air, water, Norland and PMMA sample ($n_3 = n_1$) at the back surface, respectively. The right column is the zoom-in view of the left column.

To study the threshold effect of the axial response from the planar reflector, the theoretical calculation of the planar reflection for the sample with the air back surface and the Norland back surface is plotted as a function of the refractive-index in Fig. 4.5. As the reflection from the front surface is approximately constant in both samples, the planar reflection intensity is normalised to that from the front surface. It is clear that for the sample with the air back surface, the planar reflection is stronger than that with the Norland back surface. Below the refractive-index change of 0.01, the reflection is weak and barely resolvable. Above the refractive-index change of 0.1, corresponding to the deformation of the polymer matrix, the strength of the axial response is increased dramatically. The axial response threshold effect predicted by the theoretical calculation is consistent with the experimental observation that a refractive-index change of 0.01 or above, corresponding to the recording power of 11 mW or higher, is required.

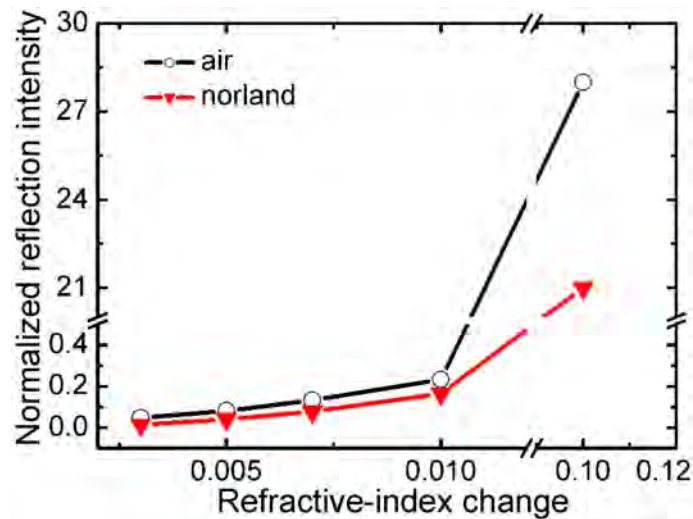


Fig. 4.5: Theoretical calculation of the confocal reflection intensity of the planar reflector normalised to the reflection intensity of the front surface is plotted as a function of the refractive-index variation. The black circle and red triangle are the sample with air and Norland at the back surface, respectively.

4.3 Confocal reflection readout threshold in a bit scattering model

Now let us turn to an alternative structure where an array of bits is recorded in a thick medium (Fig. 4.1(b)). The recording and confocal reading system is the same as that for the planar reflector model. A pattern consisting of 9 by 9 bits with a bit spacing of $1.5\ \mu\text{m}$ was recorded at $14\ \mu\text{m}$ below the front surface. The recording power is 10 mW and the exposure time for each bit is fixed 25 ms, corresponding to $200\text{ms} / \mu\text{m}^2$. We scanned the sample in the axial direction and no confocal reflection signal from the refractive-index change of the recorded bits could be detected near the recording depth position. However, the image of the recorded pattern can be reconstructed at the other positions through the multiple reflections between the strong forward scattering of bits and the back surface.

Figs.4.6 (a) and (b) show the confocal reflection images reconstructed at $10.3\ \mu\text{m}$ and $15\ \mu\text{m}$ below the front surface, respectively. The readout contrast of the bits is plotted as a function of the reading depth below the front surface, as shown in Fig. 4.6 (c). The readout contrast profile has two broad peaks shifting away from the recording position with a central position at $10.3\ \mu\text{m}$ and $15\ \mu\text{m}$, respectively. A possible explanation for the origin of two peaks is the interference between the forward scattering and the multiple reflections which forms the interference fringes [124]. From Eq. (4.1) the phase of the reflected signal is dependent on the angle of the ray which leads to the shift of the reflection peaks approximately $0.5\ \mu\text{m}$, shown in Figs. 4.4 (a) to (f). Similarly the angular dependence of the phase of the reflected forward scattering causes the shift of the peak away from the recording position.

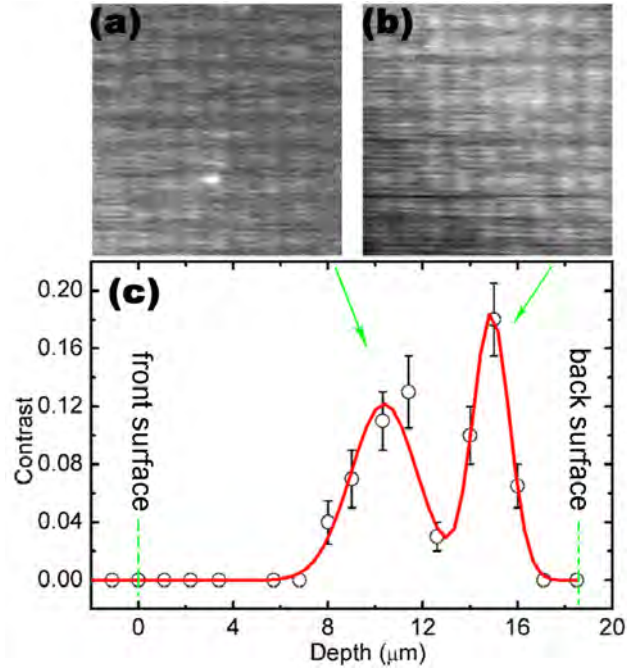


Fig. 4.6: Scattering-induced reflection image reconstruction. (a) and (b) are the scattering-induced reflection images of recorded bits readout at $10.3 \mu\text{m}$ and $15 \mu\text{m}$ below the front surface, respectively. The recording power is 10 mW and the exposure time is $200\text{ms} / \mu\text{m}^2$. (c) The readout contrast of the recorded bits is plotted as a function of the reading position.

To characterise the reconstructed image induced by bit scattering, the pattern was recorded at different depths and readout slice by slice. The readout contrast is plotted as a function of distance d_3 (see Fig. 4.1 (b)) between the recorded position and the back surface, as shown in Fig. 4.7 (a). As d_3 gradually reduces, the confocal reflection readout contrast increases dramatically. This enhancement is most probability due to the increased strength of multiple reflection between the forward scattering of bits and the back surface. This observation is confirmed by tuning the strength of multiple reflections by varying the refractive-index mismatch using different matching medium at the back surface. The image of the recorded pattern cannot be readout in the sample with Norland or water at the back surface no matter of the recording position. Here the refractive-index mismatch at the back surface is 0.168 and 0.022 respectively. As shown in Figs. 4.4 (c) to (f) multiple reflections

become weak, therefore reducing the interference of scattering beam with multiple reflections. Since multiple reflections from the back surface are enhanced as the refractive-index of the mismatching medium increases, a liquid medium with a refractive-index of $n=1.78$ (Cargille Laboratories) was placed at the back surface, where the refractive-index mismatch is 0.282. The image of recorded bits can be reconstructed and the plot of reflection contrast of the recorded bits as a function of d_3 is shown in Figs. 4.7 (a). And Fig. 4.7 (b) represents the reflection image contrast as a function of the refractive-index of the mismatching media at the back interface. It is clear that the scattering induced reflection image contrast is enhanced as the refractive-index mismatching at the back surface increases.

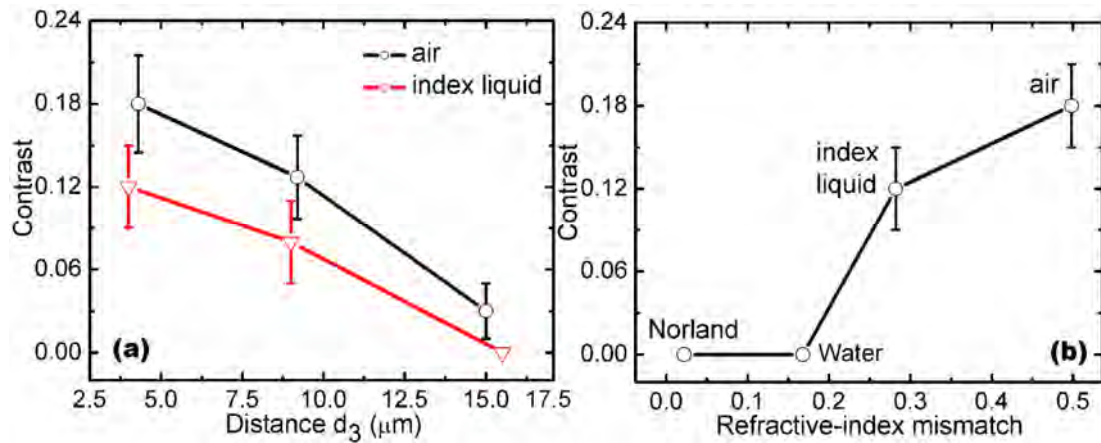


Fig. 4.7: (a) The reflection image contrast is plotted as a function of the distance between recording position and the back surface. The black circle and red triangle are the samples with air and liquid at the back surface, respectively. (b) The reflection image contrast as a function of the refractive-index mismatch at the back surface.

Fig. 4.8 shows the confocal reflection readout contrast as a function of the recording power in the sample with air at the back surface. The recorded position was fixed at $14\ \mu\text{m}$ below the front surface and exposure time was fixed at 25 ms for each bit. Generally, the recorded bits can be readout when the recording power is above 8 mW ($101\ \text{GW}/\text{cm}^2$), corresponding to calculated refractive-index change of

0.006. As we gradually increase the recording beam intensity, the readout contrast is enhanced. The readout contrast increases dramatically as the recording power is above 13 mW when the deformation of PMMA occurs.

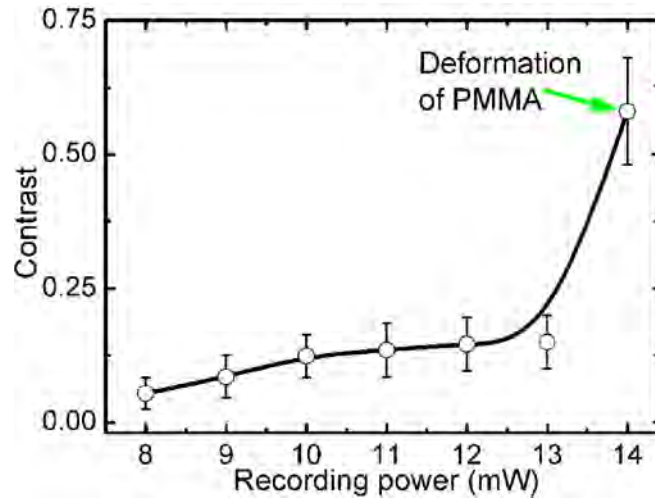


Fig. 4.8: The scattering-induced readout contrast of the recorded bits is plotted as a function of the recording power in the sample with air at the back surface.

4.4 Chapter conclusions

In this chapter, 2P induced refractive-index change in the azo-dye-dispersed PMMA sample has been investigated both theoretically and experimentally using confocal reflection microscopy, which facilitates the 4D optical data storage. Confocal reflection readout thresholds of the refractive-index change have been identified in two cases. The axial response threshold of the refractive-index change on the order of 10^{-2} is revealed from a planar reflection model. In a bit scattering model, the strong forward scattering caused by the bits leads to multiple reflection between the bit and the back surface, which enhances the image contrast and reduces the readout threshold. The understanding of 2P induced refractive-index change in azo-dye-dispersed polymers builds up the bench mark for 4D optical data storage in nanoparticle-dispersed photosomerisation polymers.

Chapter 5

Four-dimensional optical data storage in quantum-dot/rod-dispersed photoisomerisation polymers

5.1 Introduction

Nanocrystal quantum dots/rods (QDs/QRs) have been identified as an important potential key to future photonic devices [24] because of their tunable spectral response [21, 23] and large two-photon (2P) absorption cross-section [22]. In particular, QRs have polarisation dependent optical properties [24, 25, 125]. 2P excitation in a conventional solid photosensitive medium has driven all-optical devices towards three-dimensional (3D) platform architectures such as 3D photonic crystals [126-128], 3D optical circuits [129] and 3D optical memory [5, 8, 9]. The development of a QR-sensitised medium should allow for a polarisation-dependent change in refractive-index. Such a localised polarisation control inside the focus can confine the light not only in 3D but also in an additional polarisation domain.

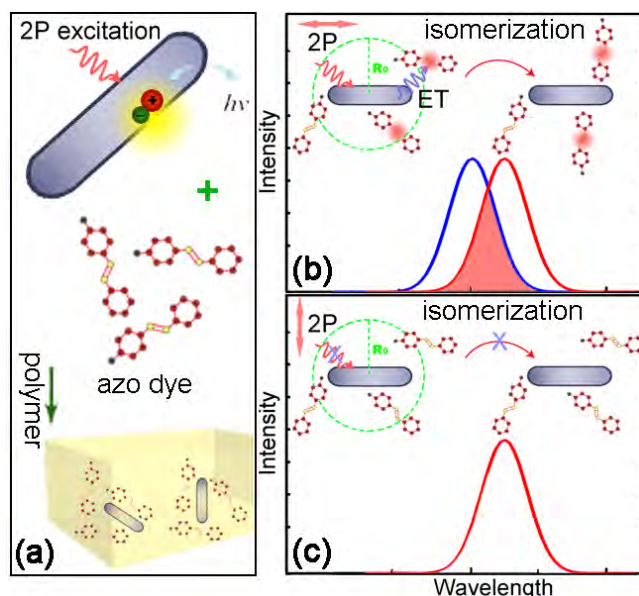


Fig. 5.1: Principle of polarisation modulated fluorescence energy transfer. (a) Random distribution of fluorescent QRs and azo dyes in the polymer matrix. (b) When a laser beam is parallelly polarised to the orientation of QRs efficient 2P excitation induced energy transfer occurs, which drives the re-orientation of azo dyes towards the perpendicular direction to the laser polarisation. (c) 2P excitation is shut off when the laser beam is perpendicularly polarised, therefore the resultant energy transfer cannot occur.

The principle of polarisation refractive-index modulation proposed in this thesis is based on energy transfer from QRs to azo dye molecules, as illustrated in Figs. 5.1 (a) to (c). Dyes and QRs are randomly dispersed in the polymer matrix as shown in Fig. 5.1 (a). Fluorescence energy transfer can occur when dyes in the proximity of the Förster distance have their absorption band (red curves) overlapped with the emission band of QRs (blue curves). QRs can pump weakly absorbing azo dye molecules when the illumination has a polarisation direction parallel to the orientation of QRs (Fig. 5.1 (b)). Consequently, the energy-transfer-driven isomerisation of the azo dyes can re-orientate their optical axis towards the perpendicular direction of the polarisation direction of the writing beam, resulting in an anisotropic change in refractive-index [106, 130]. When the illumination beam is perpendicularly polarised, QRs cannot be excited efficiently. Thus, neither can the

energy-transfer-driven isomerisation (Fig. 5.1 (c)). Provided that the difference of the 2P excitation efficiency of rods between parallelly and perpendicularly polarised irradiation is large, the selective excitation between the different polarisation angles enables the polarisation modulation of the refractive-index change.

The study in this chapter is to explore the 2P induced polarisation-encoded multilayer optical data storage in QDs/QRs sensitised photoisomerisation polymers [131-133]. The chapter is organised into five sections beginning with this introduction. Characterisation of spherical QD-sensitised photoisomerisation polymers and their application in 3D optical data storage are discussed in Section 2, which provides the fundamental understanding of energy transfer between nanocrystals and azo dyes in a polymer matrix. In order to achieve four-dimensional (4D) optical data storage, it is necessary to adopt QRs rather than QDs. Optical properties of QRs including 2P absorption cross-sections and polarisation selective excitation are characterised in Section 3. QR-driven isomerisation of azo dyes via fluorescence energy transfer processes is discussed in Section 4. The application QR- and azo-dye-dispersed polymers in 4D optical data storage as well as other polarisation controlled photonic applications are demonstrated. The chapter conclusions are drawn in Section 5.

5.2 Three-dimensional optical data storage

5.2.1 Materials preparation

This section is to explore the novel concept of using QDs as 2P sensitisers to enhance the 2P recording efficiency of azo dyes via 2P fluorescence energy transfer processes, which is the foundation for 4D optical data storage in the QR-dispersed medium. To this end, azo dye Disperse Red 1 (DR1) (Sigma Aldrich) was chosen as energy

transfer acceptors. CdS QDs of three different sizes and emission bands were prepared [134] following the controlled synthesis condition at different injection temperature. The ‘as-prepared’ QDs were labeled by their first absorption peak as CdS 366, CdS 433 and CdS 441, respectively. To prepare CdS 366 QDs, CdO (0.2 mmol), oleic acid (OA) (1 mmol), and octadecene (ODE) (9 mL) were mixed in a three-necked flask and degassed at 80 °C for 30 min. The solution was heated to 310 °C for 10 min under a nitrogen environment and vigorous stirring. The sulfur precursor of S (0.1 mmol) in 5 ml ODE was swiftly injected into the reaction pot. The growth process was left to develop for 30 s before it was quickly quenched to room temperature in chloroform. CdS 433 QDs were prepared with CdO (0.48 mmol), OA (9.6 mmol), and ODE (9 ml) before reaction. The solution was heated to 270 °C rather than 310 °C. S (0.4 mmol) in 4 ml ODE was swiftly injected into the reaction pot. The temperature was set at 200 °C for subsequent growth process. 20 min later particles stopped to grow at a size of the first extinction peak at wavelength 433 nm. CdS 441 was prepared following the same operation and injection temperature except OA was increased to 12 mmol.

Fig. 5.2 (a) shows the absorption spectra of the ‘as-prepared’ QDs in chloroform solution. Their relative fluorescence intensity spectra as well as the absorption spectra of DR1 molecules are shown in Fig. 5.2 (b). Their fluorescence quantum yields were measured using 9,10-Diphenylanthracene as standard with known $\Phi_f = 0.95$ shown in Fig. 5.2 (c). As a prediction of their energy transfer performance, Fig. 5.2 (c) lists the theoretic calculation of the Förster distance R_0 using the Förster formula [46]. With the largest Förster distance, the best fluorescence energy transfer performance is expected in CdS 433 doped polymers, where the Förster distance is almost 4 nm. The bandgap emission of CdS 366 is completely quenched by the broad emission tail from the defect states and the fluorescence quantum yield is extremely

low compared to the CdS QDs of other sizes illustrated in Fig. 5.2 (b). Therefore the lowest energy transfer efficiency is expected in CdS 366 doped polymers.

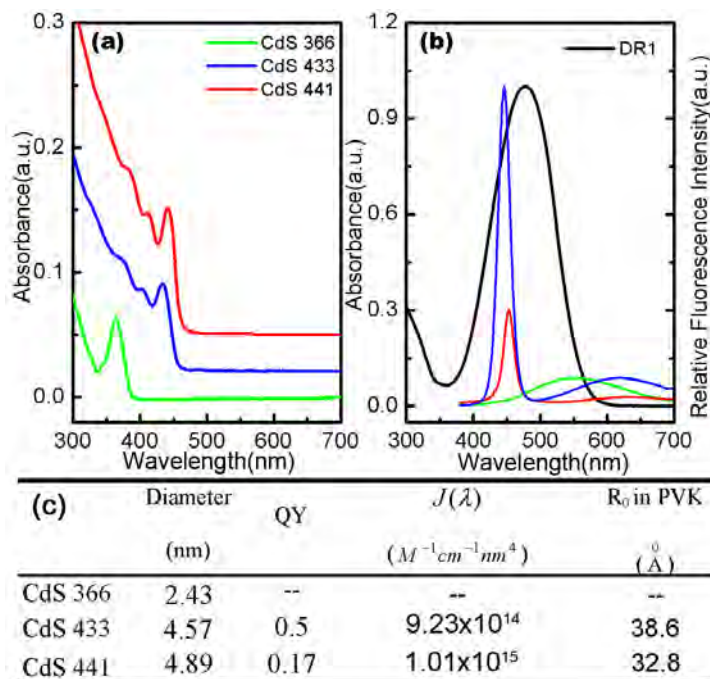


Fig. 5.2: (a) Absorbance of prepared CdS QDs. (b) Relative fluorescence intensity of CdS 366 (green), CdS 441 (red) and CdS 433 (blue), respectively as well the overlapping with the absorption spectrum of DR1 (black). (c) Calculated Förster distance using the standard Förster formula.

The polymer composites were blended using the formulation consisting of poly (N-vinyl carbazole) (PVK), 9-ethylcarbazole (ECZ), DR1 and QDs at a concentration ratio of 54mg:16mg:10mg:0.15nmol. The average distance between adjacent QDs is approximately 120 nm and between adjacent DR1 molecules is 2 nm assuming that the polymer mixture has a density close to 1g/ml.

5.2.2 Characterisation of energy transfer performance

To characterise the 2P induced energy transfer performance in the polymer matrix, the evolution kinetics of the absorbance change of DR1 was monitored by the pump

probe experiment. A Ti:sapphire ultrashort pulsed laser beam of pulse width 100 fs (Spectra-Physics Tsunami) was focused by an objective of numerical aperture (NA) 0.4 onto the films. Excitation wavelength at 720 nm which corresponds to the valley of linear absorption band of DR1 was specifically chosen to minimise the direct 2P excitation of the acceptors. A bandpass filter (53900, Newport) with a central wavelength at 560 nm and a full width at half maximum (FWHM) of 10 nm placed in front of a linearly polarised white light source was employed as a probe beam. The probe beam was attenuated to 0.2 nW before the back aperture of the objective to avoid sample depletion. The transmitted probe beam intensity was collected by a CCD (PIXIS 100, ACTON) for photon counting. Multi-spincoated thin films of 5 μm in thickness were prepared. All the samples were placed on a defocused plane with a pump diameter spot of 4 μm .

Fig. 5.3 shows the typical time evolution of the normalised absorbance change of DR1 molecules upon linearly polarised 2P excitation induced isomerisation at the intensity $10\text{ GW}/\text{cm}^2$. The *trans*-state isomers having their optical axis parallel to the polarisation of the excitation are preferentially excited and re-oriented therefore an angular hole is burning in the absorption spectra of *trans*-state isomers. The decrease of absorption in both parallel and perpendicular directions is caused by the depletion of *trans*-DR1 molecules during the isomerisation process involving both re-orientation and permanent photobleaching [41]. There was no noticeable recovery in the room condition after turning off irradiation beams. As shown in Figs. 5.3 (a) and (b), there is no isomerisation enhancement of DR1 molecules at the attendance of CdS 366 as the absorbance decreases approximately the same level as that in the controlled sample dispersed DR1 itself only in each polarisation direction. However, in the presence of CdS433 and CdS441 the absorbance of DR1 molecules in the parallel and perpendicular directions both decreases more than that in a sample

without QDs doping. A remarkable enhancement of the global absorbance decrease approximately 10% and 20%, respectively, in the CdS 441 and CdS 433 dispersed samples is observed. The physical explanation is that under 2P excitation the influx photon energy is efficiently absorbed by CdS QDs serving as energy donors and DR1 molecules in the proximity of the Förster distance serving as acceptors are excited from energy transfer, which therefore facilitates the depletion of *trans*-DR1 molecules.

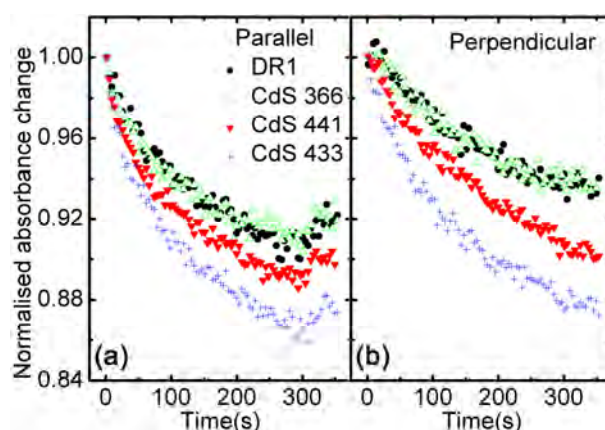


Fig. 5.3: Time evolution of normalised absorbance change of DR1 molecules when the polarisation direction of the probe beam is parallel (a) and perpendicular (b) to the pump irradiation polarisation direction, respectively. The black dots, green triangles, red filled triangles and blue crosses correspond to samples without QDs, with CdS 366, CdS 441 and CdS 433 respectively.

As a consequence of energy-transfer-driven isomerisation, a change in refractive-index was substantiated by the differential interference contrast (DIC) microscope (Olympus BX50) readout. Sandwiched samples of $20\text{ }\mu\text{m}$ in thickness were prepared for optical recording. An objective of NA 0.7 was employed to focus the infrared irradiation beam onto the sample. In the focus volume of the objective, there were over 400 QDs. The femtosecond laser was operated in a continuous-wave (CW) mode for readout. Fig. 5.4 (a) shows the DIC readout images of the bits recorded under 2P excitation, where each image comprises a pattern of 3×3 bits. To

prevent any interference between adjacent bits, the bit spacing was kept at $10\ \mu\text{m}$. The exposure time was fixed at 25 ms for each bit. Fig. 5.4 (b) shows the readout contrast as a function of the recording power. Without any QDs doping, the recording was attributed to the weak direct 2P excitation of DR1 and the refractive-index change is approximately 0.005 [117]. In the presence of QDs there is a pronounced increase in the readout contrast indicating a larger refractive-index change owing to the contribution of fluorescence energy transfer. In particular, the optimised energy transfer process in the CdS 433 doped sample leads to a contrast enhancement of approximately 30%, corresponding to an estimated refractive-index change of 0.007. This result is consistent with the theoretical calculation in Fig. 5.2 (c).

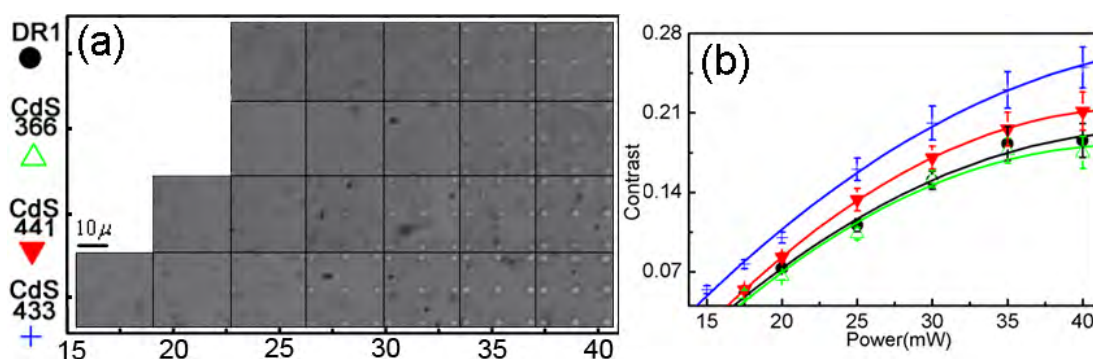


Fig. 5.4: DIC readout. (a) DIC images of recorded bits. (b) Readout contrast as a function of the recording power. The black dots, green empty triangles, red filled triangles, and blue cross correspond to samples without QDs, with CdS 366, CdS 441 and CdS 433, respectively. The scale bar is $10\ \mu\text{m}$.

5.2.3 Three-dimensional optical data storage

In order to demonstrate its feasibility in 3D optical recording, PS was used to replace the PVK:ECZ system as polymer matrix of higher rigidity is required for more stable recording. As a result, DR1 was modified into 2-{ethyl-[4-(4-nitro-phenylazo)-phenyl]-amino}-ethyl ester (DR1-EH) to make it more soluble and less crystalline in the PS matrix. The dye DR1 (2.00 g, 6.37

mmoles) and triethylamine (1.42 mL, 1.03 g, 10.2 mmoles) were dissolved in dichloromethane (40-50 ml) under argon at room temperature. Then 2-ethylhexanoyl chloride (1.42 mL, 1.34 g 8.28 mmoles) in dichloromethane (5ml) was added dropwise. The reaction was stirred overnight and reaction monitored by a thin layer chromatography (silica ether:hexane 3:1, product has a very high *rf* and starting material has a very low *rf* under these solvent conditions). The reaction was worked up by washing with water, sodium bicarbonate solution, and brine before drying with magnesium sulfate and evaporation to a red mass. This was purified by chromatography (silca gel with ether:hexane 3:1 volume ratio) to give 1.5g (53%) of dark red solid.

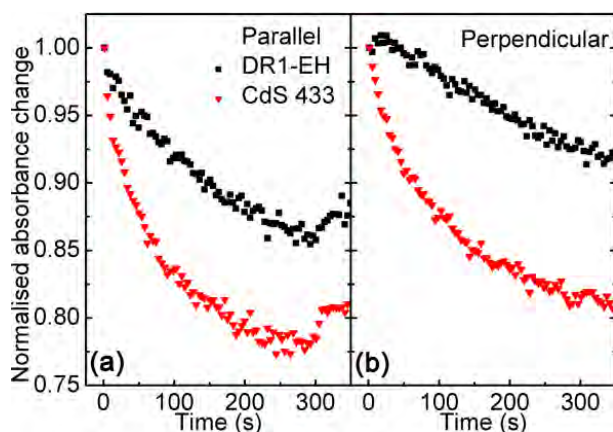


Fig. 5.5: Time evolution of normalised absorbance change of DR1-EH molecules when the polarisation direction of the probe beam is parallel (a) and perpendicular (b) to the pump irradiation polarisation direction. Black squares and red triangles are data from sample without QDs and sample sensitised by CdS 433 respectively. The film thickness is $5\ \mu\text{m}$ and the pump intensity is $15\ \text{GW}/\text{cm}^2$.

A similar fluorescence energy transfer driven isomerisation was observed in a CdS 433 and DR1-EH doped PS sample, with a concentration ratio of PS:DR1-EH:CdS433 at 70mg:10mg:0.15nmol, as shown in Figs. 5.5 (a) and (b). Pronounced absorbance change was observed in each polarisation direction when

CdS 433 QDs acted as 2P energy transfer donors. The recording performance as a function of recording powers is shown in Figs. 5.6 (a) and (b). In Figs. 5.6 (c) to (e) we demonstrated the ability to record information in multiple layers in the CdS 433 and DR1-EH doped PS sample and read out distinctly. Each layer contains a letter consisting of a pattern of 24×24 bits with a bit spacing of $2.6 \mu\text{m}$. Letters I, E and C were recorded in the first, second and third layers respectively, with a layer spacing of $30 \mu\text{m}$.

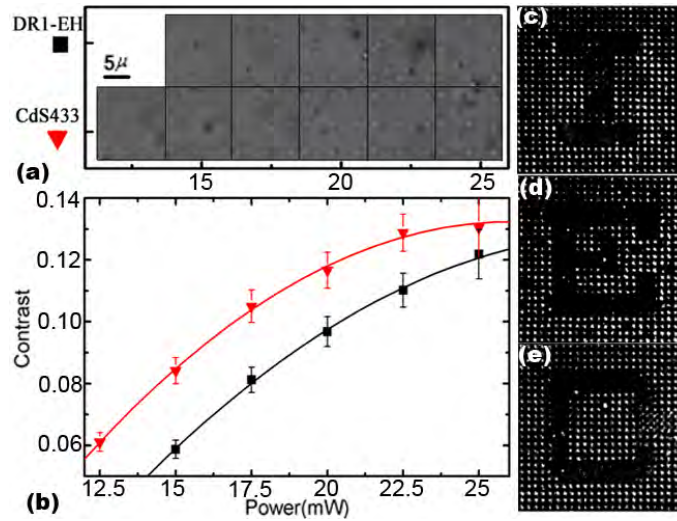


Fig. 5.6: Demonstration of 3D optical memory. (a) DIC image of recorded bits of DR1-EH without QDs and with CdS 433 doping in PS. Scale bar is $5 \mu\text{m}$. (b) Readout contrast as a function of the recording power. (c) to (e) demonstrate letters I, E and C recorded in the first, second and third layers, respectively.

5.2.4 Anisotropy evolution

As discussed in Section 2.3 the unique property of azo groups is that under linearly polarised illumination their optical axis can be re-oriented to the perpendicular direction of the polarisation of a writing beam through multiple isomerisation process. Therefore an anisotropic refractive-index variation can be introduced [18, 39]. It has been demonstrated in Section 5.2.3 using CdS QDs as 2P energy transfer donors can

greatly enhance the recording efficiency of azo dyes with small 2P absorption cross-sections. However, the spherical QDs absorbing excitation from all polarised angles have no angular selective excitation property. Azo dye acceptors close to QDs in the proximity of the Förster distance will be excited by fluorescence energy transfer from QDs donors, where no polarisation can be preserved during the energy transfer process.

This prediction was confirmed by the anisotropy evolution experiment which is similar experimental setup described in Section 5.2.2. The anisotropy is defined as [41]

$$A = (A_{//} - A_{\perp}) / A_0, \quad (5.1)$$

where $A_{//}$ is the absorbance of the film parallel to the polarisation of the pump beam, A_{\perp} is the absorbance of the film in the perpendicular direction, and A_0 is the absorbance prior to the irradiation. The optical axis of DR1 can be re-oriented to the perpendicular direction of the polarisation direction of the 2P excitation to introduce anisotropy, as shown in Fig. 5.7 (a), although direct 2P excitation is weak. Whereas the excitation by fluorescence energy transfer from QDs to DR1 breaks the selective excitation law of azo molecules, a progressive degradation of anisotropy has been observed as the energy transfer efficiency increases using QDs of different sizes, as shown in Figs. 5.7 (b) to (d). In particular, the CdS 433 sensitised sample showing the best recording performance in terms of refractive-index change has the worst performance in preserving the polarisation sensitivity.

The success of incorporating QDs as 2P into azo-dye-dispersed polymers via a 2P energy transfer process has opened the horizon for multi-dimensional optical data storage. To further enhance the impact and break the limitation of the polarisation sensitivity, nanoparticles such as QRs which have large 2P absorption cross-sections and sharp polarisation selective excitation properties are necessary.

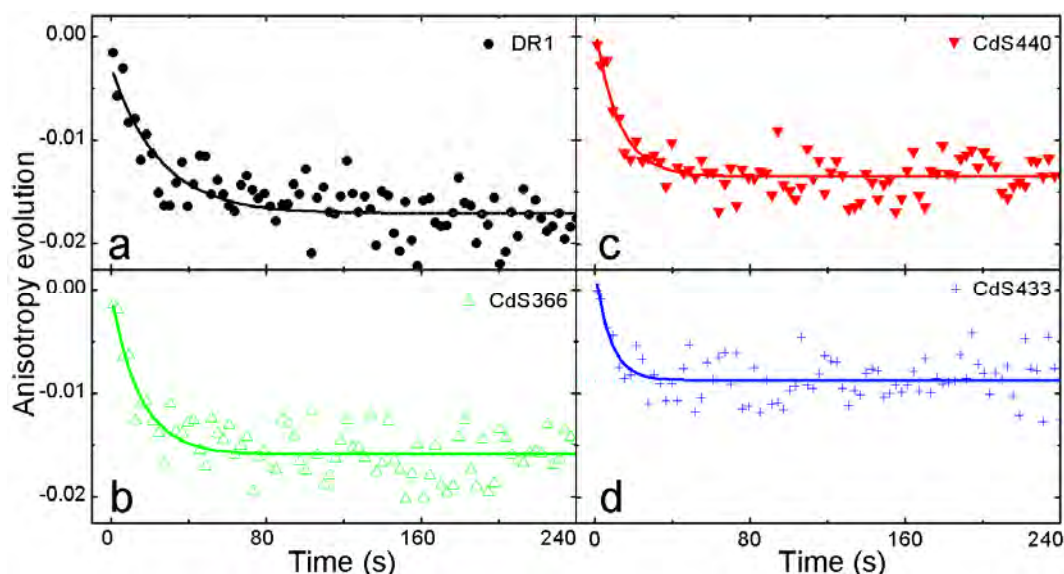


Fig. 5.7: Time evolution of anisotropy of film loaded with DR1 molecules (a), CdS 366 QDs (b), CdS 441 (c) and CdS 433 (d) respectively. Solid lines are guides for eyes.

5.3 Two-photon characterisation of quantum rods

5.3.1 Two-photon absorption cross-sections

It has been known that the extinction coefficients of nanocrystals are primarily dependent on their volume [135]. Recent work demonstrated that elongating CdSe nanocrystals into a rod-shape can pronouncedly increase their linear absorption cross-sections due to expanded volumes [136]. Here, the shape control of CdS nanocrystals is explored in this section as a means to enhance the nonlinear absorption cross-sections [133]. Furthermore, wavefunction confinement by a rod-shape particle enables additional polarisation selective absorption and linearly polarised emission properties [24], where spherical QD does not have. Those unique optical properties of QRs are desirable for 4D optical data storage.

To this end, we first measure the dependence of the 2P absorption cross-section of CdS QDs on the size. CdS QDs of different diameters were synthesized by

injecting the sulfur (S) precursor at different temperatures [134]. The absorption spectra of three different size QDs are labelled as CdS 430, CdS 437 and CdS 451, respectively, corresponding to the diameters of 4.45, 4.7 and 5.32 nm, respectively, determined from the first absorption peak [137]. The 2P absorption was measured using open aperture z-scan methods [138] employing a Spitfire amplified pulsed laser at the wavelength of 800 nm (a pulse width of 100 fs and a repetition rate of 1 kHz). The laser beam was focused by a lens of focal length 250 mm, which gives a focal spot radius of $25\ \mu\text{m}$ provided that the diameter of the collimated beam is 7.5 mm [3]. The QDs were well washed and re-dispersed in chloroform solution in a 1 mm quartz cuvette.

Fig. 5.8 (a) shows the open aperture z-scan response of CdS QDs of three different sizes at the incident intensity of $127\ \text{GW}/\text{cm}^2$. The normalised transmittance of open aperture z-scan is given by [139]

$$T(z) = \frac{1}{\sqrt{\pi}q_0} \int_{-\infty}^{\infty} \ln[1 + q_0 \exp(-x^2)] dx, \quad (5.2)$$

where $q_0 = \beta_2 I_0 L_{\text{eff}}$, $L_{\text{eff}} = [1 - \exp(-al)]/a$, a is the linear absorption coefficient, l is the sample path length, β_2 is the 2P absorption coefficient and I_0 is the incident intensity within the focus. By fitting the open aperture transmittance using Eq. (5.2) the 2P absorption coefficient can be obtained. From β_2 2P absorption cross-section can be deduced as [139]

$$\sigma_2 = \beta_2 h\nu / N_0, \quad (5.3)$$

where $h\nu$ is the photon energy and N_0 is the particle concentration in the solution. At excitation wavelength of 800 nm all QDs have no linear absorption. Given a density of $N_0 = 1.2 \times 10^{16}\ \text{cm}^{-3}$ the 2P absorption cross-sections are determined 0.44×10^{-46} , 0.53×10^{-46} and $0.84 \times 10^{-46}\ \text{cm}^4 \cdot \text{s} \cdot \text{photon}^{-1}$ for CdS QDs with diameter of 4.45, 4.7 and 5.3 nm respectively. This result is comparable with previous reported

value $7 \times 10^{-47} \text{ cm}^4 \cdot \text{s} \cdot \text{photon}^{-1}$ at the excitation of 800 nm of CdS QDs of similar diameters [140].

Fig. 5.8 (b) shows the log-log plot of the measured 2P absorption cross-sections of CdS QDs versus their diameters. The linear fitting yields a power-law dependence of 3.6 on the diameters in the range of 4.4-5.4 nm. Similarly, 2P absorption cross-sections of CdSe QDs showing a power-law dependence of 3.5 ± 0.5 on their diameters in the range 2.4 to 4.8 nm was reported before [141]. Within experimental error and different states involved in the 2P transition [141] these results imply the correlation of 2P absorption cross-sections of CdS QDs with their volumes which are proportional to the cubical diameters. In other words, expanding the volume of CdS nanocrystals may lead to the pronounced increase in 2P absorption coefficient.

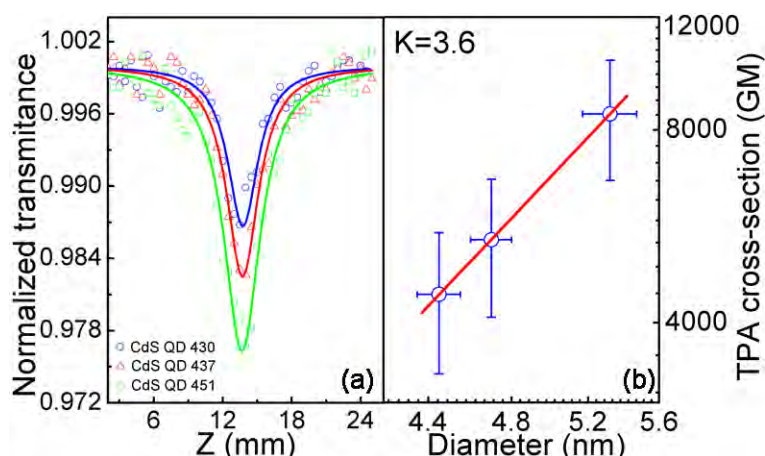


Fig. 5.8: (a) Open aperture z-scan response of CdS QDs of three different sizes. Blue circles, red triangles and green squares are data of CdS 430, CdS 437 and CdS 451 respectively. The solid lines are fitting with Eq. (5.2). (b) Log-log plot of two-photon absorption (TPA) cross-sections of CdS QDs versus their diameters ($1\text{GM} = 10^{-50} \text{ cm}^4 \cdot \text{s} \cdot \text{photon}^{-1}$). Red line is the linear fitting yields a power-law proportionality of 3.6.

CdS QRs were synthesised by slight modification of the developed recipe [142]. The S precursor was prepared separately by dissolving S powders into 1-octadecene

(ODE) at concentration of 0.1 mM and heated to 120 °C. 0.065 g CdO (0.89 mmol), 0.4 g n-tetradecylphosphonic acid (TDPA) (0.155 mmol) and 7 g of trioctylphosphine oxide (TOPO) were degassed at 80 °C for two hours. The mixture was then heated to 340 °C under nitrogen pressure to form the Cd precursors. Then the mixture was cooled to desired injection temperature of 300 °C. Rods were synthesised by dropwising the S precursor in a speed of 0.5 ml volumes every 2 minutes. CdS QRs of uniform size were obtained after 45 minutes. Fig. 5.9 (a) shows the absorption spectra as well as the fluorescence spectra of as-prepared CdS QRs in chloroform. The narrow emission peak with a full width at half maximum (FWHM) of 20 nm is consistent with a narrow particle size distribution. A high resolution TEM image of the as-prepared QRs is shown in the Fig. 5.9 (b). The statistics in Fig. 5.9 (c) show that as-prepared QRs have a uniform size distribution with an average width of 4.4 ± 0.4 nm and a length of 43 ± 3.5 nm (aspect ratio ~ 10). The volume of a single QR is calculated to be approximately 15 times that of a QD of diameter 4.45 nm, assuming that the QR and the QD have cylindrical and spherical shapes, respectively.

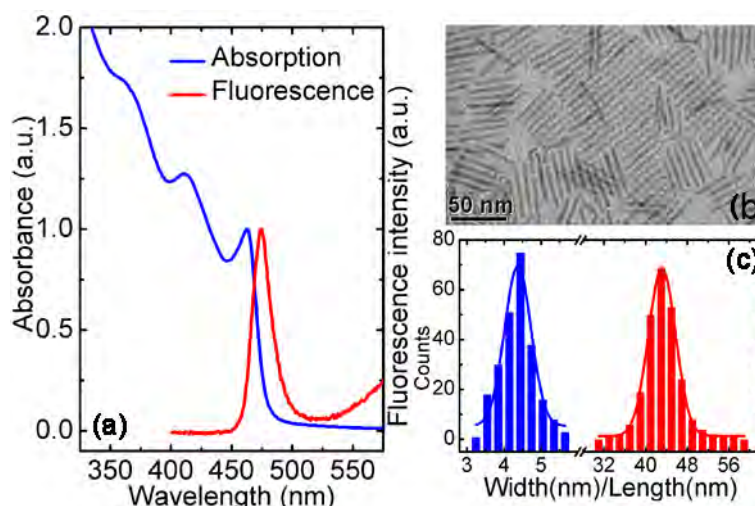


Fig. 5.9: (a) Absorption (blue) and fluorescence (red) spectra of as-prepared CdS QRs. (b) TEM images of well washed QRs. (c) Counts of statistics of width (blue) and length (red) of CdS QRs.

Well washed QRs were re-dispersed in solution for 2P measurement. The concentration of CdS QRs was determined by weighting the mass of the precipitation after centrifugating the well washed sample, giving the molar mass of as-prepared QRs calculated using the dimensions measured in high resolution TEM images. Fig. 5.10 shows the open aperture z-scan response of CdS QRs in chloroform solution at the irradiance of 127 GW/cm^2 . It has been found that under 2P excitation the absorption of QRs is strongly polarisation dependent via $\cos^4(\theta)$, where θ is the angle between the laser polarisation and the 2P transition dipole of the QR [125]. This feature implies that for a specific linearly polarised excitation source, QRs can absorb the incident energy only when their orientation has a component parallel to the laser polarisation. Thus, Eq. (5.3) is not valid in this case as it assumes that all particles within the focus absorb the excitation. It is safe to assume a homogenous orientation distribution of QRs dispersed in solution. Thus, the 2P absorption cross-section of QRs can be corrected by an orientation factor given as [112]

$$\sigma_2 = 5\beta_2 hv / N_0 . \quad (5.4)$$

By fitting the normalised transmittance in Fig. 5.10 using Eqs. (5.2) and (5.4), the 2P absorption cross-section of CdS QRs is obtained $20.9 \cdot 10^{-46} \text{ cm}^4 \cdot \text{s} \cdot \text{photon}^{-1}$ at wavelength 800 nm. The 2P absorption cross-section of QR is one order of magnitude larger compared to that of QDs.

To investigate the 2P absorption cross-section dependence on the excitation wavelength, 2P induced fluorescence [143-145] measurement was performed. A Titanium:sapphire ultrashort pulsed laser of a pulse width of 100 fs and a repetition rate of 80 MHz, operating in the wavelength range of 700-1000 nm was employed as a 2P excitation source. The laser beam was focused by a high NA objective (NA=0.95) and the fluorescence was collected by the same objective and projected onto a CCD for fluorescence photon counting. Using the 2P induced fluorescence

data the 2P absorption cross-sections can be expressed as [143-145]

$$F \sim \eta \phi \sigma_2 N I^2, \quad (5.5)$$

where F is the fluorescence counts, η is the fluorescence quantum yield, ϕ is the system collection efficiency, N is the number of particles inside the focus and I is the incident intensity.

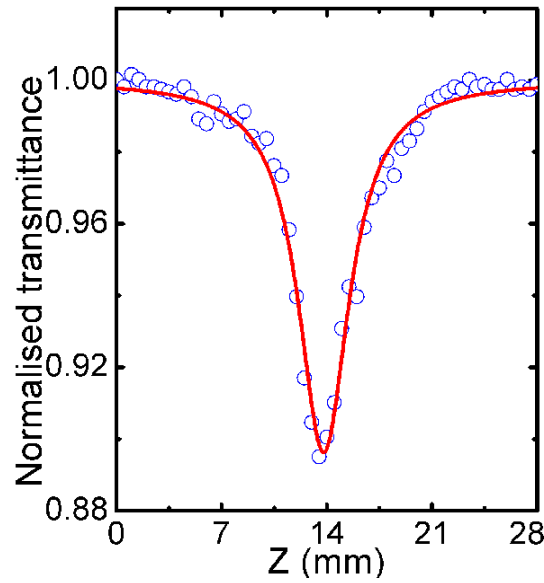


Fig. 5.10: Open aperture z-scan response of CdS QRs in chloroform solution. Blue circles are measured normalised transmittance and red line is fitting with Eq. (5.2).

We assume that the system collection efficiency and the fluorescence quantum yield are constant for the CdS nanocrystal-dispersed solution in the whole investigated window of 720-960 nm. With the given value measured by the z-scan method at wavelength 800 nm the 2P absorption cross-sections of CdS QRs at different excitation wavelength can be obtained using Eq. (5.5) and are plotted in Fig. 5.11 (blue circles). CdS QDs of similar diameter of 4.45 nm was also measured and plotted in Fig. 5.11 (red squares). The log-log plot of photoluminescence versus excitation power yields a linear slope close to 2 in both QDs and QRs solutions (not shown here), which confirms the 2P induced emission in both cases. From Fig. 5.11

it is clear to see that in the whole investigated spectral range the QRs show superior 2P sensitivity compared to QDs of similar diameters. Especially in the window of 800-960 nm, which has been widely applied in 2P fluorescence bio-imaging [146], 3D optical data storage [12] and micro-fabrication [147], the 2P absorption cross-section of QR is one to two orders of magnitude larger than that of QDs.

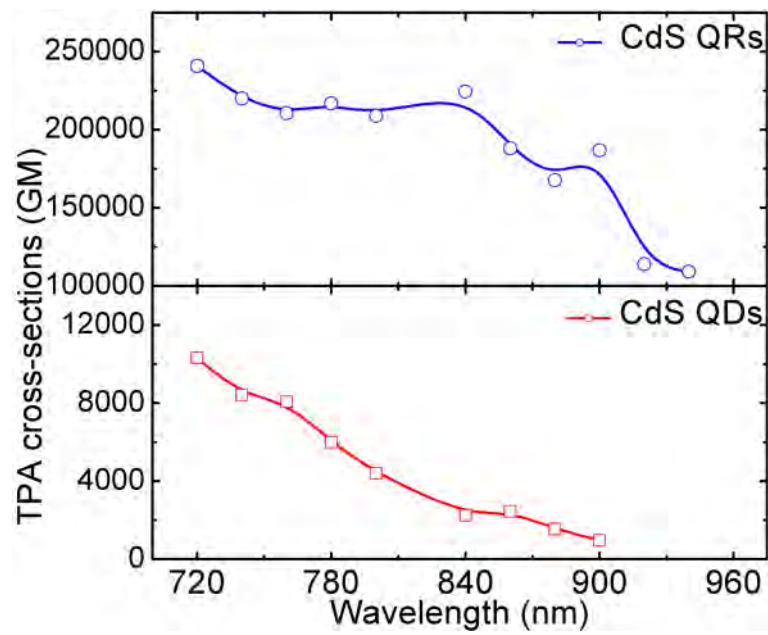


Fig. 5.11: Plot of TPA cross-sections of CdS QRs (blue circles) and CdS QDs 430 (red squares) as a function of the excitation wavelength.

The z-scan measurement is confirmed by the 2P induced fluorescence study of single QR. The action cross-sections $\eta\sigma_2$ were obtained by averaging the intensity of 10 particles to give $1.15 \cdot 10^{-48} \text{ cm}^4 \cdot \text{s} \cdot \text{photon}^{-1}$ at wavelength 800 nm. Giving the fluorescence quantum yield of QDs decrease 100-fold when the temperature increases from $\sim 5\text{K}$ to room temperature [145], the 2P absorption cross-sections of CdS QRs is on the order of $10^{-46} \text{ cm}^4 \cdot \text{s} \cdot \text{photon}^{-1}$ and consistent with the z-scan measurement of QRs in solution.

5.3.2 Two-photon orientation microscopy

A strong polarised behaviour of QRs in both emission and excitation has been demonstrated in fluorescence studies of single rod under single-photon excitation [24, 25]. It is of most importance to establish the angular selective excitation property under 2P excitation before using QRs as energy transfer donors in the azo dye mixed polymer matrix for 4D optical data storage.

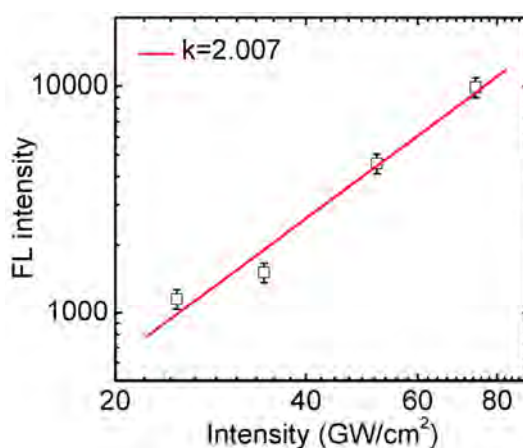


Fig. 5.12: Fluorescence intensity dependence of the CdS QRs emission under 2P excitation on a log-log scale. The slope of linear fitting is 2.007.

The CdS QRs were well washed and prepared in chloroform solution with a extreme low concentration. The solution was spin coated on a pre-cleaned cover glass. A Ti:sapphire ultrashort pulsed laser beam of pulse width 100 fs (Spectra-Physics Tsunami) at a wavelength of 720 nm was focused by an objective of NA 1.4 onto the films. The fluorescence intensity was collected by the same objective and acquired by a CCD (PIXIS 100, ACTON) for spectra acquisition or a PMT for fluorescence images. The scattered laser light was blocked by a short pass filter. The dependence of the emission intensity on the excitation power is plotted in Fig. 5.12 on a log-log scale. The linear fit yields a slop of 2.007 which is the feature of the 2P absorption induced emission.

The study of emission polarisation was performed by rotating the analyser in front of the CCD and acquiring the images at each angle simultaneously. Fig. 5.13 (a) shows a pair of fluorescence images obtained at emission polarisation angles of 0 and 90 degrees, respectively, where the excitation polarisation was fixed at the vertical polarisation direction of 0 degree. It is highly fluorescent when the analyser is rotated at 0 degree, whereas it is nearly non-fluorescent when the analyser is rotated at 90 degrees. The emission intensity of the circled spot is plotted as a function of the analyser angle, shown in Fig. 5.13 (b). It is clear to show that the circled emission spot has strong linearly polarised emission property, where it follows a dependence of $\cos^2(\theta)$ as observed under single-photon excitation [24, 25].

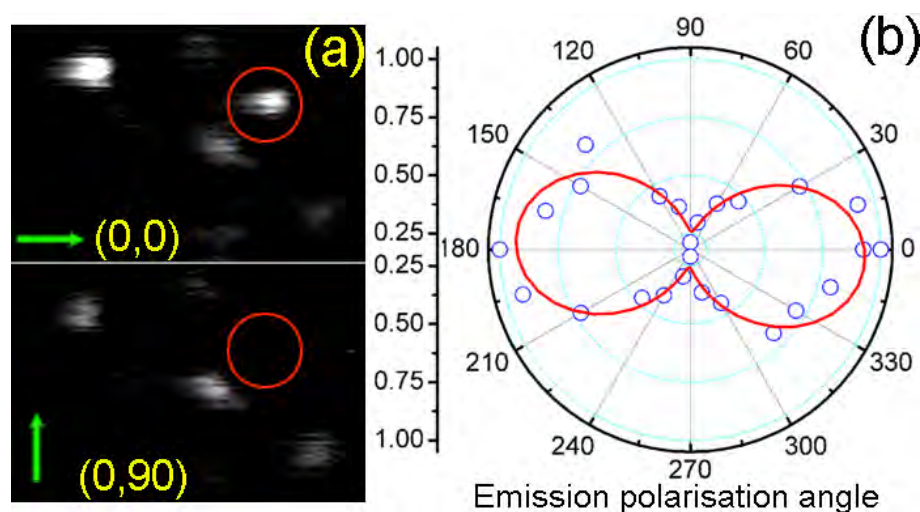


Fig. 5.13: (a) Fluorescence images of a circled emitting spot acquired at emission polariser angles of 0 and 90 degrees, respectively. The image scale is $5\ \mu\text{m}$. (b) The emission intensity of the circled emitting spot is plotted as a function of the emission polarisation angle. The solid line is fitting with $\cos^2(\theta)$.

To study the polarisation selective excitation of CdS QRs under 2P irradiance, the fluorescence images are acquired by rotating the polariser to control the incident polarisation state. Fig. 5.14 (a) shows the images of a circled emitting spot obtained at excitation polarisation angles of 0, 30, 75 and 90 degrees, respectively, where the

fluorescence analyser was fixed at the vertical direction. Distinct polarisation selective excitation of the circled emitting spot can be discerned in the images. The sharp angular dependence of 2P absorption can be evident in Fig. 5.14 (b) where the emission intensity is plotted as a function of the excitation polarisation angle. The data can be fitted well via a correlation of $\cos^4(\theta)$ (solid lines), which is consistent with previous investigations [125]. This result indicates QRs can be excited efficiently when the laser polarisation direction is rotated parallel to the rods orientation, whereas the excitation is nearly shut off when the polarisation direction of the laser is normal to this angle. It is worth to note that the $\cos^4(\theta)$ dependence of the angular selectivity for the 2P absorption case is much sharper than the $\cos^2(\theta)$ dependence under single-photon excitation [25].

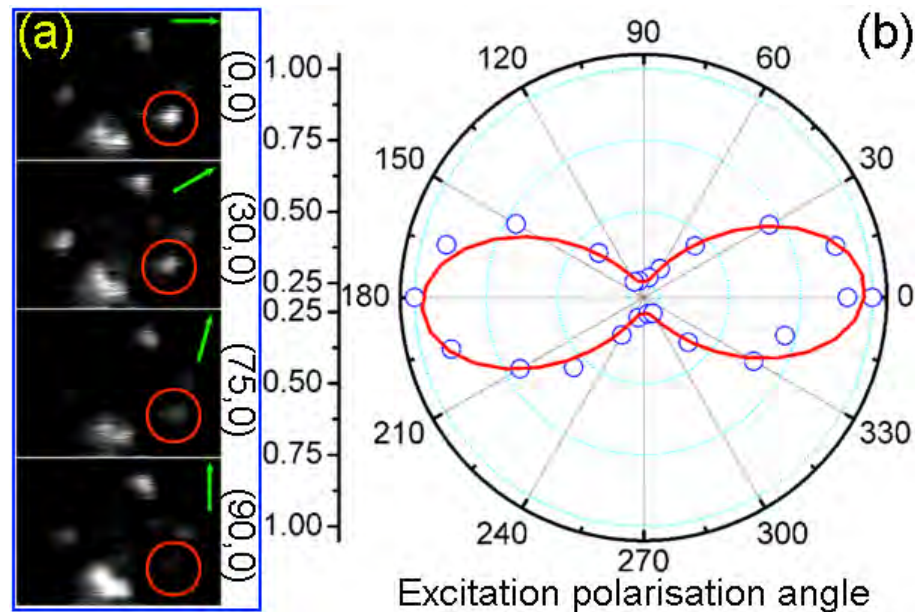


Fig. 5.14: (a) Fluorescence images of a circled emitting spot acquired at excitation polarisation angles of 0, 30, 75 and 90 degrees, respectively, where the emission polariser was fixed at the vertical direction. The image length scale is $5 \mu m$. (b) The emission intensity of the circled emitting spot is plotted as a function of the excitation polarisation angle. The solid line is fitting with a dependence of $\cos^4(\theta)$.

5.4 Four-dimensional optical data storage

5.4.1 Characterisation of quantum-rod-driven energy transfer

Before demonstrating 4D optical data storage in the QR-sensitised medium, we need to confirm that local fluorescence energy transfer can indeed occur from QRs to azo dyes. DR1 was modified into DR1-EH to make it more soluble in the PS matrix. The absorption band of DR1-EH, which gives sufficient spectral overlapping with the emission band of the QRs, is plotted in Fig. 5.15. CdS QRs were prepared following the developed recipe discussed in Section 5.2, with an average size tuned to

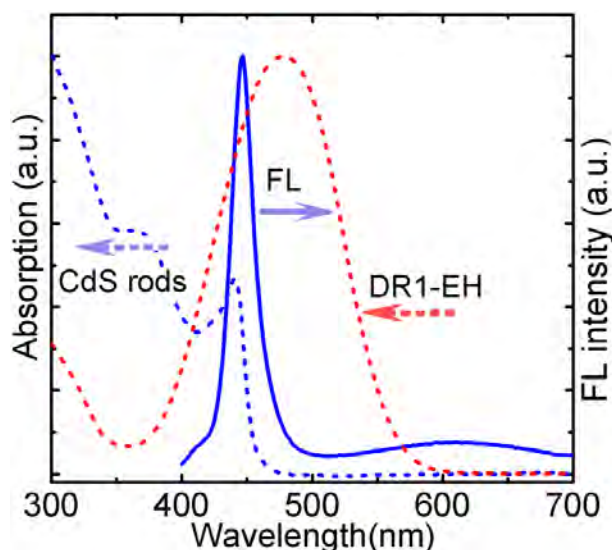


Fig. 5.15: Absorption and emission spectra of CdS QRs as well as sufficient spectral overlapping with the absorption spectra of DR1-EH.

4.6 nm by 32 nm. The measured fluorescence (FL) quantum yield of CdS rods was 0.06 using 9,10-Diphenylanthracene as standard with known $\Phi_f = 0.95$. The calculated Förster distance R_0 is 2.9 nm using the Förster formula [46]. CdS rods were dispersed in the PS matrix at a concentration of an average inter-particle

distance of 86 nm for the given density of the polymer composition equal to 1 g/ml. A Ti:sapphire ultrashort pulsed laser beam of pulse width 100 fs (Spectra-Physics Tsunami) was employed as a 2P excitation source. The wavelength was specifically chosen at 720 nm to avoid the direct laser excitation of DR1-EH so that most irradiation energy is absorbed by QRs and transferred to dyes (see the absorption spectra in Fig. 5.15).

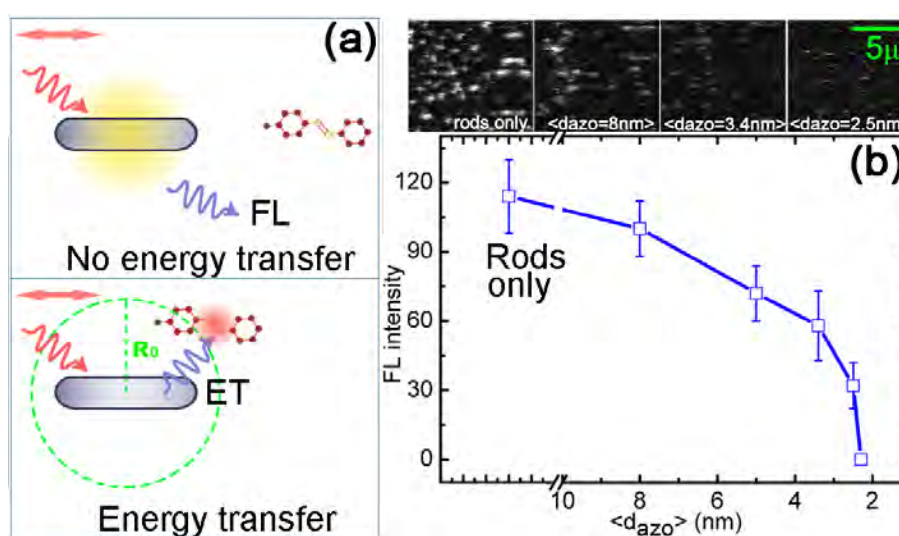


Fig. 5.16: (a) Schematic illustration when donors are far away from acceptors, no energy transfer (ET) occurs and FL is emitted from QRs. If donors and acceptors are within the Förster distance, azo dyes are excited by ET. (b) The FL intensity of the QR-dispersed PS sample is plotted as a function of the inter-molecule separation of DR1-EH. The inset is the FL images for different concentrations of azo dyes.

When the acceptors are far away from the donors, no energy transfer occurs and strong FL emission of QRs is observed as illustrated in Fig. 5.16 (a). The FL intensity of QRs is plotted as a function of the average inter-molecule distance between DR1-EH $\langle d_{\text{azo}} \rangle$ as shown in Fig. 5.16 (b). The FL images acquired at the emission peak of QRs at wavelength 450 nm by progressive increasing the concentration of azo dyes are shown in the inset. The concentration of azo dyes is visualised as the mean molecule separation $\langle d_{\text{azo}} \rangle$ between DR1-EH. As we gradually increased the

concentration of DR1-EH, which corresponds to the decrease in the inter-molecule distance between dyes, the FL intensity of QRs was reduced as a result of ET from QRs to DR1-EH. When the inter-molecule separation between DR1-EH is below 2.5 nm, the FL of QRs was quenched completely.

5.4.2 Characterisation of energy-transfer-driven isomerisation

As schematic illustration in Fig. 5.16 (a), when donors and acceptors are within R_0 azo dyes are excited as a result of the occurrence of fluorescence energy transfer. To observe the energy-transfer-driven isomerisation induced refractive-index change several bits were recorded in a sample doped with DR1-EH at a concentration of 9.1 wt.% corresponding to an inter-molecule separation of 2.4 nm and DIC microscopy was used to readout the refractive-index change of the written bits. QRs were diluted to an inter-particle separation of 104 nm to avoid aggregation. Assuming a homogeneous QRs distribution, each rod consumes a volume of radius r . Within the volume of radius R_0 azo dyes are excited via energy transfer from QRs and in the rest part excited by direct laser excitation. The volume absorption cross-section is given as $a = V \cdot \sigma_2$. With the given 2P absorption cross-section of QRs is $20.9 \cdot 10^{-46} \text{ cm}^4 \cdot \text{s} \cdot \text{photon}^{-1}$ and the cross-section of azo dye at excitation 720nm is approximately $5 \cdot 10^{-50} \text{ cm}^4 \cdot \text{s} \cdot \text{photon}^{-1}$ [148]. Special care is taken for surface capping which can give a reasonable homogeneous distribution $r = 25 \text{ nm}$. The energy transfer induced excitation is given $a = \frac{4\pi R_0^3}{3} \sigma_2 = 2.2 \cdot 10^{-64} \text{ cm}^7 \cdot \text{s} \cdot \text{photon}^{-1}$, whereas the background absorption from the 2P excitation of dye molecules is given $a_{\text{dye}} = \frac{4\pi r^3}{3} \sigma_2 = 1 \cdot 10^{-66} \text{ cm}^7 \cdot \text{s} \cdot \text{photon}^{-1}$, which is two orders of magnitude

smaller than energy transfer induced excitation. In our experiment condition, to avoid aggregation we decreased concentration of QRs with $r=52\text{nm}$. The energy transfer induced excitation is still one order of magnitude larger than 2P excitation of dyes where $a = \frac{4\pi r^3}{3} \sigma_2 = 5.3 * 10^{-65} \text{ cm}^7 \cdot \text{s} \cdot \text{photon}^{-1}$. As a result the contribution of direct 2P excitation of dye molecules to the refractive-index change is nearly negligible.

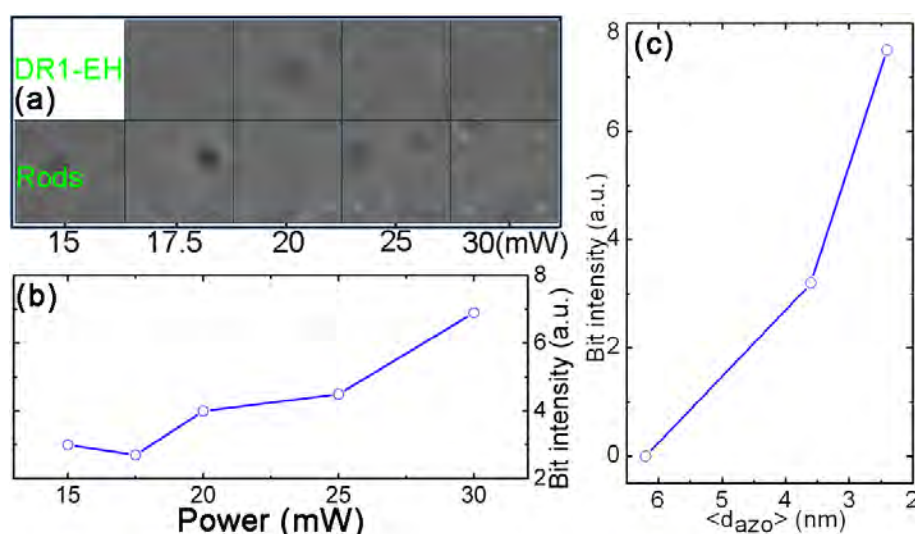


Fig. 5.17: (a) DIC images of written bits recorded at the power range from 15 to 30 mW. (b) The readout bit intensity of pure energy-transfer-driven isomerisation induced recording is plotted as a function of the recording power. (c) The readout bit intensity of pure energy-transfer-driven isomerisation induced recording at 30 mW in samples blended with azo dyes of different concentrations.

The DIC images of written bits are shown in Fig. 5.17 (a). It can be discerned that the readout intensity is much weaker in the whole recording range from 17.5 mW to 30 mW in a sample doped with DR1-EH only. Using QRs as energy transfer donors the readout contrast of written bits are greatly enhanced. The readout bit intensity of pure energy-transfer-driven isomerisation induced recording is simply given by subtracting the background recording of DR1-EH itself and plotted as a function of the recording power, as shown in Fig. 5.17 (b). Increase in the recording power leads to significant increase of the readout intensity due to complete transfer

of QRs absorbed 2P energy to surrounding azo dyes. Reducing the concentration of azo dyes leads to incomplete energy transfer and decreases the recording efficiency. This is observed in Fig. 5.17 (c). The readout bit intensity of pure energy-transfer-driven isomerisation induced recording at 30 mW is plotted as a function of mean separation between azo dyes. It is evident that the readout intensity of energy-transfer induced recording is gradually increased as the progressive increase of energy transfer efficiency by reducing of $\langle d_{\text{azo}} \rangle$.

Energy-transfer-driven isomerisation induced by angular selective excitation of QRs introduces polarisation sensitivity which is characterised by the pump-probe experiment. A linearly polarised white light source with central wavelength at 520 nm and a full width at half maximum of 10 nm was employed as a probe beam. The transmitted probe beam intensity was monitored by a CCD (PIXIS 100, ACTON). Spincoated samples of thickness of 4 μm with an inter-molecule separation of 2.4 nm between DR1-EH and the inter-particle distance of 104 nm between rods were prepared. Generally *trans* molecules have a larger extinction coefficient compared with *cis* molecules. They are selectively photobleached and re-orientated during the isomerisation process leading to angular hole burning absorption [41]. The absorption decrease is much stronger when the laser polarisation is parallel to the probe beam than it is normal to the probe beam.

Fig. 5.18 (a) shows the normalised absorbance evolution of the controlled sample loaded with DR1-EH only under the irradiance intensity of $15 \text{ GW}/\text{cm}^2$. Fig. 5.18 (b) shows the pure energy-transfer-driven isomerisation induced absorbance change after baselined to the controlled sample to subtract the background recording. The absorbance decrease here is due to angular hole burning of *trans* molecules induced by pure energy-transfer-driven isomerisation. The early isomerisation rates in the first 40 seconds were fitted with a linear dependence. It is clear to see that the

rate of the absorbance change in the parallel direction is significantly faster than that in the perpendicular direction where the difference is over 5 times. This is primarily attributed to the strength of the angular selective excitation property of QRs where the excitation is nearly shut off in the perpendicular direction.

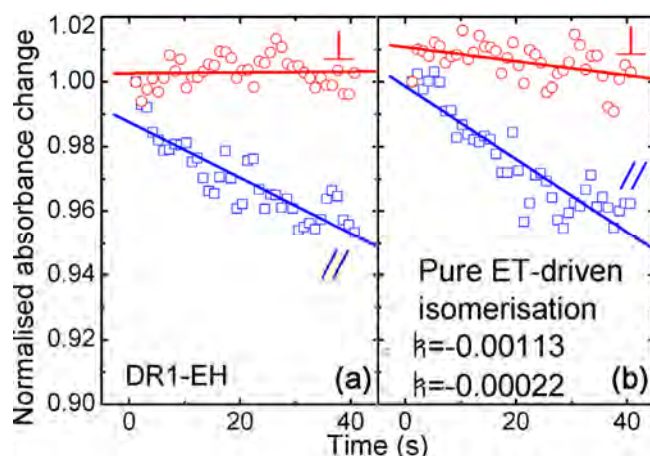


Fig. 5.18: (a) Normalised absorption change of the controlled sample dispersed DR1-EH only. (b) Pure energy-transfer-driven isomerisation induced absorbance evolution. Blue squares and red circles are data acquired when the excitation polarisation is parallel and perpendicular to the probe polarisation direction, respectively. The solid lines are the early isomerisation rate fitting with a linear dependence.

The large difference in the isomerisation rates of the pure energy-transfer-driven isomerisation in parallel and perpendicular directions builds up the anisotropy as well as the localised polarisation sensitivity. Fig. 5.19 (a) shows pure energy-transfer-driven anisotropy evolution defined in Eq. (5.1) in the QR-sensitised sample. The anisotropy increases exponentially and reaches the maximum within 120 s and slowly reverses after that. The pronounced polarisation selective excitation property of QRs creates a maximum anisotropy of approximately -0.03 which is abundant to enable the following localised polarisation modulated photonic applications.

For a comparison a CdS QD-sensitised sample was prepared at the same

concentration. As spherical QDs have no angular selective excitation property no polarisation sensitivity can be preserved during QD-driven energy transfer process as discussed in Section 5.2. The residual polarisation sensitivity is mainly attributed to weak background recording by direct excitation of dyes. Fig. 5.19 (b) shows the plot of the anisotropy enhancement defined as $R(t) = A_{rods}(t)/A_{dots}(t)$, where $A_{rods}(t)$ and $A_{dots}(t)$ are anisotropy in QR- and QD-sensitised samples, respectively. From Fig. 5.19 (b) it clearly indicates that the polarisation sensitivity is preserved during QR-driven energy transfer process. This energy-transfer-preserved polarisation has been confirmed by the polarisation readout of several bits recorded by a parallelly-polarised beam. The polarisation sensitivity of recorded bits was readout in the polarisation interference setup described in Chapter 3. After baseline the bit intensity at each reading polarisation angle to the controlled sample dispersed DR1-EH only, the polarisation ratio of pure energy-transfer-driven isomerisation induced recording is plotted as a function of reading polarisation angles in Fig. 5.19 (c). It can be seen that the pronounced polarisation sensitivity is preserved in the QR-driven energy transfer process whereas the polarisation in the QD-sensitised sample is negligible.

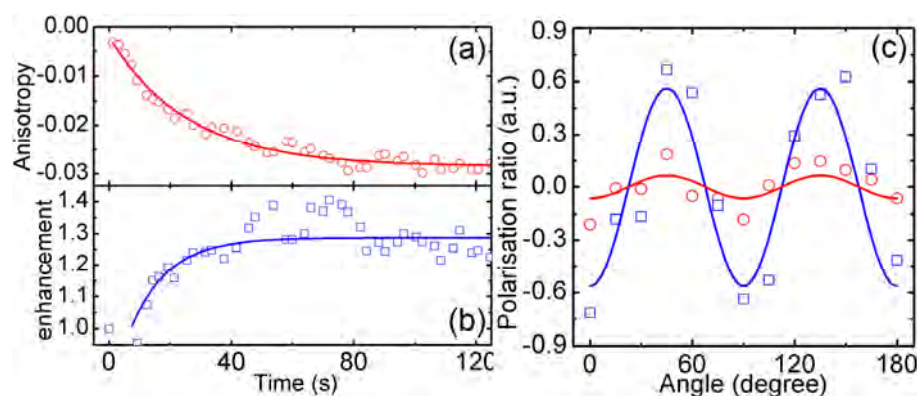


Fig. 5.19: (a) Anisotropy evolution of the QR-sensitised sample under linearly polarised illumination. The solid line is the guide for eyes. (b) Anisotropy enhancement of a QR-sensitised sample compared to the QD-sensitised sample is plotted as a function of time. The solid line is the guide for eyes. (c) Plot of the energy-transfer-preserved polarisation ratio of recorded bits as a function of the reading polarisation angle after baseline correction. Red circles and blue squares

are data from QD- and QR-sensitised samples, respectively. Solid curves are fitting with $\cos(4\theta)$.

5.4.3 Four-dimensional optical data storage and other photonic applications

The 2P excitation can introduce a polarisation dependent refractive-index change in the QR-sensitised polymer loaded with azo dyes. To demonstrate 2P induced polarisation-encoded 4D optical data storage in such a medium, a thick sample of $80\ \mu\text{m}$ was prepared. Patterns of letters I/J, E/F and C/D were encoded at the 0 and 45

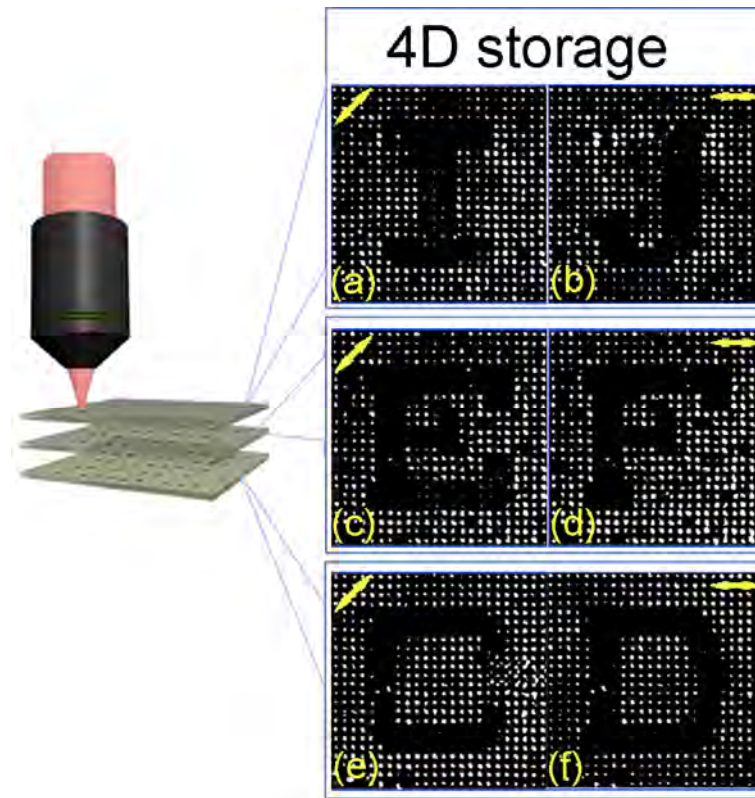


Fig. 5.20: Demonstration of polarisation-encoded 4D optical data storage. (a) to (f) are letters I/J, E/F and C/D recorded in the first, second and third layers, respectively, in the polarisation direction of 45 and 0 degrees and retrieved back using corresponding polarised reading beams.

degrees of the writing polarisation direction in the first, second and third layers,

respectively. Each pattern consists of 24×24 bits, with bit separation of $2.6 \mu\text{m}$. The spacing between adjacent layers is $20 \mu\text{m}$. Data can be retrieved back using the reading beam with the corresponding polarisation direction in the polarisation interference setup developed in Chapter 3. Figs. 5.20 (a) to (f) demonstrate that the encoded patterns can be readout distinctly with minor cross-talks, which are mainly attributed to the permanent photobleaching of azo dyes under the intense illumination at 720nm [41]. The storage capacity achieved is approximately 50Gbits/disc . The QR-sensitised photoisomerisation polymer loaded with azo dyes cannot only allow 2P recording with enhanced efficiency but also enable multiplexing information in additional polarisation domain of a writing beam, which can significantly enhance the impact in this field.

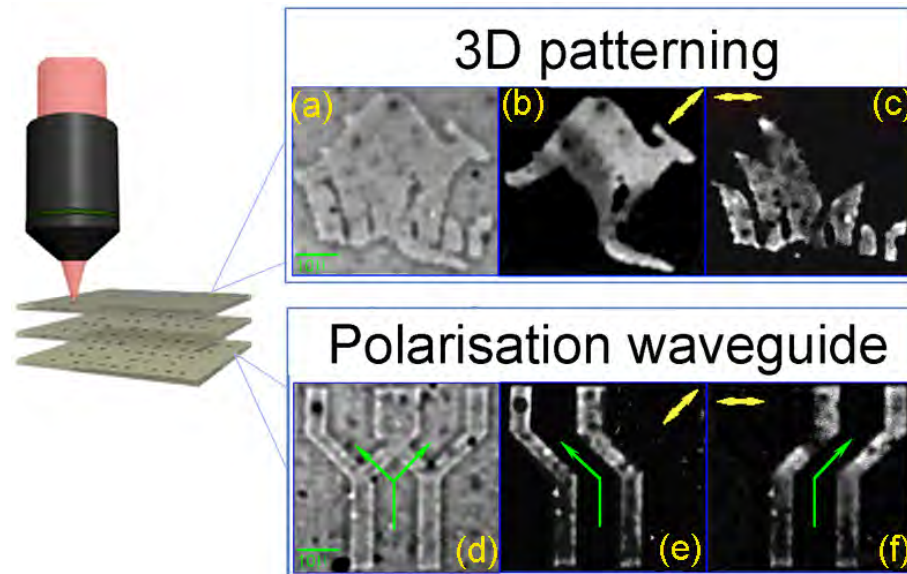


Fig. 5.21: Photonic applications of localised polarisation control. (a) DIC images of polarisation multiplexed patternings. Top-view images of distinct patterns are retrieved by rotating the polarisation direction of the reading beam at 45° (b) and 0° (c) degrees, respectively. (d) DIC images of polarisation controlled waveguide fabrication. Top-view images of upper and lower arms are readout at a polarisation angle of 45° (e) and 0° (f) degrees, respectively.

The localised polarisation sensitivity offers an additional dimension to

manipulate the beam in the polarisation domain, which holds a great potential of other multi-dimensional photonic applications. Figs. 5.21 (a) to (f) demonstrate polarisation multiplexed 3D patterning and fabrication of waveguides. Patterns of a kangaroo and the Sydney Opera House have been multiplexed in the same position when the polarisation direction of the writing beam is orientated at 0 and 45 degrees, respectively. Refractive-index variation is shown in the DIC readout image in Fig. 5.21 (a). The DIC readout is sensitive to refractive-index variation only, which is non-polarisation dependent. Therefore all patterns can be readout in the DIC mode simultaneously. However, the patterned images can be retrieved distinctly using a reading beam of a polarisation angle at 45 and 0 degrees, respectively, as shown in Figs. 5.21 (b) and (c). Similarly, a Y-shape waveguide channel was fabricated with the support region of upper and lower arms exposed to linearly polarised writing beams at polarisation direction of 0 and 45 degrees, respectively. The DIC image is shown in Fig. 5.21 (d). The top view images readout by corresponding polarised reading beams are shown in Figs. 5.21 (e) and (f). As the localised anisotropy introduces polarisation sensitive refractive-index variation, this polarisation-multiplexed waveguide could be used to split and guide differently polarised beams.

5.5 Chapter conclusions

This chapter has demonstrated 2P induced polarisation-encoded 4D optical data storage in QR-sensitised photoisomerisation polymers. QRs have been incorporated into photoisomerisation polymers via 2P energy transfer, which allows not only efficient 2P recording but also the polarisation modulated refractive-index variation.

To gain an understanding of 2P energy transfer between nanocrystals and azo dyes in a polymer matrix, the feasibility of using CdS QDs as 2P energy transfer

donors to excite azo dyes with low 2P absorption cross-sections dispersed in polymer matrix has also been demonstrated. The characterisation of energy-transfer-driven isomerisation kinetics evidently reveals the enhanced recording efficiency via an energy transfer process from QDs to surrounding azo dyes. It has been found that the polarisation sensitivity is significantly degraded as the spherical QDs have no angular selective excitation property and the polarisation sensitivity cannot be preserved during the energy transfer process.

A volume dependence of 2P absorption cross-sections of CdS nanocrystals has been found. CdS QRs of a uniform size distribution have been synthesised for enhanced 2P absorption. The 2P absorption cross-section has been characterised by both the z-scan method and the 2P induced fluorescence study. The 2P absorption cross-section of CdS QRs is found to be one order of magnitude larger than that of CdS QDs. Not only large 2P absorption cross-sections, but also the strong linearly polarised emission and the sharp polarisation selective excitation property of CdS QRs have been observed in the orientation microscopy study.

As a consequence of energy transfer an enhanced refractive-index change has been observed in QR-sensitised photoisomerisation polymers. The sharp angular selective excitation property has built up the large difference of isomerisation rates between the direction parallel and perpendicular to the laser polarisation. Characterisation of the anisotropy evolution clearly reveals the preservation of polarisation sensitivity during the energy transfer from QRs to surrounding azo dyes, which allows the localised control of light in the additional polarisation domain. The application of 3D localised polarisation control has been successfully demonstrated in polarisation-encoded 4D optical data storage as well as in polarisation-controlled 3D patterning and fabrication of waveguides.

Chapter 6

Multi-dimensional optical data storage in quantum-dot/rod-doped photorefractive polymers

6.1 Introduction

Photorefractivity with the ability of reversible spatial modulation of refractive-index and storing information in the volume of a medium has been seen as an important optical data storage system. Improving the recording performance has been an increasing interest since the observation of photorefractivity in polymers [69, 70], owing to their low cost and simple procedure to prepare. Due to their attractive optical properties of quantum dots/rods (QDs/QRs) such as narrow emission bands, the emission wavelength tunability on their sizes and the photostability [149, 150], the fuse of nanotechnology with photorefractive polymers has greatly enhanced its impact in the volume data storage. The emergency of two-photon (2P) excitation has provided a new platform for application of both photorefractive crystals [11] and photorefractive polymers [12] into three-dimensional (3D) bit by bit optical data

storage. QDs/QRs have large 2P absorption cross-sections as discussed in Chapter 5. Therefore, developing 2P induced optical memory in QD/QR-sensitised photorefractive polymers is of significance, which holds great potentials towards multi-dimensional optical data storage.

It has been known that the surface states of QDs can significantly affect their optical properties as well as their photorefractive performance. Facilitating a high efficiency of the charge generation as well as a fast grating build-up response was reported in the 2BC characterisation setup by surface processing of QDs [87, 94]. It has been found that without an external electric field surface capping can greatly affect the local charge separation between QDs and surrounding polymers [99]. In a typical 2P excitation configuration, no external electric field is used. Thus, it is of great importance to process the surface of QDs to facilitate the local charge separation and enhance the photorefractive performance.

The goal of this chapter is to develop 2P induced multi-dimensional optical data storage in a QD/QR-doped photorefractive polymer [151]. This chapter is organised as following. Section 6.1 presents the introduction. In Section 6.2 the feasibility of 2P excitation in QD-sensitised photorefractive polymers and their application in 3D optical data storage are explored. In particular, the photorefractive performance of QDs with different surface stoichiometry is characterised in multi-modes readout under 2P excitation. In Section 6.3 the feasibility of 2P excitation in photorefractive polymers sensitised by QRs is investigated. The chapter conclusion is drawn in Section 6.4.

6.2 Three-dimensional optical data storage

6.2.1 Surface modification of quantum dots

It has been recognised that charge separation and transfer occurs at the interface between QDs and conjugated polymers with an electron affinity gradient even in the absence of external electric field [99]. Charge separation and transfer processes should be fast enough to inhibit the radiative relaxation of QDs [152]. It has been well established that the surface properties of QDs significantly affects their photoluminescence (PL). In addition, surface states arising from unpassivated atoms

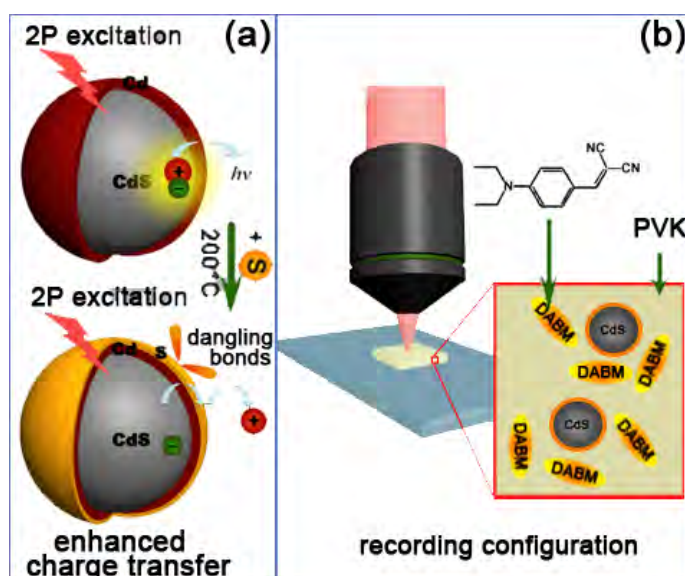


Fig. 6.1: Charge transfer enhancement by surface modification. (a) Gradual deposition of unpassivated S atoms on the surface of QDs serves as hole traps leading to suppression of radiative recombination of photoexcited QDs. (b) The experimental configuration for 2P induced recording. Surface modified QDs were incorporated into photorefractive polymers, blending with nonlinear dye and PVK matrix.

fall within the electronic band gap of QDs. The successive ionic layer adsorption and reaction (SILAR) technique originally developed for the deposition of thin films on solid substrates from solution baths was recently introduced to grow precisely

controlled epitaxial shells with atomic monolayer control on the surface of QDs [153]. This research has employed the SILAR method to control the surface stoichiometry of CdS QDs from cadmium (Cd) rich to sulfur (S) rich and study their photorefractive recording performance under intense 2P excitation. The gradual transition from Cd to S rich surface leads to an enrichment of surface states associated with unpassivated surface S atoms, suppressing the radiative recombination, and therefore reinforcing the charge separation rate, as illustrated in Fig. 6.1.

CdS core particles were prepared using a well established recipe [134]. CdO (0.48 mmol), oleic acid (9.6 mmol), and octadecene (ODE) (9 ml) were mixed in a three-necked flask and degassed at 80 °C for 30 min. The solution was heated to 270 °C for 10 min under a nitrogen environment and vigorous stirring. The sulfur precursor of S (0.4 mmol) in 4 ml ODE was swiftly injected into the reaction pot. The temperature was set at 200 °C for subsequent growth process. 20 min later particles stopped to grow at a size of the first extinction peak at wavelength 433 nm. The ratio of Cd:S used to prepare the QDs was 1.2:1, and the ‘as-prepared’ CdS core particles were consequently expected to possess a surface excess of Cd. The only passivating ligand available in our system is oleic acid, which is expected to bind solely to surface Cd atoms, leaving any surface S atoms unpassivated.

Using the SILAR chemistry, we subsequently tuned the surface stoichiometry of CdS QDs from Cd to S rich by systematically injecting of additional S precursors [153]. Tuning the surface stoichiometry of CdS QDs from Cd to S rich was achieved in a one-pot method by systematically injecting controlled amounts of additional S precursors [153]. For each injection the quantity of S precursors was fixed at 0.05 mmol in 0.5 ml ODE and the growth time was fixed at 5 min. After six injections (the mol concentration ratio S:Cd of 1.5 : 1), the final S rich particles were achieved

with a rather small increase of diameter 0.6 nm compared to the Cd rich particles. The size of QDs was determined from the first extinction peak [137]. This indicated the deposition efficiency of S precursors was below 70%. Both the absorption and fluorescence spectra were measured immediately after taken from the reaction pot without any washing process to change the surface.

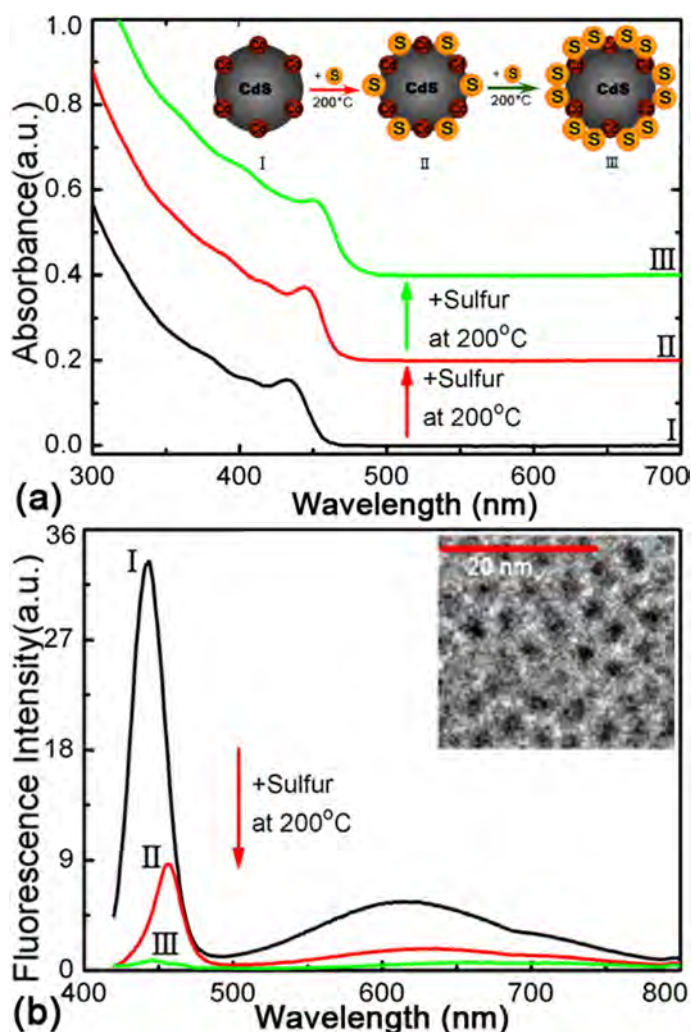


Fig. 6.2: Surface stoichiometry engineering using SILAR method. (a) Dynamic evolution of absorption spectra after injection of additional S precursors. I corresponds to QDs of Cd rich surface achieved when the mol concentration ratio of Cd to S is 1.2:1 in the reaction pot. II and III correspond to mixed surface and S rich surface at mol concentration ratio of 1:1.25 and 1:1.5 respectively. (b) Relative PL intensity of QDs I, II and III divided by the absorbance of illuminating beam at the wavelength of 400 nm. The inset shows the TEM image of S rich surface QDs. The scale bar is 20 nm.

The deposition of S atoms onto the CdS particles was monitored using UV-vis spectroscopy as shown in Fig. 6.2 (a). A red-shift of the first absorption peak due to particle growth was observed with the adhesion of S. The inset is the schematic illustration of the progressive deposition of S atoms on the surface of core particles. When the initial Cd precursors were exhausted the absorption peak stopped to red-shift, and an S rich surface was achieved. The increase in the surface density of unpassivated dangling bonds of S atoms led to a marked reduction in photoluminescence (PL) efficiency of the QDs [154, 155]. Fig. 6.2 (b) shows the relative fluorescence intensity of the surface modified CdS QDs. A systematic reduction of PL was observed with increased additional S precursors. The emission intensity of the S rich QDs was quenched by approximately two orders of magnitude lower than that of the original Cd rich QDs, while the size of QDs did not change significantly. The inset shows the high resolution TEM images of as-prepared S rich CdS QDs. This fluorescence quenching is attributed to the accumulation of surface trap density during the surface stoichiometry modification rather than any size effect or aggregation.

6.2.2 Two-photon localised photorefractive performance

To investigate the effect of the enhanced charge separation on the change in refractive-index under 2P excitation, we prepared a photorefractive polymer formulation consisting of poly (N-vinyl carbazole) (PVK): 9-ethylcarbazole (ECZ) and 4-(diethylaminobenzylidene)-malononitrile (DABM). The molecule structure of DABM is shown Fig. 6.1 (b). The QD-based photorefractive polymer for 2P excitation was prepared as follows. One millilitre aliquots of raw QDs were taken from the reaction pot, washed and precipitated by chloroform and 2-propanol. The precipitated particles were re-dissolved in chloroform and stored in the dark. No change in the optical properties of the QDs was observed due to the washing process

monitored using the absorption and emission spectra. The mixture of 54 mg of PVK, 16 mg of ECZ, 30 mg of DABM and 0.12 nmol QDs were dissolved in chloroform. The solution was drop casted to a glass slide and dried at 60 °C for 20 min. The sample was heated to 150 °C for 3 min and subsequently sandwiched with a Teflon spacer thickness of 20 μm .

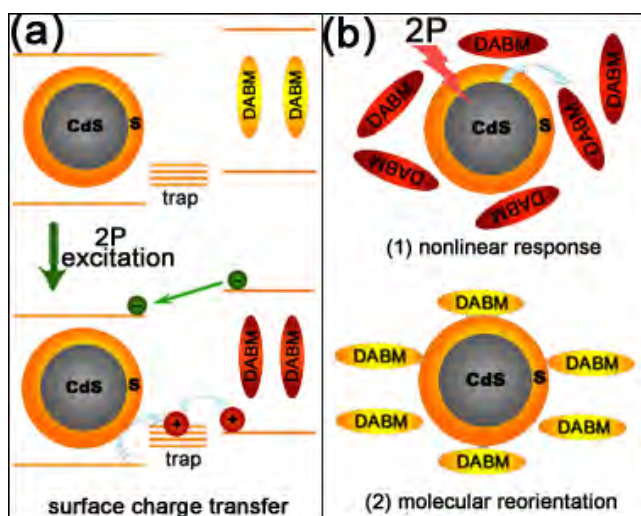


Fig. 6.3: Scheme of localised photorefractivity. (a) Energy levels and local charge transfer at the interface between QDs and DABM molecules. (b) Nonlinear response and enhancement by molecule re-orientation as a consequence of local electric field introduced by charge transfer at the interface.

The Highest Occupied Molecular Orbitals (HOMO) energy level of CdS QDs is in the range 6.2-6.6 eV [152]; hence they are favourable to be hole donors only when blended with materials of a higher HOMO level [152] like DABM where the HOMO level is in the range 5.9-6 eV [156], as illustrated in Fig. 6.3 (a). Since no external electric field is introduced, the charge separation should be fast enough to compete with radiative decay processes. The surface trap density of the CdS QDs engineered by the progressive deposition using the SILAR method exhibits the unpassivated dangling bonds of S atoms, which serve as hole traps on the order of picoseconds [155]. Under 2P excitation, space charges can be continuously produced from the

QDs in the focal region of an, swiftly separated and transferred at the interface. As a consequence of the change in the local electric field, the nonlinear response of DABM molecules near the interface is possible and a refractive-index enhancement is observed, as shown in Fig. 6.3 (b).

Since the QDs have no linear absorption beyond wavelength 600 nm, a Ti:sapphire ultrashort pulsed laser beam of pulse width 100 fs (Spectra-Physics Tsunami) at a wavelength of 780 nm was employed for 2P excitation. A high numerical aperture (NA) objective (NA=0.7; 20x) was used to focus the beam onto the recording sample. For readout of the stored information a commercial microscope (Olympus BX50) and a high NA objective (NA=1.4) were used. Since the charge transfer occurs at the interface it is necessary to have a large interfacial area in the focus volume. In our experiment there were over 500 QDs in the focal volume of an objective of NA 0.7 [109].

Fig. 6.4 (a) shows the fluorescence readout images of bits written at series of power condition from 7.5 to 35 mW. Each image comprises a pattern of 3×3 bits. To prevent any interference between adjacent bits, the bit spacing was kept at $10 \mu\text{m}$. The exposure time was fixed at 30 ms for each bit. The fluorescence collected by a photo multiplier tube (PMT) was fixed at the wavelength of 550 nm, corresponding to the emission band of DABM. The readout contrast of the recorded bits is plot as a function of the recording power, shown in Fig. 6.4 (b). The fluorescence intensity is substantially depressed upon radiation where QDs were present, indicating the surface charge transfer between the DABM molecules and QDs. Furthermore, as the surface of the QDs was engineered from Cd rich to S rich the fluorescence was suppressed significantly although not completely. This quenching is consistent with progressive adhesion of unpassivated S atoms, which facilitates the swift separation of electron-hole pairs at the interface, therefore inhibiting the radiative emission of

DABM.

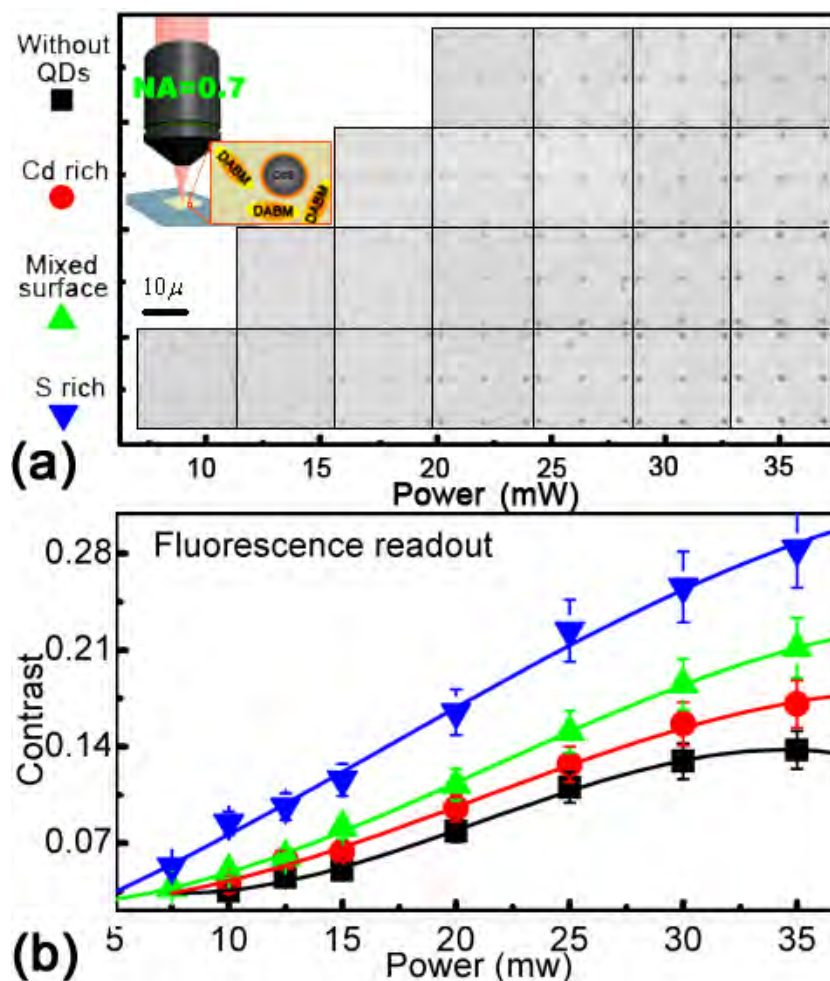


Fig. 6.4: (a) PL readout images of recorded bits at the recording power from 7.5 to 35 mW. The scale bar is $10\ \mu\text{m}$. The inset shows the recording configuration. (b) The readout contrast of recorded bits is plotted as a function of the recording power. Black squares, red dots, green triangles and blue triangles are data from the controlled sample dispersed DABM only and samples dispersed CdS QDs with Cd rich surface, mixed surface and S rich surface, respectively.

As a consequence of the space charge separation the local electric field change can introduce a change in refractive-index through a possible electrooptic effect in DABM molecules, as illustrated in Fig. 6.3. This refractive-index change was substantiated by transmission readout results as well as differential interference contrast (DIC) readout. The images of transmission readout are shown in Fig. 6.5 (a)

and the contrast of recorded bits is plotted as a function of the recording power in Fig. 6.5 (b). The images of DIC readout and the plot of contrast as a function of recording power are shown in Figs. 6.5 (c) and (d), respectively. It is evident that in the presence of QDs there is a substantial increase in the readout contrast confirmed in both transmission readout and DIC mode. In addition, as the progressive increase of surface states and dangling bonds on the surface of QDs by gradual deposition of unpassivated S atoms, the readout contrast is dramatically increased further. This result is consistent with that of FL readout, which indicates the resultant refractive-index change observed here is attributed to the local charge transfer at the interface between QDs and DABM molecules.

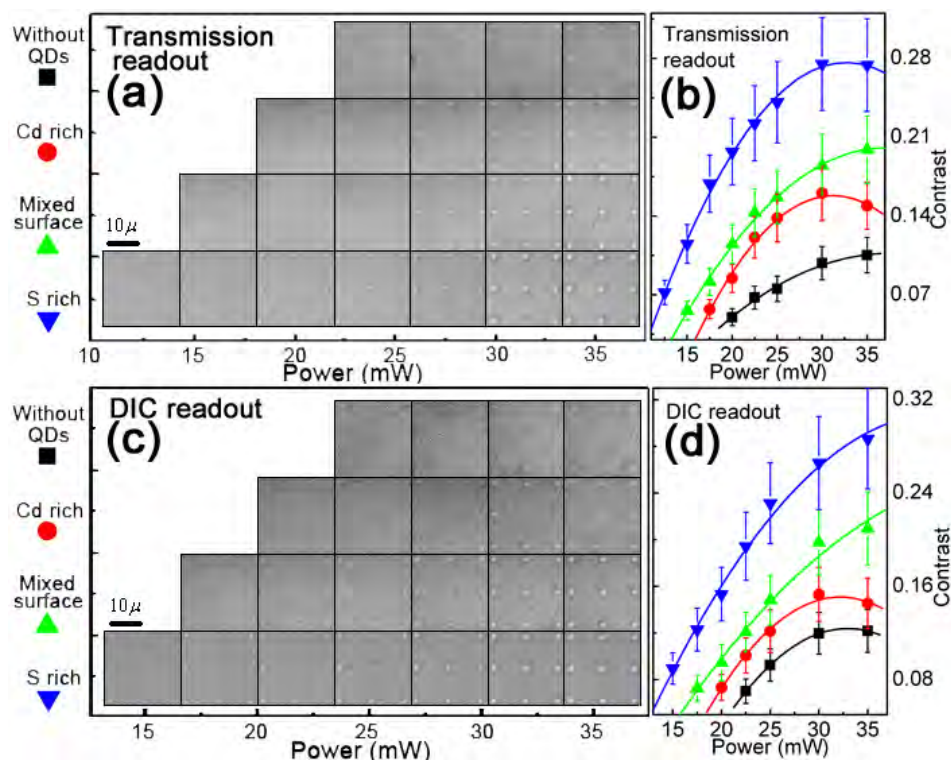


Fig. 6.5: Transmission (a) and DIC (c) readout images of recorded bits at the recording power from 12.5 to 35 mW. All scale bars are 10 μm . Transmission (b) and DIC (d) readout contrasts of recorded bits are plotted as a function of the recording power. The black squares, red dots, green triangles, and blue triangles correspond to the controlled sample dispersed DABM only and samples dispersed with CdS QDs of Cd rich surfaces, mixed surfaces and S rich surfaces, respectively.

6.2.3 Dynamic margin

Inspecting Fig. 6.4 and Fig. 6.5 reveals that the threshold of recording power decreases monotonically with the progressive increase in the surface state density on the QD surface. In the presence of CdS QDs with S rich surfaces the threshold power drops nearly 30% compared to that of the controlled sample without QDs doping. This is primarily due to enhanced charge transfer at the assistance of S rich surfaces. An important feature of photorefractivity is the erasability and rewritability. The stored information can be erased complete when exposed to homogeneous illumination. Interestingly, the recorded bits in the QD-doped samples below the

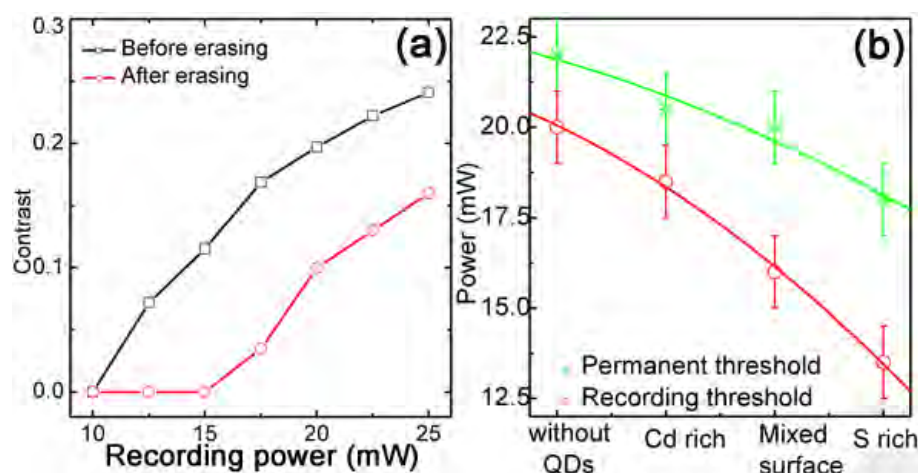


Fig. 6.6: (a) DIC readout contrast of recorded bits in samples dispersed with CdS QDs of S rich surfaces before (black squares) and after (red circles) exposed to UV illumination is plotted as a function of the recording power. (b) The recording threshold power (red circle) and permanent recording threshold power (green asterisk) as a function of surface stoichiometry. Solid lines are guide for eyes.

threshold of permanent recording power can be erased completely after exposure to a UV beam for 5 mins. Fig. 6.6 (a) shows the DIC readout contrast of recorded bits before erasing and after erasing in CdS QDs of S rich surface doped sample as a function of the recording power. It clearly reveals that the recording can be erased when the recording power is below 18 mW using the objective (NA=0.7). Above the

threshold power, permanent recording occurs mainly due to the bleaching of DABM molecules and damage to the polymer matrix.

The margin between the thresholds of the erasable and permanent recording power is plotted in Fig. 6.6 (b). The dynamic margin is gradually enlarged as the progressive transition of the QD surface from Cd to S rich. After incorporating of CdS QDs with an S rich surface, the rewritable recording range of the sample is more than 200% that of the controlled sample without QDs doping. The gradually widened dynamic margin in QD-sensitised samples indicates the refractive-index modulation in the erasable power range is primarily induced by the local electric field as a consequence of charge transfer at the interface between QDs and DABM molecules.

6.2.4 Three-dimensional optical data storage

The ability to record information as refractive-index change in QD-doped photorefractive polymers under 2P excitation compels its application in 3D optical data storage. We demonstrated multilayer information can be efficiently recorded and retrieved distinctly in the media, as shown in Figs. 6.7 (a) to(c). Three layers of information were stored in the volume of the sample at the presence of CdS QDs of an S rich surface. Each layer contains a pattern of 24×24 bits with a bit spacing of

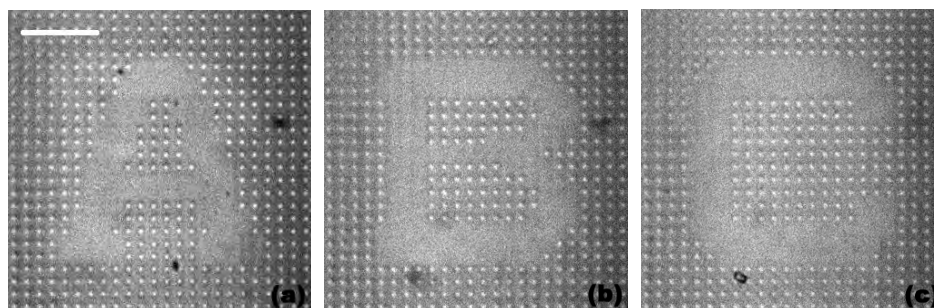


Fig. 6.7: Demonstration of multilayer information storage in photorefractive polymers sensitised by CdS QDs of S rich surfaces. Letter A (a), Letter B (b) and Letter C (c) are recorded in the first, second and third layer, respectively. The scale bar is $20 \mu m$.

3.2 μm . A letter A was recorded in the first layer whilst letter B and C were recorded in the second and third layer respectively with a layer spacing of 20 μm , which leads to a storage density of approximately 5Gbits per disc.

6.3 Feasibility of incorporating quantum rods for multi-dimensional optical data storage

To gain the ability to control the beam in the polarisation domain and towards erasable polarisation-encoded multi-dimensional optical data storage, 2P sensitisers with sharp polarisation selective excitation property such as QRs are necessary. This section is to investigate the feasibility of incorporating QRs into photorefractive polymers for 2P excitation.

CdS QRs of a uniform size distribution were synthesised following the operation described in Chapter 5. The ‘as-prepared’ QRs are expected to have Cd rich surfaces as there is excess of Cd precursors in the reaction solution. Then QRs were precipitated and refluxed into oleic acid (OA) to change the surface capping to OA, which gives QDs a good solubility inside the PVK matrix. Since the volume of a QR is much larger compared with that of a QD, QRs are easier to aggregate to change their optical properties during the sample preparation process. To avoid heavy aggregations QRs were dispersed with reduced concentration in the formulation consisting of 54 mg of PVK, 16 mg of ECZ, 30 mg of DABM and 0.04 nmol QRs. Samples of 20 μm thickness were prepared for 2P characterisation.

The 2P characterisation setup is the same as described in Section 6.2. A Ti:sapphire ultrashort pulsed laser beam at a wavelength of 780 nm was employed for 2P excitation. An objective (NA=0.7; 20x) was used to focus the beam onto the recording sample. Figs. 6.8 (a) and (b) show the DIC and FL readout images of

several bits recorded in the QR-sensitised photorefractive polymer, respectively. The bits were recorded at a condition of the power of 40 mW and exposure time of 25 ms. The fluorescence intensity of DABM molecules is substantially depressed within the recorded bits in the QR-doped sample, as shown in Fig. 6.8 (b), indicating the surface charge transfer between the DABM molecules and QRs. As a consequence of possible nonlinear response to the local electric field, refractive-index change was substantiated in DIC readout, shown in Fig. 6.8 (a). It reveals clearly that 2P excitation can be applied in QR-sensitised photorefractive polymers to achieve localised refractive-index change.

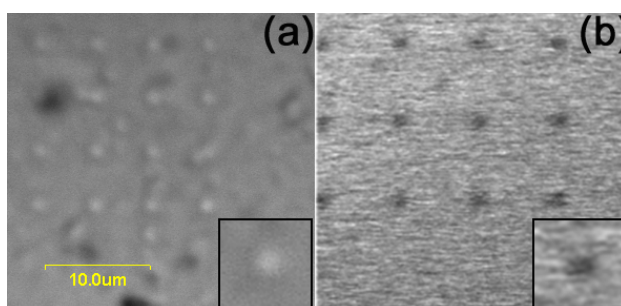


Fig. 6.8: DIC (a) and FL (b) readout images of recorded bits in QR-sensitised photorefractive polymers. The recording power is 40 mW and exposure time is 25 ms for each bit. The insets are the zoom-in views of one bit. The scale bar is 10 μm .

According to Fig. 6.8, the refractive-index is so small that it cannot produce a pronounced contrast to the background, which impedes the feasible demonstration of polarisation-encoded 4D optical data storage in the QR-sensitised photorefractive polymer. This is primarily attributed to the diluted concentration of QRs to avoid heavy aggregations. Due to the larger surface area, QRs tend to aggregate much more easily than QDs. To increase the doping concentration of QRs and improve the recording performance, complicated surface processing for QRs is required, which is still a challenge.

6.4 Chapter conclusions

In this chapter, the feasibility of applying 2P excitation in QD/QR-sensitised photorefractive polymers towards 4D optical data storage has been demonstrated. The 2P localised refractive-index change has been introduced in CdS QD-sensitised photorefractive polymers and characterised with different surface stoichiometry of QDs. S rich surface states facilitate the local charge transfer at the interface between QDs and DABM molecules, therefore leading to enhanced recording efficiency substantiated in fluorescence, transmission and DIC readout modes. Photorefractive polymers sensitised by QDs with S rich surfaces not only enhance the recording efficiency but also enlarge the dynamic range between erasable recording and permanent recording thresholds. As a consequence, multilayer data storage has been demonstrated successfully. The 2P induced localised refractive-index change has been demonstrated in QR-sensitised photorefractive polymers, which is a bench mark for future four-dimensional optical recording.

Chapter 7

Conclusion

7.1 Thesis conclusions

The main research in this thesis provides a comprehensive insight into the development of polarisation-encoded multi-dimensional optical data storage in quantum dot/rod (QD/QR)-sensitised polymer composites, which is a conceptual breakthrough to the current three-dimensional (3D) optical data storage. Four major areas of research have been explored and concentrated on the following key areas.

1. Development and characterisation of two-photon (2P) induced two-state polarisation encoding in photoisomerisation polymers. It is the first demonstration of erasable and rewritable polarisation-encoded multilayer optical data storage.
2. Theoretical analysis and experimental characterisation of 2P induced refractive-index change of azo dyes inside a polymer matrix in confocal reflection microscope.

3. Introducing a novel polarisation-encoded four-dimensional (4D) optical data storage in QD/QR-sensitised photoisomerisation polymers via 2P energy transfer.
4. Developing a novel 2P induced localised refractive-index change towards multi-dimensional optical data storage in QD/QR-sensitised photorefractive polymers.

The feasibility of the 2P induced polarisation encoding technique for multilayer bit by bit data storage has been demonstrated in azo dye 2,5-dimethyl-4-(p-nitrophenylazo)anisole (DMNPAA) doped polymers. A polarisation interference setup has been introduced to readout the 2P induced polarisation sensitivity, which serves as a key reading system for polarisation-encoded multilayer optical data storage in this thesis. An angular dependence of the readout intensity via a relation of $\sin^2(2\theta)$ has been found, which establishes the possibility of two-state polarisation multiplexing with a polarisation angle of 45 degrees. In addition, the optical axis of azo dyes can be randomly re-orientated back and the stored information can be erased when exposing the sample to UV illumination, which is desirable for rewritable 4D optical data storage. The first demonstration of polarisation-encoded 4D optical data storage in such a medium leads to a conceptual breakthrough in the field of optical data storage.

The 2P induced refractive-index change of azo dyes inside a polymer matrix has been investigated in confocal reflection microscope. A confocal reflection readout threshold of the axial response from a planar reflector with a refractive-index change on the order of 10^{-2} is revealed. It has been found that the strong forward scattering caused by the recorded bits leads to multiple reflection between the bit and the back surface, which enhances the image contrast and reduces the readout threshold. This

2P induced refractive-index change, together with the 2P induced polarisation sensitivity, builds up a scientific foundation for polarisation-encoded 4D optical data storage in QD/QR-sensitised polymers.

The incorporation of QDs into the polymer loaded with azo dyes via 2P energy transfer processes leads to a novel recording medium with further improved 2P sensitivity. It has been found that the 2P recording efficiency are significantly dependent on the energy transfer efficiency, determined by the spectral overlapping between the absorption band of azo dyes and the emission band of QDs, which can be tuned by the sizes of QDs. The optimised 2P energy transfer efficiency in CdS QD-sensitised polymers gives rise an enhancement of refractive-index change for 10 to 20%, which allows a higher efficiency for 3D optical data storage. However, the high efficiency comes at the cost of degradation of the polarisation sensitivity.

An investigation in the unique optical properties of QRs under 2P excitation compels the QR-sensitised medium. Z-scan measurement has revealed an significantly high cross-section of CdS QR of $20.9 \times 10^{-46} \text{ cm}^4 \cdot \text{s} \cdot \text{photon}^{-1}$. It has been found that the 2P absorption cross-sections of QRs are one to two orders of magnitude larger compared to those of QDs in the infrared wavelength window from 720 nm to 960 nm. More importantly, a comprehensive characterisation of QRs under 2P orientation microscopy has been undertaken. Strong linearly polarised emission and sharp polarisation selective excitation on the dependence of $\cos^4(\theta)$ of CdS QRs have been observed. This feature of polarisation selective excitation is of the most importance for polarisation encoding technique, whereas spherical QDs are missing.

The new knowledges mentioned above have led to the development of QR-sensitised photoisomerisation polymers for multi-dimensional optical data

storage. The recording performance of azo-dye-doped polymers using QRs as 2P energy transfer donors has been further enhanced. It has been shown an enhanced refractive-index change as a consequence of QR-driven energy transfer at the optimised condition for complete energy transfer from QRs to surrounding azo dyes. In particular, the isomerisation of azo dyes using QRs as 2P energy transfer donors has been characterised in the pump probe experiment. It has been shown that the QR-sensitised polymer builds up large difference in the isomerisation rates between the orthogonal polarisation directions. A large anisotropy of -0.03 has been built up, which gives abundant room to localised polarisation sensitive refractive-index modulation. In comparison no polarisation sensitivity has been preserved in the QD-driven energy transfer. The application of this novel medium in polarisation-encoded 4D optical data storage as well as in polarisation controlled 3D patterning and waveguide fabrication has been successfully demonstrated.

The applicaiton of CdS QDs/QRs in 2P induced optical data storage has been further expanded in photorefractive polymers. The recording performance has been characterised in polymers sensitised by CdS QDs of different surface stoichiometry. It has been found that S rich surfaces can facilitate the local charge transfer at the interface between QDs and nonlinear dye molecules and the 2P recording efficiency is enhanced in fluorescence, transmission and differential interference contrast (DIC) readout modes. Furthermore, it has been shown that using CdS QDs of S rich surfaces as 2P sensitisers in photorefractive polymers enlarges the dynamic range between erasable recording and permanent recording thresholds close to 200% that of the controlled sample. Application of such a medium for 2P induced multilayer data storage has been successfully demonstrated. The ability of QR-sensitised photorefractive polymers to record the refractive-index change under 2P excitation has also been demonstrated, which is a bench mark for future 4D optical data storage.

In conclusion, the research conducted in this thesis has demonstrated polarisation-encoded multi-dimensional optical data storage in QD/QR-sensitised polymers, which opens the new horizon for high density optical data storage. Taking the advantages of QDs/QRs with large 2P absorption cross-sections, tunable spectra property and polarisation functionality the fuse of nanotechnology and polymer science will induce significant impact in the field of optical data storage.

7.2 Future work

7.2.1 Quantum-rod-sensitised photorefractive polymers

As we discussed in Chapter 5, one of the important feature of QRs is the sharp polarisation selective excitation property. The excitation can be selectively switch on or off by controlling the polarisation direction of a laser beam parallel or perpendicular to the orientation of a QR. Therefore, it brings the possibility of polarisation controlled refractive-index modulation as a response to the change of local charge separation introduced by differently polarised writing beams. The ability of QR-sensitised photorefractive polymers to record the refractive-index change has been demonstrated. The challenges impeding the demonstration of polarisation-encoded 4D optical data storage are surface processing of QRs to improve the solubility and optimise the doping concentration. First, the surface cappings need to bond strongly on the surface of QRs to prevent the aggregation. Second, they need to be soluble in PVK to disperse QRs homogeneously in the matrix. Third, they need to facilitate the charge separation at the interface between QRs and surrounding matrix for the occurrence of localised photorefractive effect. This technique can provide new opportunity for polarisation-encoded multi-dimensional optical data storage as well as other polarisation controlled

multi-dimensional photonic applications.

7.2.2 Five-dimensional optical data storage

The research conducted in this thesis has demonstrated the polarisation encoding technique in QD/QR-dispersed polymers, which leads to the 4D optical data storage. The optical properties of QDs/QRs are also dependent on their shapes and sizes, which can be tuned during the preparation process [21]. Therefore, it opens the possibility of wavelength selective excitation which is the most important prerequisite for spectral encoding techniques [105, 157, 158]. The feasibility of the spectral encoding technique in polymers loaded with gold nanorods of different sizes has been demonstrated [105, 157, 158]. However, the concept of encoding information in the spectral domain of a writing beam in QD/QR-sensitised polymers has never been explored. It is expected that applying spectral encoding and polarisation encoding techniques simultaneously in QD/QR-sensitised polymers can significantly expand the storage capacity further, which can lead to five-dimensional optical data storage.

7.2.3 Compact optical system for multi-dimensional optical data storage

A compact optical system can be designed for recording and reading the multi-dimensional optical data storage. A broad wavelength light source and polarisation control components are integrated. Such a system compatible with current the DVD technique can also encode the polarisation information or spectral information in the volume of an optical disc under 2P excitation. In addition, multiplexed information can be readout distinctly using the same compact optical

system. It is expected that the compact optical recording and reading system will speed up the multi-dimensional high capacity optical data storage coming of age.

Bibliography

- [1] D. Day, M. Gu, and A. Smallridge, Review of optical data storage, in *Infrared holography for optical communications*(Springer Berlin, Heidelberg, 2003), pp. 1-22.
- [2] D. McPhail, and M. Gu, Use of polarization sensitivity for three-dimensional optical data storage in polymer dispersed liquid crystals under two-photon illumination. *Appl. Phys. Lett.* **81**, 1160 (2002).
- [3] M. Gu, *Principles of three-dimensional imaging in confocal microscopes* (World Scientific, Singapore, 1996).
- [4] C. F. Bohern, and D. R. Huffman, *Absorption and scattering of ligh by small particles* (J.Wiley & Sons, New York, 1983).
- [5] D. A. Parthenopoulos, and P. M. Rentzepis, Three-dimensional optical storage memory. *Science* **245**, 843-845 (1989).
- [6] J. H. Strickler, and W. W. Webb, Three-dimensional optical-data storage in refractive media by 2-photon point excitation. *Opt. Lett.* **16**, 1780-1782 (1991).
- [7] Y. R. Shen, *Principles of nonlinear optics* (Wiley, New York, 1984).
- [8] E. Walker, and P. M. Rentzepis, Two-photon technology: a new dimension.

- Nat. Photonics* **2**, 406 - 408 (2008).
- [9] B. H. Cumpston, S. P. Ananthavel, S. Barlow, D. L. Dyer, J. E. Ehrlich, L. L. Erskine, A. A. Heikal, S. M. Kuebler, I.-Y. S. Lee, D. McCord-Maughon, J. Qin, H. Rockel, M. Rumi, X.-L. Wu, S. R. Marder, and J. W. Perry, Two-photon polymerization initiators for three-dimensional optical data storage and microfabrication. *Nature* **398**, 51-54 (1999).
 - [10] A. Toriumi, J. M. Herrmann, and S. Kawata, Nondestructive readout of a three-dimensional photochromic optical memory with a near-infrared differential phase-contrast microscope. *Opt. Lett.* **22**, 555-557 (1997).
 - [11] Y. Kawata, H. Ishitobi, and S. Kawata, Use of two-photon absorption in a photorefractive crystal for three-dimensional optical memory. *Opt. Lett.* **23**, 756-758 (1998).
 - [12] D. Day, M. Gu, and A. Smallridge, Use of two-photon excitation for erasable-rewritable three-dimensional bit optical data storage in a photorefractive polymer. *Opt. Lett.* **24**, 948-950 (1999).
 - [13] J. D. Bhawalkar, N. D. Kumar, J. Swiatkiewicz, and P. N. Prasad, Three dimensional optical data storage in a photobleachable dye-doped polymer using two-photon laser scanning microscopy. *Mol. Cryst. Liq. Cryst. Sci. Technol., Sect. B* **19**, 249-257 (1998).
 - [14] M. Gu, and D. Day, Use of continuous-wave illumination for two-photon three-dimensional optical bit data storage in a photobleaching polymer. *Opt. Lett.* **24**, 288-290 (1999).
 - [15] E. N. Glezer, M. Milosavljevic, L. Huang, R. J. Finlay, T.-H. Her, J. P. Callan, and E. Mazur, Three-dimensional optical storage inside transparent materials. *Opt. Lett.* **21**, 2023-2025 (1996).
 - [16] D. Day, and M. Gu, Formation of voids in a doped polymethylmethacrylate

- polymer. *Appl. Phys. Lett.* **80**, 2404 (2002).
- [17] D. Day, and M. Gu, Effects of refractive-index mismatch on three-dimensional optical data-storage density in a two-photon bleaching polymer. *Appl. Opt.* **37**, 6299-6304 (1998).
 - [18] S. Alasfar, M. Ishikawa, Y. Kawata, C. Egami, O. Sugihara, N. Okamoto, M. Tsuchimori, and O. Watanabe, Polarization-multiplexed optical memory with urethane-urea copolymers. *Appl. Opt.* **38**, 6201-6204 (1999).
 - [19] B. Yao, M. Lei, L. Ren, N. Menke, Y. Wang, T. Fischer, and N. Hampp, Polarization multiplexed write-once-read-many optical data storage in bacteriorhodopsin films. *Opt. Lett.* **30**, 3060-3062 (2005).
 - [20] W. M. Gibbons, T. Kosa, P. Palffy-Muhoray, P. J. Shannon, and S. T. Sun, Continuous grey-scale image storage using optically aligned nematic liquid crystals. *Nature* **377**, 43-46 (1995).
 - [21] A. P. Alivisatos, Semiconductor clusters, nanocrystals, and quantum dots. *Science* **271**, 933-937 (1996).
 - [22] D. R. Larson, W. R. Zipfel, R. M. Williams, S. W. Clark, M. P. Bruchez, F. W. Wise, and W. W. Webb, Water-soluble quantum dots for multiphoton fluorescence imaging in vivo. *Science* **300**, 1434-1436 (2003).
 - [23] X. Peng, L. Manna, W. Yang, J. Wickham, E. Scher, A. Kadavanich, and A. P. Alivisatos, Shape control of CdSe nanocrystals. *Nature* **404**, 59-61 (2000).
 - [24] J. Hu, L.-S. Li, W. Yang, L. Manna, L.-W. Wang, and A. P. Alivisatos, Linearly polarized emission from colloidal semiconductor quantum rods. *Science* **292**, 2060-2063 (2001).
 - [25] X. Chen, A. Nazzal, D. Goorskey, M. Xiao, Z. Adam Peng, and X. Peng, Polarization spectroscopy of single CdSe quantum rods. *Phys. Rev. B: Condens. Matter* **64**, 2453041-2453044 (2001).

- [26] V. Biju, T. Itoh, A. Anas, A. Sujith, and M. Ishikawa, Semiconductor quantum dots and metal nanoparticles: Syntheses, optical properties, and biological applications. *Anal. Bioanal. Chem.* **391**, 2469-2495 (2008).
- [27] P. Reiss, J. Bleuse, and A. Pron, Highly luminescent CdSe/ZnSe core/shell nanocrystals of low size dispersion. *Nano Lett.* **2**, 781-784 (2002).
- [28] E. Rothenberg, M. Kazes, E. Shaviv, and U. Banin, Electric field induced switching of the fluorescence of single semiconductor quantum rods. *Nano Lett.* **5**, 1581-1586 (2005).
- [29] S. Kawata, and Y. Kawata, Three-dimensional optical data storage using photochromic materials. *Chem. Rev.* **100**, 1777-1788 (2000).
- [30] A. Toriumi, S. Kawata, and M. Gu, Reflection confocal microscope readout system for three-dimensional photochromic optical data storage. *Opt. Lett.* **23**, 1924 (1998).
- [31] T. Todorov, L. Nikolova, and N. Tomova, Polarization holography. 1: A new high-efficiency organic material with reversible photoinduced birefringence. *Appl. Opt.* **23**, 4309-4312 (1984).
- [32] Z. Sekkat, J. Wood, and W. Knoll, Reorientation mechanism of azobenzenes within the trans \rightarrow cis photoisomerization. *J. Phys. Chem.* **99**, 17226-17234 (1995).
- [33] A. Natansohn, P. Rochon, J. Gosselin, and S. Xie, Azo polymers for reversible optical storage. 1. Poly[4-[[2-(acryloyloxy)ethyl]ethylamino]-4-nitroazobenzene]. *Macromolecules* **25**, 2268-2273 (1992).
- [34] V. P. Pham, T. Galstyan, A. Granger, and R. A. Lessard, Novel azo dye-doped poly(methyl methacrylate) films as optical data storage media. *Jpn. J. Appl. Phys., Part 1* **36**, 429-438 (1997).

- [35] M. Maeda, H. Ishitobi, Z. Sekkat, and S. Kawata, Polarization storage by nonlinear orientational hole burning in azo dye-containing polymer films. *Appl. Phys. Lett.* **85**, 351-353 (2004).
- [36] Z. Sekkat, and M. Dumont, Photoassisted poling of azo dye doped polymeric films at room temperature. *Appl. Phys. B* **54**, 486-489 (1992).
- [37] Z. Sekkat, D. Morichere, M. Dumont, R. Loucif-Saibi, and J. A. Delaire, Photoisomerization of azobenzene derivatives in polymeric thin films. *J. Appl. Phys.* **71**, 1543-1546 (1992).
- [38] W. M. Gibbons, P. J. Shannon, S.-T. Sun, and B. J. Swetlin, Surface-mediated alignment of nematic liquid crystals with polarized laser light. *Nature* **351**, 49-50 (1991).
- [39] T. D. Ebralidze, and A. N. Mumladze, Light-induced anisotropy in azo-dye-colored materials. *Appl. Opt.* **29**, 446-447 (1990).
- [40] Z. Sekkat, D. Yasumatsu, and S. Kawata, Pure photoorientation of azo dye in polyurethanes and quantification of orientation of spectrally overlapping isomers. *J. Phys. Chem. B.* **106**, 12407-12417 (2002).
- [41] H. Ishitobi, Z. Sekkat, and S. Kawata, Photo-orientation by multiphoton photoselection. *J. Opt. Soc. Am. B: Opt. Phys.* **23**, 868-873 (2006).
- [42] P.-A. Blanche, P. C. Lemaire, C. Maertens, P. Dubois, and R. Jerome, Polarised light induced birefringence in azo dye doped polymer: A new model and polarised holographic experiments. *Opt. Commun.* **139**, 92-98 (1997).
- [43] C. Wang, H. Fei, Y. Yang, Z. Wei, Y. Qiu, and Y. Chen, Photoinduced anisotropy and polarization holography in azobenzene side-chain polymer. *Opt. Commun.* **159**, 58-62 (1999).
- [44] E. Hamada, T. Fujii, Y. Tomizawa, and S. Iimura, High density optical recording on dye material discs: An approach for achieving 4.7 GB density.

- Jpn. J. Appl. Phys., Part 1* **36**, 593-594 (1997).
- [45] Z. Sekkat, Isomeric orientation by two-photon excitation: A theoretical study. *Opt. Commun.* **229**, 291-303 (2004).
- [46] J. R. Lakowicz, *Principles of fluorescence spectroscopy* (Kluwer Academic/Plenum, New York, 1999).
- [47] L. Stryer, Fluorescence energy transfer as a spectroscopic ruler. *Annu. Rev. Biochem.* **47**, 819-846 (1978).
- [48] L. Tolosa, H. Malak, G. Raob, and J. R. Lakowicz, Optical assay for glucose based on the luminescence decay time of the long wavelength dye Cy5. *Sens. Actuators, B* **45**, 93-99 (1997).
- [49] T. Nagai, K. Ibata, E. S. Park, M. Kubota, K. Mikoshiba, and A. Miyawaki, A variant of yellow fluorescent protein with fast and efficient maturation for cell-biological applications. *Nat. Biotechnol.* **20**, 87-90 (2002).
- [50] L. Giordano, T. M. Jovin, M. Irie, and E. A. Jares-Erijman, Diheteroarylethenes as thermally stable photoswitchable acceptors in photochromic fluorescence resonance energy transfer (pcFRET). *J. Am. Chem. Soc.* **124**, 7481-7489 (2002).
- [51] H. Tian, and S. Yang, Recent progresses on diarylethene based photochromic switches. *Chem. Soc. Rev.* **33**, 85-97 (2004).
- [52] C. C. Corredor, Z.-L. Huang, and K. D. Belfield, Two-photon 3D optical data storage via fluorescence modulation of an efficient fluorene dye by a photochromic diarylethene. *Adv. Mater.* **18**, 2910-2914 (2006).
- [53] C. C. Corredor, Z.-L. Huang, K. D. Belfield, A. R. Morales, and M. V. Bondar, Photochromic polymer composites for two-photon 3D optical data storage. *Chem. Mater.* **19**, 5165-5173 (2007).
- [54] A. A. Angeluts, N. I. Koroteev, S. A. Krikunov, S. A. Magnitskii, D. V.

- Malakhov, V. V. Shubin, and P. M. Potokov, Enhancement of two-photon initiated coloration by energy transfer from dye to photochromic molecules in polymer films. *Proc. SPIE-Int. Soc. Opt. Eng.* **3732**, 232-238 (1999).
- [55] N. Tian, and Q.-H. Xu, Enhanced two-photon excitation fluorescence by fluorescence resonance energy transfer using conjugated polymers. *Adv. Mater.* **19**, 1988-1991 (2007).
- [56] A. R. Clapp, I. L. Medintz, and H. Mattoussi, Forster resonance energy transfer investigations using quantum-dot fluorophores. *ChemPhysChem* **7**, 47-57 (2006).
- [57] A. R. Clapp, I. L. Medintz, J. M. Mauro, B. R. Fisher, M. G. Bawendi, and H. Mattoussi, Fluorescence resonance energy transfer between quantum dot donors and dye-labeled protein acceptors. *J. Am. Chem. Soc.* **126**, 301-310 (2004).
- [58] I. L. Medintz, A. R. Clapp, H. Mattoussi, E. R. Goldman, B. Fisher, and J. M. Mauro, Self-assembled nanoscale biosensors based on quantum dot FRET donors. *Nat. Mater.* **2**, 630-638 (2003).
- [59] L. Zhu, M.-Q. Zhu, J. K. Hurst, and A. D. Q. Li, Light-controlled molecular switches modulate nanocrystal fluorescence. *J. Am. Chem. Soc.* **127**, 8968-8970 (2005).
- [60] C. A. Leatherdale, W.-K. Woo, F. V. Mikulec, and M. G. Bawendi, On the absorption cross section of CdSe nanocrystal quantum dots. *J. Phys. Chem. B.* **106**, 7619-7622 (2002).
- [61] C. R. Kagan, C. B. Murray, M. Nirmal, and M. G. Bawendi, Electronic energy transfer in CdSe quantum dot solids. *Phys. Rev. Lett.* **76**, 1517-1520 (1996).
- [62] A. R. Clapp, T. Pons, I. L. Medintz, J. B. Delehanty, J. S. Melinger, T. Tiefenbrunn, P. E. Dawson, B. R. Fisher, B. O'Rourke, and H. Mattoussi,

- Two-photon excitation of quantum-dot-based fluorescence resonance energy transfer and its applications. *Adv. Mater.* **19**, 1921-1926 (2007).
- [63] B. O. Dabbousi, J. Rodriguez-Viejo, F. V. Mikulec, J. R. Heine, H. Mattoussi, R. Ober, K. F. Jensen, and M. G. Bawendi, (CdSe)ZnS core-shell quantum dots: Synthesis and characterization of a size series of highly luminescent nanocrystallites. *J. Phys. Chem. B.* **101**, 9463-9475 (1997).
- [64] F. Chen, and D. Gerion, Fluorescent CdSe/ZnS nanocrystal-peptide conjugates for long-term, nontoxic imaging and nuclear targeting in living cells. *Nano Lett.* **4**, 1827-1832 (2004).
- [65] L. Y. Lee, S. L. Ong, J. Y. Hu, W. J. Ng, Y. Feng, X. Tan, and S. W. Wong, Use of semiconductor quantum dots for photostable immunofluorescence labeling of *Cryptosporidium parvum*. *Appl. Environ. Microbiol.* **70**, 5732-5736 (2004).
- [66] I. L. Medintz, S. A. Trammell, H. Mattoussi, and J. M. Mauro, Reversible modulation of quantum dot photoluminescence using a protein-bound photochromic fluorescence resonance energy transfer acceptor. *J. Am. Chem. Soc.* **126**, 30-31 (2004).
- [67] X. Sheng, A. Peng, H. Fu, Y. Liu, Y. Zhao, Y. Ma, and J. Yao, Modulation of a fluorescence switch based on photochromic spirooxazine in composite organic nanoparticles. *Nanotechnology* **18**, (2007).
- [68] X. Li, J. W. M. Chon, and M. Gu, Nanoparticle-based photorefractive polymers. *Aust. J. Chem.* **61**, 317-323 (2008).
- [69] S. Ducharme, J. C. Scott, R. J. Twieg, and W. E. Moerner, Observation of the photorefractive effect in a polymer. *Phys. Rev. Lett.* **66**, 1846-1849 (1991).
- [70] K. Meerholz, B. L. Volodin, Sandalphon, B. Kippelen, and N. Peyghambarian, A photorefractive polymer with high optical gain and diffraction efficiency near 100%. *Nature* **371**, 497 (1994).

- [71] F. Wurthner, R. Wortmann, and K. Meerholz, Chromophore design for photorefractive organic materials. *ChemPhysChem* **3**, 17-31 (2002).
- [72] W. E. Moerner, A. Grunnet-Jepsen, and C. L. Thompson, Photorefractive polymers. *Annu. Rev. Mater. Sci.* **27**, 585-623 (1997).
- [73] W. E. Moerner, and S. M. Silence, Polymeric photorefractive materials. *Chem. Rev.* **94**, 127-155 (1994).
- [74] O. Ostroverkhova, and W. E. Moerner, Organic photorefractives: Mechanisms, materials, and applications. *Chem. Rev.* **104**, 3267-3314 (2004).
- [75] P. M. Lundquist, C. Poga, R. G. DeVoe, Y. Jia, W. E. Moerner, M.-P. Bernal, H. Coufal, R. K. Grygier, J. A. Hoffnagle, C. M. Jefferson, R. M. Macfarlane, R. M. Shelby, and G. T. Sincerbox, Holographic digital data storage in a photorefractive polymer. *Opt. Lett.* **21**, 890-892 (1996).
- [76] D. Wright, M. A. Diaz-Garcia, J. D. Casperson, M. Declue, W. E. Moerner, and R. J. Twieg, High-speed photorefractive polymer composites. *Appl. Phys. Lett.* **73**, 1490-1492 (1998).
- [77] B. Kippelen, S. R. Marder, E. Hendrickx, J. L. Maldonado, G. Guillemet, B. L. Volodin, D. D. Steele, Y. Enami, Sandalphon, Y. J. Yao, J. F. Wang, H. Rockel, L. Erskine, and N. Peyghambarian, Infrared photorefractive polymers and their applications for imaging. *Science* **279**, 54-57 (1998).
- [78] P. N. Prasad, Polymer science and technology for new generation photonics and biophotonics. *Curr. Opin. Solid State Mater. Sci.* **8**, 11-19 (2004).
- [79] J. G. Winarz, L. Zhang, M. Lal, C. S. Friend, and P. N. Prasad, Photogeneration, charge transport, and photoconductivity of a novel PVK/CdS-nanocrystal polymer composite. *Chem. Phys.* **245**, 417-428 (1999).
- [80] J. G. Winarz, L. Zhang, M. Lal, C. S. Friend, and P. N. Prasad, Observation of the photorefractive effect in a hybrid organic-inorganic nanocomposite. *J. Am.*

- Chem. Soc.* **121**, 5287-5295 (1999).
- [81] J. G. Winiarz, L. Zhang, J. Park, and P. N. Prasad, Inorganic: Organic hybrid nanocomposites for photorefractivity at communication wavelengths. *J. Phys. Chem. B.* **106**, 967-970 (2002).
 - [82] J. G. Winiarz, and P. N. Prasad, Photorefractive inorganic-organic polymer-dispersed liquid-crystal nanocomposite photosensitized with cadmium sulfide quantum dots. *Opt. Lett.* **27**, 1330-1332 (2002).
 - [83] K. R. Choudhury, Y. Sahoo, S. Jang, and P. N. Prasad, Efficient photosensitization and high optical gain in a novel quantum-dot-sensitized hybrid photorefractive nanocomposite at a telecommunications wavelength. *Adv. Funct. Mater.* **15**, 751-756 (2005).
 - [84] K. R. Choudhury, Y. Sahoo, and P. N. Prasad, Hybrid quantum-dot-polymer nanocomposites for infrared photorefractivity at an optical communication wavelength. *Adv. Mater.* **17**, 2877-2881 (2005).
 - [85] D. J. Binks, D. P. West, S. Norager, and P. O'Brien, Field-independent grating formation rate in a photorefractive polymer composite sensitized by CdSe quantum dots. *J. Chem. Phys.* **117**, 7335-7341 (2002).
 - [86] D. J. Binks, S. P. Bant, D. P. West, P. O'Brien, and M. A. Malik, CdSe/CdS core/shell quantum dots as sensitizer of a photorefractive polymer composite. *J. Mod. Opt.* **50**, 299-310 (2003).
 - [87] F. Aslam, D. J. Binks, M. D. Rahn, D. P. West, P. O'Brien, and N. Pickett, Photorefractive performance of polymer composite sensitized by CdSe nanoparticles passivated by 1-hexadecylamine. *J. Mod. Opt.* **Vol. 52**, 945 (2005).
 - [88] F. Aslam, D. J. Binks, M. D. Rahn, D. P. West, P. O'Brien, N. Pickett, and S. Daniels, Photorefractive performance of a CdSe/ZnS core/shell

- nanoparticle-sensitized polymer. *J. Chem. Phys.* **122**, 1-6 (2005).
- [89] F. Aslam, J. Stevenson-Hill, D. J. Binks, S. Daniels, N. L. Pickett, and P. O'Brien, Effect of nanoparticle composition on the performance of photorefractive polymers. *Chem. Phys.* **334**, 45-52 (2007).
- [90] J. G. Winiarz, Enhancement of the photorefractive response time in a polymeric composite photosensitized with CdTe nanoparticles. *J. Phys. Chem. C* **111**, 1904-1911 (2007).
- [91] D. J. Suh, O. O. Park, T. Ahn, and H.-K. Shim, Observation of the photorefractive behaviors in the polymer nanocomposite based on p-PMEH-PPV/CdSe-nanoparticle matrix. *Opt. Mater.* **21**, 365-371 (2003).
- [92] J. H. Park, and O. O. Park, Photorefractive properties in poly (N-vinylcarbazole)/CdSe nanocomposites through chemical hybridization. *Appl. Phys. Lett.* **89**, (2006).
- [93] L. Ding, D. Jiang, and J. Huang, Photorefractive effect of polymer sensitized by CdS nanoparticles. *Guangxue Xuebao/Acta Optica Sinica* **26**, 1526-1531 (2006).
- [94] C. Fuentes-Hernandez, D. J. Suh, B. Kippelen, and S. R. Marder, High-performance photorefractive polymers sensitized by cadmium selenide nanoparticles. *Appl. Phys. Lett.* **85**, 534-536 (2004).
- [95] J. Zhang, Z. Chen, Y. Liu, M. Huang, Q. Wei, and Q. Gong, Improvement on the photorefractive performance of a monolithic molecular material by introducing electron traps. *Appl. Phys. Lett.* **85**, 1323-1325 (2004).
- [96] K. R. Choudhury, M. Samoc, A. Patra, and P. N. Prasad, Charge carrier transport in poly(N-vinylcarbazole):CdS quantum dot hybrid nanocomposites. *J. Phys. Chem. B* **108**, 1556-1562 (2004).
- [97] K. R. Choudhury, J. G. Winiarz, M. Samoc, and P. N. Prasad, Charge carrier

- mobility in an organic-inorganic hybrid nanocomposite. *Appl. Phys. Lett.* **82**, 406-408 (2003).
- [98] W.-S. Kim, J.-W. Lee, and J.-K. Park, Enhancement of the recording stability of a photorefractive polymer composite by the introduction of a trapping layer. *Appl. Phys. Lett.* **83**, 3045-3047 (2003).
- [99] N. C. Greenham, X. Peng, and A. P. Alivisatos, Charge separation and transport in conjugated-polymer/semiconductor-nanocrystal composites studied by photoluminescence quenching and photoconductivity. *Phys. Rev. B: Condens. Matter* **54**, 17628-17637 (1996).
- [100] B. E. A. Saleh, and M. C. Teich, *Fundamentals of photonics* (Wiley, New York, 1991).
- [101] P. Cheben, F. Del Monte, D. J. Worsfold, D. J. Carlsson, C. P. Grover, and J. D. Mackenzie, A photorefractive organically modified silica glass with high optical gain. *Nature* **408**, 64-67 (2000).
- [102] P. A. Blanche, B. Kippelen, A. Schulzgen, C. Fuentes-Hernandez, G. Ramos-Ortiz, J. F. Wang, E. Hendrickx, N. Peyghambarian, and S. R. Marder, Photorefractive polymers sensitized by two-photon absorption. *Opt. Lett.* **27**, 19-21 (2002).
- [103] J. H. Strickler, and W. W. Webb, Three-dimensional optical data storage in refractive media by two-photon point excitation. *Opt. Lett.* **16**, 1780 (1991).
- [104] M. Watanabe, S. Juodkazis, H.-B. Sun, S. Matsuo, and H. Misawa, Two-photon readout of three-dimensional memory in silica. *Appl. Phys. Lett.* **77**, 13-15 (2000).
- [105] J. W. M. Chon, P. Zijlstra, M. Gu, J. Van Embden, and P. Mulvaney, Two-photon-induced photoenhancement of densely packed CdSe/ZnSe/ZnS nanocrystal solids and its application to multilayer optical data storage. *Appl.*

- Phys. Lett.* **85**, 5514-5516 (2004).
- [106] X. Li, J. W. M. Chon, S. Wu, R. A. Evans, and M. Gu, Rewritable polarization-encoded multilayer data storage in 2,5-dimethyl-4-(p-nitrophenylazo)anisole doped polymer. *Opt. Lett.* **32**, 277-279 (2007).
- [107] X. Li, J. W. M. Chon, S. Wu, R. Evans, and M. Cu, Two-photon-induced two-state polarisation encoding in 2,5-dimethyl-4-(p- nitrophenylazo)anisole doped polymer, in *ACOFT/AOS 2006 - Australian Conference on Optical Fibre Technology/Australian Optical Society*(2006).
- [108] B. A. Reinhardt, L. L. Brott, S. J. Clarson, A. G. Dillard, J. C. Bhatt, R. Kannan, L. Yuan, G. S. He, and P. N. Prasad, Highly active two-photon dyes: Design, synthesis, and characterization toward application. *Chem. Mater.* **10**, 1863-1874 (1998).
- [109] M. Gu, *Advanced optical imaging theory* (Springer, Verlag, 2000).
- [110] K. Choi, P. Zijlstra, J. W. M. Chon, and M. Gu, Fabrication of low-threshold 3D void structures inside a polymer matrix doped with gold nanorods. *Adv. Funct. Mater.* **18**, 2237-2245 (2008).
- [111] A. Toriumi, S. Kawata, and M. Gu, Reflection confocal microscope readout system for three-dimensional photochromic optical data storage. *Opt. Lett.* **23**, 1924-1926 (1998).
- [112] M. A. Bopp, Y. Jia, G. Haran, E. A. Morlino, and R. M. Hochstrasser, Single-molecule spectroscopy with 27 fs pulses: Time-resolved experiments and direct imaging of orientational distributions. *Appl. Phys. Lett.* **73**, 7-9 (1998).
- [113] C. J. R. Sheppard, M. Gu, and X. Q. Mao, Three-dimensional coherent transfer function in a reflection-mode confocal scanning microscope. *Opt. Commun.*

- 81**, 281-284 (1991).
- [114] T. Wilson, Y. Kawata, and S. Kawata, Readout of three-dimensional optical memories. *Opt. Lett.* **21**, 1003-1005 (1996).
- [115] G. U. Min, Confocal readout of three-dimensional data bits recorded by the photorefractive effect under single-photon and two-photon excitation. *Proc. IEEE* **87**, 2021-2029 (1999).
- [116] M. Gu, J. O. Amistoso, A. Toriumi, M. Irie, and S. Kawata, Effect of saturable response to two-photon absorption on the readout signal level of three-dimensional bit optical data storage in a photochromic polymer. *Appl. Phys. Lett.* **79**, 148-150 (2001).
- [117] T. Hattori, T. Shibata, S. Onodera, and T. Kaino, Fabrication of refractive index grating into azo-dye-containing polymer films by irreversible photoinduced bleaching. *J. Appl. Phys.* **87**, 3240-3244 (2000).
- [118] M. Ivanov, T. Todorov, L. Nikolova, N. Tomova, and V. Dragostinova, Photoinduced changes in the refractive index of azo-dye/polymer systems. *Appl. Phys. Lett.* 2174 (1995).
- [119] Z. Sekkat, H. Ishitobi, and S. Kawata, Two-photon isomerization and orientation of photoisomers in thin films of polymer. *Opt. Commun.* **222**, 269-276 (2003).
- [120] X. Li, J. W. M. Chon, and M. Gu, Confocal reflection readout thresholds in two-photon-induced optical recording. *Appl. Opt.* **47**, 4707-4713 (2008).
- [121] C. J. R. Sheppard, and M. Gu, Axial imaging through an aberrating layer of water in confocal microscopy. *Opt. Commun.* **88**, 180-190 (1992).
- [122] C. J. R. Sheppard, M. Gu, K. Brain, and H. Zhou, Influence of spherical aberration on axial imaging of confocal reflection microscopy. *Appl. Opt.* **33**, 616-624 (1994).

- [123] M. Born, and E. Wolf, *Principles of optics* (Pergamon, Oxford, 1975).
- [124] D. Ganic, X. Gan, and M. Gu, Near-field imaging by a micro-particle: A model for conversion of evanescent photons into propagating photons. *Opt. Express* **12**, 5325-5335 (2004).
- [125] E. Rothenberg, Y. Ebenstein, M. Kazes, and U. Banin, Two-photon fluorescence microscopy of single semiconductor quantum rods: Direct observation of highly polarized nonlinear absorption dipole. *J. Phys. Chem. B.* **108**, 2797-2800 (2004).
- [126] V. R. Almeida, C. A. Barrios, R. R. Panepucci, and M. Lipson, All-optical control of light on a silicon chip. *Nature* **431**, 1081-1084 (2004).
- [127] M. Deubel, G. Von Freymann, M. Wegener, S. Pereira, K. Busch, and C. M. Soukoulis, Direct laser writing of three-dimensional photonic-crystal templates for telecommunications. *Nature* **3**, 444-447 (2004).
- [128] S. Noda, M. Fujita, and T. Asano, Spontaneous-emission control by photonic crystals and nanocavities. *Nat. Photonics* **1**, 449-458 (2007).
- [129] K. Minoshima, A. M. Kowalevich, I. Hartl, E. P. Ippen, and J. G. Fujimoto, Photonic device fabrication in glass by use of nonlinear materials processing with a femtosecond laser oscillator. *Opt. Lett.* **26**, 1516-1518 (2001).
- [130] Z. Sekkat, J. Wood, E. F. Aust, W. Knoll, W. Volksen, and R. D. Miller, Light-induced orientation in a high glass transition temperature polyimide with polar azo dyes in the side chain. *J. Opt. Soc. Am. B: Opt. Phys.* **13**, 1713-1724 (1996).
- [131] X. Li, J. W. M. Chon, R. A. Evans, and M. Gu, Two-photon energy transfer enhanced three-dimensional optical memory in quantum-dot and azo-dye doped polymers. *Appl. Phys. Lett.* **92**, 063309 (2008).
- [132] X. Li, J. W. M. Chon, R. A. Evans, and M. Gu, Quantum-rod dispersed

- photopolymers for multi-dimensional photonic applications. *Opt. Express* **17**, 2954-2961 (2009).
- [133] X. Li, J. Van Embden, J. W. M. Chon, and M. Gu, Enhanced two-photon absorption of CdS nanocrystal rods. *Appl. Phys. Lett.* **94**, 103117 (2009).
- [134] W. W. Yu, and X. Peng, Formation of high-quality CdS and other II-VI semiconductor nanocrystals in noncoordinating solvents: Tunable reactivity of monomers. *Angew. Chem. Int. Ed.* **41**, 2368-2371 (2002).
- [135] V. I. Klimov, Optical nonlinearities and ultrafast carrier dynamics in semiconductor nanocrystals. *J. Phys. Chem. B.* **104**, 6112-6123 (2000).
- [136] H. Htoon, J. A. Hollingworth, A. V. Malko, R. Dickerson, and V. I. Klimov, Light amplification in semiconductor nanocrystals: Quantum rods versus quantum dots. *Appl. Phys. Lett.* **82**, 4776-4778 (2003).
- [137] W. W. Yu, L. Qu, W. Guo, and X. Peng, Experimental determination of the extinction coefficient of CdTe, CdSe, and CdS nanocrystals. *Chem. Mater.* **15**, 2854-2860 (2003).
- [138] M. Sheik-Bahae, A. A. Said, T.-H. Wei, D. J. Hagan, and E. W. Van Stryland, Sensitive measurement of optical nonlinearities using a single beam. *IEEE J. Quantum Electron.* **26**, 760-769 (1990).
- [139] J. He, Y. Qu, H. Li, J. Mi, and W. Ji, Three-photon absorption in ZnO and ZnS crystals. *Opt. Express* **13**, 9235-9247 (2005).
- [140] J. He, W. Ji, G. H. Ma, S. H. Tang, E. S. W. Kong, S. Y. Chow, X. H. Zhang, Z. L. Hua, and J. L. Shi, Ultrafast and large third-order nonlinear optical properties of CdS nanocrystals in polymeric film. *J. Phys. Chem. B.* **109**, 4373-4376 (2005).
- [141] S.-C. Pu, M.-J. Yang, C.-C. Hsu, C.-W. Lai, C.-C. Hsieh, S. H. Lin, Y.-M. Cheng, and P.-T. Chou, The empirical correlation between size and two-photon

- absorption cross section of CdSe and CdTe quantum dots. *Small* **2**, 1308-1313 (2006).
- [142] F. Shieh, A. E. Saunders, and B. A. Korgel, General shape control of colloidal CdS, CdSe, CdTe quantum rods and quantum rod heterostructures. *J. Phys. Chem. B.* **109**, 8538-8542 (2005).
- [143] M. A. Albota, C. Xu, and W. W. Webb, Two-photon fluorescence excitation cross sections of biomolecular probes from 690 to 960 nm. *Appl. Opt.* **37**, 7352-7356 (1998).
- [144] C. Xu, and W. W. Webb, Measurement of two-photon excitation cross sections of molecular fluorophores with data from 690 to 1050 nm. *J. Opt. Soc. Am. B: Opt. Phys.* **13**, 481-491 (1996).
- [145] J. W. M. Chon, M. Gu, C. Bullen, and P. Mulvaney, Three-photon excited band edge and trap emission of CdS semiconductor nanocrystals. *Appl. Phys. Lett.* **84**, 4472-4474 (2004).
- [146] K.-T. Yong, J. Qian, I. Roy, H. H. Lee, E. J. Bergey, K. M. Tramposch, S. He, M. T. Swihart, A. Maitra, and P. N. Prasad, Quantum rod bioconjugates as targeted probes for confocal and two-photon fluorescence imaging of cancer cells. *Nano Lett.* **7**, 761-765 (2007).
- [147] S. Maruo, O. Nakamura, and S. Kawata, Three-dimensional microfabrication with two-photon-absorbed photopolymerization. *Opt. Lett.* **22**, 132-134 (1997).
- [148] L. De Boni, J. J. Rodrigues Jr., D. S. Dos Santos Jr., C. H. T. P. Silva, D. T. Balogh, O. N. Oliveira Jr., S. C. Zilio, L. Misoguti, and C. R. Mendonça, Two-photon absorption in azoaromatic compounds. *Chem. Phys. Lett.* **361**, 209-213 (2002).
- [149] C. B. Murray, D. J. Norris, and M. G. Bawendi, Synthesis and characterization

- of nearly monodisperse CdE (E = S, Se, Te) semiconductor nanocrystallites. *J. Am. Chem. Soc.* **115**, 8706-8715 (1993).
- [150] W. C. W. Chan, and S. Nie, Quantum dot bioconjugates for ultrasensitive nonisotopic detection. *Science* **281**, 2016-2018 (1998).
- [151] X. Li, C. Bullen, J. W. M. Chon, R. A. Evans, and M. Gu, Two-photon-induced three-dimensional optical data storage in CdS quantum-dot doped photopolymer. *Appl. Phys. Lett.* **90**, (2007).
- [152] M. G. Bawendi, W. L. Wilson, L. Rothberg, P. J. Carroll, T. M. Jedju, M. L. Steigerwald, and L. E. Brus, Electronic structure and photoexcited-carrier dynamics in nanometer-size CdSe clusters. *Phys. Rev. Lett.* **65**, 1623-1626 (1990).
- [153] J. J. Li, Y. A. Wang, W. Guo, J. C. Keay, T. D. Mishima, M. B. Johnson, and X. Peng, Large-scale synthesis of nearly monodisperse CdSe/CdS core/shell nanocrystals using air-stable reagents via successive ion layer adsorption and reaction. *J. Am. Chem. Soc.* **125**, 12567-12575 (2003).
- [154] V. I. Klimov, C. J. Schwarz, D. W. McBranch, C. A. Leatherdale, and M. G. Bawendi, Ultrafast dynamics of inter- and intraband transitions in semiconductor nanocrystals: Implications for quantum-dot lasers. *Phys. Rev. B: Condens. Matter* **60**, (1999).
- [155] V. Klimov, P. Haring Bolivar, and H. Kurz, Ultrafast carrier dynamics in semiconductor quantum dots. *Phys. Rev. B: Condens. Matter* **53**, 1463-1467 (1996).
- [156] J. Thomas, C. Fuentes-Hernandez, M. Yamamoto, K. Cammack, K. Matsumoto, G. A. Walker, S. Barlow, B. Kippelen, G. Meredith, S. R. Marder, and N. Peyghambarian, Bistriarylamine polymer-based composites for photorefractive applications. *Adv. Mater.* **16**, 2032-2036 (2004).

- [157] H. Ditlbacher, J. R. Krenn, B. Lamprecht, A. Leitner, and F. R. Aussenegg, Spectrally coded optical data storage by metal nanoparticles. *Opt. Lett.* **25**, 563-565 (2000).
- [158] J. W. M. Chon, C. Bullen, P. Zijlstra, and M. Gu, Spectral encoding on gold nanorods doped in a silica sol-gel matrix and its application to high-density optical data storage. *Advanced Functional Materials* **17**, 875-880 (2007).

Publications of the author

Journal Publications

Xiangping Li, James W.M. Chon, Wu Shuhui, Richard A. Evans and Min Gu. Rewritable polarisation-encoded multilayer data storage in 2,5-dimethyl-4-(p-nitrophenylazo)anisole doped polymer. *Opt. Lett.*, **32**: 277-279, 2007.

Xiangping Li, Bullen Craig, James W.M. Chon, Richard A. Evans and Min Gu. Two-photon-induced three-dimensional optical data storage in CdS quantum-dot doped photopolymer. *Appl. Phys.Lett.*, **90**: 161116, 2007.

Xiangping Li, James W.M. Chon, Richard A. Evans and Min Gu. Two-photon energy transfer enhanced three-dimensional optical memory in quantum-dot and azo-dye doped polymers. *Appl. Phys.Lett.*, **92**: 063309, 2008. (Highlight by *Nature Photonics* **2**, 402 (2008)).

Xiangping Li, James W.M. Chon, and Min Gu. Nanoparticle-based photorefractive

polymers. *Aust. J. Chem.*, **61**: 317-323, 2008.

Xiangping Li, James W.M. Chon, and Min Gu. Confocal reflection readout thresholds in two-photon-induced optical recording. *Appl. Opt.*, **47**: 4707-4713, 2008.

Xiangping Li, James W.M. Chon, Richard A. Evans and Min Gu. Quantum-rod dispersed photopolymers for multi-dimensional photonic applications. *Opt. Express.*, **17**: 2954-2961, 2009.

Xiangping Li, Joel Van Embden, James W. M. Chon and Min Gu. Enhanced two-photon absorption of CdS nanocrystal rods. *Appl. Phys. Lett.* **94**: 103117, 2009.

Conferences

Xiangping Li, James W.M. Chon, Wu Shuhui, Richard A. Evans and Min Gu. Two-photon-induced two-state polarisation encoding in 2,5-dimethyl-4-(p-nitrophenylazo)anisole doped polymer. *Australian Conference on Optical Fibre Technology/Australian Optical Society*, Melbourne, Australia, July 10-13, 2006.

Xiangping Li, James W.M. Chon, Wu Shuhui, Bullen Craig and Min Gu. Two-photon induced optical recording in quantum-dot-based photorefractive materials. *International Conference on Nanoscience and Nanotechnology*, Brisbane, Australia, July 3-7, 2006.

Xiangping Li, Craig Bullen, James W.M. Chon, Richard A. Evans, Min Gu. Two-photon Induced Refractive Index Change In Quantum Dot Doped

Photorefractive Polymer. *European Conference on Lasers and Electro-Optics and the International Quantum Electronics Conference*, Munich, Germany, June 17-22, 2007.

Xiangping Li, James W.M. Chon, Richard A. Evans, Min Gu. Three-dimensional optical memory in nanocrystal and azo-dye dispersed polymers via two-photon energy transfer. *21st International Commission for Optics*, Sydney, Australia, July 7-10, 2008.

Xiangping Li, James Chon, Joel Leonard Van Embden, Min Gu. Two-photon-induced-photoluminance of CdS quantum rod ensembles. *2008 International Conference On Nanoscience and Nanotechnology*, Melbourne, Australia, February 25-29, 2008.

Xiangping Li, James W.M. Chon, Min Gu. Two-photon induced refractive-index modulation in quantum-rod-dispersed photopolymers. *Frontiers in Optics 2008/Laser Science XXIV*, Rochester, USA, October 19-24, 2008.

Xiangping Li, James W.M. Chon, Richard A. Evans, Min Gu. Quantum-rod sensitized four-dimensional optical data storage. *29th Conference on Lasers and Electro Optics and the 27th International Quantum Electronics Conference*, Baltimore, USA, May 31 – June 5, 2009.